ACTUATION STRATEGIES FOR CYCLE-TO-CYCLE CONTROL OF HOMOGENEOUS CHARGE COMPRESSION IGNITION COMBUSTION ENGINES

A DISSERTATION
SUBMITTED TO THE DEPARTMENT OF MECHANICAL ENGINEERING
AND THE COMMITTEE ON GRADUATE STUDIES
OF STANFORD UNIVERSITY
IN PARTIAL FULFILLMENT OF THE REQUIREMENTS
FOR THE DEGREE OF
DOCTOR OF PHILOSOPHY

Adam F. Jungkunz
March 2013

© Copyright by Adam F. Jungkunz 2013
All Rights Reserved

I certify that I have read this dissertation and that, in my opinion, it is fully adequate in scope and quality as a dissertation for the degree of Doctor of Philosophy.

(J. Christian Gerdes) Principal Adviser

I certify that I have read this dissertation and that, in my opinion, it is fully adequate in scope and quality as a dissertation for the degree of Doctor of Philosophy.

(Christopher F. Edwards)

I certify that I have read this dissertation and that, in my opinion, it is fully adequate in scope and quality as a dissertation for the degree of Doctor of Philosophy.

(J. Edward Carryer)

Approved for the University Committee on Graduate Studies

Abstract

The mounting evidence of anthropogenic climate change necessitates a significant effort to improve the internal combustion (IC) engine and reduce its adverse environmental impacts due to its ubiquitous use powering ground transportation in the world today. Homogenous Charge Compression Ignition (HCCI) engines present a promising opportunity to reduce the environmental consequences of using IC engines by reusing exhaust from one engine cycle to initiate combustion on the following engine cycle. The presence of high retained exhaust ratios in HCCI engines results in dilute, low-temperature combustion that achieves greater efficiencies and lower CO_2 and NO_x emissions than conventional spark-ignited or diesel engines. However, three critical obstacles prevent them from being widely adopted: first, unlike conventional IC engines, HCCI engines lack a direct combustion trigger to determine when combustion occurs, and that lack of a direct trigger makes specifying combustion timing challenging. Second, the high quantities of retained exhaust create a strong physical link between engine cycles, resulting in undesirable dynamics that could potentially lead to engine misfire at certain operating conditions. Finally, the high quantities of retained exhaust also prevent the engine from inducting as much fuel and air as possible, limiting the load range of the engine.

This dissertation addresses all three of those obstacles by investigating the abilities of different actuators to control combustion timing and improve the dynamics at certain HCCI operating conditions that could be used to expand the load range of HCCI engines. A simple, physical model that represents one engine cycle as a discrete-time, nonlinear system captures the oscillatory dynamics present at certain HCCI operating conditions on an experimental engine. The physical model provides

physical intuition about the sources driving the oscillations and the control actions needed to reduce them. A linearized version of the model depicts the source of those oscillations on a root locus, and shows that a negative real axis pole in a discrete-time, linear dynamical system drives the oscillations.

Three different actuators, exhaust valve closing timing, pilot fuel injection timing, and main fuel injection mass, each reduce the oscillations. For each actuator, a linearization of the physical model illustrates how each actuator can be used with simple linear control laws to improve the dynamics at HCCI operating conditions. Then, the actuators are compared to each other on three bases: the difficulty of the control problem associated with using the particular actuator to reduce the oscillations, the difficulty of implementing the actuator in a production vehicle, and the effectiveness of each actuator at reducing the oscillations.

Acknowledgements

Sometimes you want to go
Where everybody knows controls
And they're experts at zeros and poles
You want to be where Ax + Bu
Tells you where the system goes
You want to be where everybody knows controls.

I'm not sure how many other graduate students can proudly proclaim that their advisors likened themselves to John Ratzenberger's character Cliff Clavin on the venerable 1980's NBC sitcom *Cheers* while introducing them for their PhD defense, but I know I can. I've had the pleasure of learning an exceptional amount about dynamics, controls, '80's rock, communicating, selecting the proper sander for a woodworking project, how to moonwalk to Michael Jackson's "Bad" after passing one's qualifying exam, and many other things from Chris Gerdes over the past eight years. Thanks for all your help and support during my time here at Stanford, Chris.

Thanks also to my other two reading committee members, Chris Edwards and Ed Carryer, for their help not only in providing me feedback on my dissertation, but also for other advice they've given me throughout my Stanford career. I came to know both of them during my first quarter at Stanford through the joint Stanford-GM-Bosch HCCI control project and in Ed's case through ME 218. They both provided help with the design of the test engine featured prominently in this dissertation as well as help with thermodynamic modeling help in Chris's case well before I began writing my dissertation.

I appreciate the assistance I received from Steve Rock and Allison Okamura, who

both served on my oral committee at my defense. They both had some valuable insight for me about my work, and they gave me some important tips on ways to better present the material in the dissertation and in future presentations.

I cannot imagine how much more difficult completing my PhD would have been without the help of Scott Sutton, the engine lab mechanical technician, and Godwin Zhang, the Dynamic Design Lab (DDL) electronics technician. I learned a considerable amount from both of them about engines and electronics, and the engine would not run nearly as well as it does or maybe even at all if not for their help setting it up and maintaining it. To them, I am truly indebted.

I found the support of the two DDL administrators, Denise Curti and Jennifer Rahn, invaluable during my time at Stanford. Denise was a huge help in ordering pretty much all of the equipment for the test engine, and made all of my acquisitions for the engine flow more smoothly. Jennifer has been a big help with all sorts of things over the last few years—filing travel reimbursements, scheduling conference rooms, printing material for courses, making sure paperwork was in order—and I greatly appreciate all that she has done for me.

I owe a big thanks to our corporate sponsors at General Motors and Robert Bosch. Not only did they generously provide us the resources to build a totally awesome, state-of-the-art engine testbed, they provided us with valuable advice and feedback about whatever modeling and control concepts we were considering. Thanks to Chen-Fang Chang, Jun-Mo Kang, Nicole Wermuth, Jason Chen, Tang-Wei Kuo, Paul Najt, and Man-Feng Chang at GM and Aleksander Kojic, Jasim Ahmed, Sungbae Kim, Han Ho Song, and Nalin Chaturvedi for their help.

I could not possibly write an acknowledgements section without recognizing the other members of the Combustion Unit of the Dynamic Design Lab, or the C-Unit, as we affectionately refer to ourselves. Matt Roelle, Nikhil Ravi, Hsien-Hsin Liao, Steve Erlien, and Greg Shaver have provided invaluable advice, modeling help, experimental help, testbed help, comedic relief, and friendship throughout my time in the lab. Thanks guys.

The other members of the DDL family have been a significant help too. From advice on classes, electronics, managing my path through graduate school, giving me

advice on conference talks, or just spending time having a beer at the Treehouse or catching an A's game at the Oakland Coliseum, many thanks to Matt Schwall, Josh Switkes, Chris Gadda, Sam Chang, Shad Laws, Judy Hsu, Kirstin Talvala, Craig Beal, Carrie Bobier, Rami Hindiyeh, Mick Kritayakirana, Holly Butterfield, Hyungchai Park, Paul Theodosis, John Kegelman, Avinash Balachandran, Joe Funke, Nitin Kapania, Russell Patton, Marcial Hernandez, Stephanie Kato, and John Goh.

Thanks to all my many friends and family for your friendship, help, and support throughout my time here at Stanford. You all certainly made my time more enjoyable, and for that, I am grateful.

I thank my parents, Dave and Julie Jungkunz, for providing the foundation upon which I could develop and grow. By ensuring that I never needed to work while in school, they provided me the opportunity to focus on my schoolwork and be successful enough to attend Stanford. Thanks to to my sister, Katie Becker, for her support throughout my graduate career as well.

My west coast family, cousins Elizabeth and Marla Feierabend, were a huge part of my time at Stanford. I thank them for all their companionship, meals, camping and hiking trips, and support during my time at Stanford.

Finally, my lovely wife, Laura Crenwelge, has been very supportive, patient, understanding, and encouraging of my graduate career. Thank you for your love, your help, and for moving halfway across the country to share this journey with me. Additionally, I am grateful that our son, Harmon, decided to remain in the womb until his due date, thus allowing me to defend five days prior to his birth. Thanks little guy!

Contents

List of Tables

List of Figures

Chapter 1

Introduction

1.1 Background

One of the most significant challenges facing humanity in the 21st Century is finding more sustainable ways to use energy. According to the World Bank, worldwide energy usage more than doubled between 1971 and 2008 [42] as illustrated in Figure 1.1. The rising energy usage creates two concerns: first, the world has a finite supply of fossil fuels to meet the demand for energy, and second, there are adverse environmental impacts from burning fossil fuels. One notable environmental trend is the rise in carbon dioxide (CO_2) emissions over the same span [41], illustrated in Figure 1.2. The adverse impacts of rising CO_2 emissions are best mitigated by reducing those emissions.

The transportation sector provides an excellent opportunity for reducing carbon dioxide emissions. The sector accounted for 28% of all energy used in the United States in 2010, and, as Figure 1.3 depicts, 94% of the energy used for transportation came from petroleum-based sources [45]. In the developing world, the growth in demand for transportation can be seen clearly when comparing the number of automobiles per capita between nations. China perhaps best exemplifies this trend: from 2003 to 2008, the number of passenger cars per person grew by a factor of 2.7 [43], shown in Figure 1.4. Thus, technologies that use petroleum-based resources more efficiently have the potential to reduce greenhouse gas emissions.

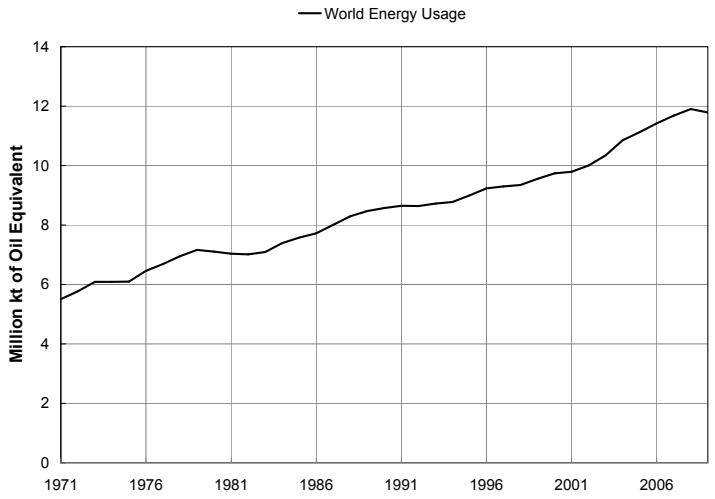

Figure 1.1: World energy usage from 1971-2008 [42]

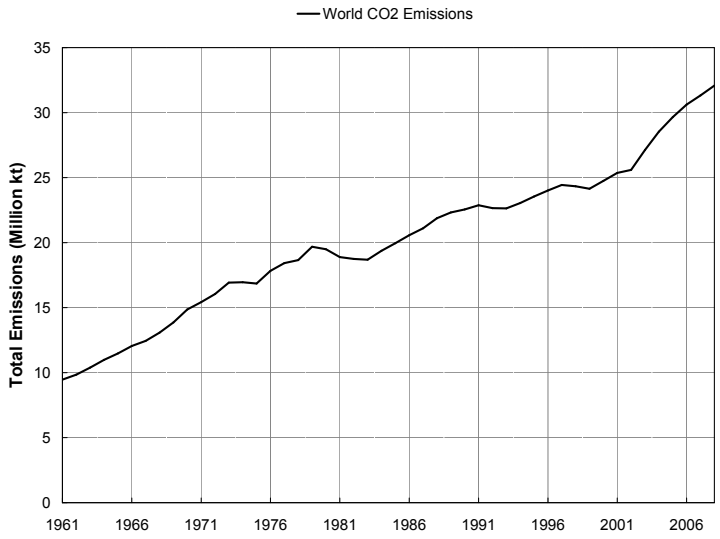

Figure 1.2: World carbon dioxide emissions from 1961-2008 [41]

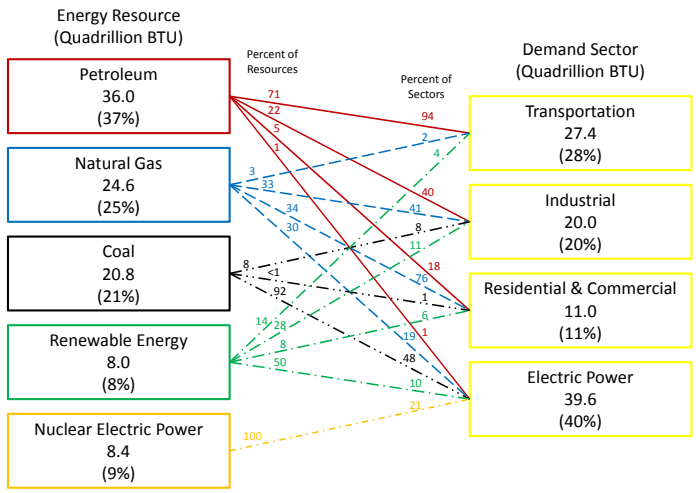

Figure 1.3: Primary U.S. energy flows for 2010 [45]

Batteries, fuel cells, hybrids, and advanced internal combustion (IC) engine strategies all exhibit promising technologies for reducing greenhouse gas emissions in the transportation sector and making it more sustainable. Batteries and fuel cells pose great opportunities for reducing the environmental impacts of automobiles in the long term, but they currently do not offer the energy density [6], the cost-effectiveness, or, in the case of batteries, the recharge times that IC engines and liquid fuels offer. Homogeneous Charge Compression Ignition (HCCI) engines provide one technology with the promise to reduce CO_2 emissions while still maintaining the convenience of current automobiles.

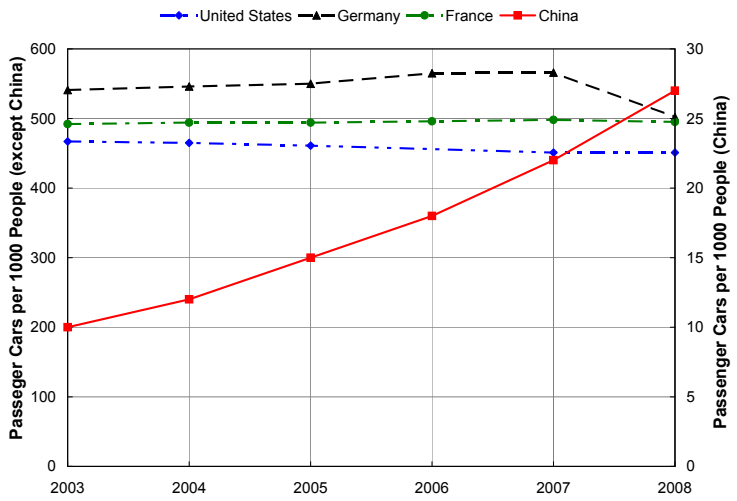

Figure 1.4: Passenger cars per 1000 people for China, USA, Germany, and France from 2003-2008

[43]

1.2 Homogeneous Charge Compression Ignition Description

Homogeneous Charge Compression Ignition (HCCI) presents a promising technology for internal combustion engines that reduces oxides of nitrogen (NO_x) emissions relative to current on-road engine technologies [27, 44, 7]. HCCI combustion also delivers better efficiency and therefore fewer CO_2 emissions than spark-ignited (SI) engines, and it emits less particulate matter than diesel engines [7].

HCCI combustion accomplishes these improvements largely due to the way in which combustion begins in each engine cycle. In a conventional SI cycle, fuel and air enter the cylinder and mix homogeneously during the intake stroke. During the compression stroke, the piston compresses that mixture and prepares it for combustion. Near the end of the compression stroke, a spark plug ignites the mixture, initiating a flame that passes through the charge, burning the reactants. This flame has a drawback: it produces local temperatures which are very high and results in the production of oxides of nitrogen (NO_x).

In a conventional diesel engine, only air enters the cylinder during the intake stroke. During the compression stroke, the piston compresses the air, similar to during the SI cycle. Near the end of the compression stroke, an injector sprays fuel into the cylinder; the fuel burns as it diffuses into the cylinder. However, it is not well-mixed with the air, so the resulting combustion produces particulate matter. Additionally, the local temperatures are again high enough to produce NO_x.

In an HCCI engine, fuel and air enter the cylinder during the intake stroke and mix, as in an SI engine. Then, the piston compresses the charge during the compression stroke. However, unlike in an SI engine, the mixture autoignites once the piston transfers sufficient energy into the mixture. The autoignition results in a bulk combustion event that occurs throughout the cylinder at temperatures cold enough to prevent NO_x from forming.

One major difference exists between the homogeneous charge in an SI engine and the homogeneous charge in a gasoline-burning HCCI engine. Gasoline and air do not autoignite at moderate compression ratios; thus, in an HCCI engine, additional

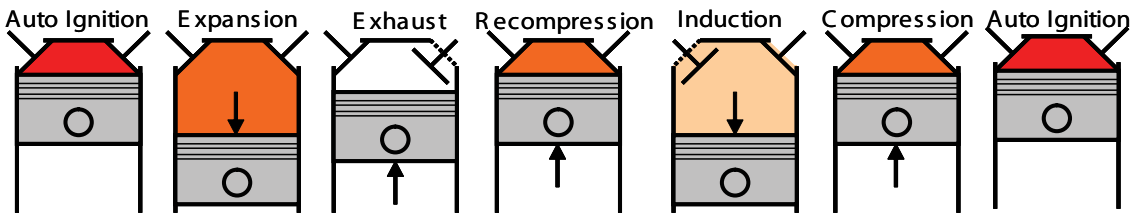

Figure 1.5: Depiction of the different stages of a recompression HCCI engine cycle

energy needs to be added to the homogeneous charge prior to compression so that the mixture ignites when desired. Different actuation strategies can provide this energy and are discussed further in Section 1.3. An exhaust recompression strategy supplies the energy needed to initiate combustion in all of the experimental results presented in this dissertation.

Figure 1.5 depicts one recompression HCCI engine cycle. The figure shows the six steps in the cycle: autoignition, expansion, exhaust, recompression, induction, and compression. First, the image depicts an autoignition event followed by expansion, where the charge does work on the piston. An exhaust event, in which some of the exhaust leaves the cylinder, follows the expansion event. During the exhaust stroke, the exhaust valve closes well before top dead center and retains some of the hot residual exhaust in the cylinder to provide energy for the next engine cycle. The piston recompresses the retained residual in the cylinder, and then travels downward during the intake stroke. The intake valve opens, allowing fresh air into the cylinder. Although it is not shown, fuel is also injected directly into the cylinder during the intake stroke. Finally, the intake valve closes and the piston compresses the mixture and autoignition occurs.

1.3 Background on HCCI

HCCI engines are not without their drawbacks. One major difficulty in operating HCCI engines is controlling the timing at which the mixture autoignites. In reinduction HCCI, where exhaust gases from the exhaust manifold are brought back into

the cylinder to promote autoignition, and recompression HCCI, the mass of exhaust present in the cylinder on each engine cycle must be carefully controlled to ensure that combustion occurs when desired on the subsequent engine cycle. Furthermore, retaining high amounts of exhaust on each engine cycle leads to cycle-to-cycle coupling that occurs because a large fraction of the matter in the cylinder on any given engine cycle remains in the cylinder on the following cycle [32, 36, 37]. The cyclic coupling in recompression HCCI is much greater than in SI or diesel engines, because those strategies do not rely upon significant fractions of retained exhaust from the previous cycle to initiate combustion.

The need to retain exhaust from the previous engine cycle to initiate combustion limits the load range in which recompression HCCI engines operate [39]. This exhaust limits the amount of fresh charge that can be burned in the cylinder significantly below what a comparably sized SI or diesel cylinder would burn.

Expanding HCCI's upper load operating capability would make it a more viable technology. One method that can be used to increase the high-load capabilities of HCCI engines is to phase combustion at later angles [49], which can be achieved in recompression HCCI by retarding the exhaust valve closing angle and retaining less exhaust in the cylinder, delaying the angle at which combustion begins. However, Wagner et al. [46] and Shahbakhti and Koch [35] found there is a significant increase in cyclic variation in indicated mean effective pressure, IMEP, and the start of combustion angle, θ_{SOC}, as exhaust valve closing is retarded. The dynamics at late combustion phasing conditions driving these cycle-to-cycle oscillations need to be further understood in order to harness the potential of those conditions for load range expansion.

1.3.1 Actuation Strategies for HCCI Combustion Timing Control

One of the steps in dealing with the cycle-to-cycle dynamics of HCCI is determining what actuation strategies have the ability to improve them. Several different actuation strategies for controlling HCCI combustion timing—intake heating, variable

compression ratio, exhaust reinduction, exhaust recompression, multiple fuel, and multiple injection strategies—are discussed in this section, highlighting their various benefits and challenges.

Intake Heating

Intake heating, used by Najt and Foster [27], was one of the original methods used to achieve HCCI combustion. Martinez-Frias et al. [25] implemented a control system that relied upon a heat exchanger which preheats the intake air with exhaust. However, the actuator's bandwidth was too slow to be considered for cycle-to-cycle control.

Haraldsson et al. [11] developed one potential method for improving the bandwidth of intake heating. Their process, called Fast Thermal Management, mixed hot and cold air streams to control the inlet air temperature, and was able to affect combustion timing with an eight cycle time-constant, which is still too slow for cycle-to-cycle control. Widd et al. [47] implemented Fast Thermal Management along with variable valve actuation and a model predictive controller to control combustion phasing; these results showed promise for controlling combustion timing cycle-to-cycle, but they relied on the valve actuation system to achieve that ability.

Multiple Fuels

Multiple fuel strategies can control combustion timing in HCCI by changing the propensity of the fuel to autoignite. Olsson et al. [28] illustrated the use of a dual-fuel, turbocharged HCCI engine to achieve high load operating conditions. Bengtsson et al. [1] utilized a dual-fuel combustion timing control scheme in order to characterize different methods for calculating combustion timing. One disadvantage to a multiple fuel strategy is that it would require drivers to monitor two different fuel levels in their vehicles. Any vehicle using a dual fuel input would require a second fuel system, which would add cost to a vehicle. Another disadvantage to a dual fuel system is that an infrastructure for delivering the second fuel would need to be in place. Clearly these obstacles are solvable, but they depend upon customers to change their habits.

Variable Compression Ratio

Variable compression ratio (VCR) possesses tremendous potential as an actuator for controlling combustion timing in HCCI. VCR engines operate by changing the amount of compression achieved during the compression stroke. At increased compression ratios, the temperatures are higher during compression, and combustion timing advances. Christensen et al. [5] showed the usefulness of variable compression ratio as an input for HCCI combustion timing and its ability to work with a wide variety of fuels on a single cylinder engine. Haraldsson et al. [10] and Hyvönen et al. [13] both demonstrated the effectiveness of using variable compression ratio as an input to control combustion timing on a multi-cylinder Saab Variable Compression (SVC) engine. However, one major disadvantage to the variable compression ratio input on the Saab engine is that the compression ratio of each cylinder changes simultaneously, making that implementation of VCR difficult to use as a cylinder-individual cycle-to-cycle control input. Other variable compression ratio technologies [4] could potentially work well for cylinder-individual, cycle-to-cycle control of HCCI, but they have yet to be tested with any HCCI combustion to date.

Exhaust Reinduction

Exhaust reinduction HCCI operates by inducting exhaust from the previous engine cycle back into the cylinder during the intake stroke along with fresh air. Caton et al. [3] showed the viability of reinduction HCCI and illustrated its ability to work as an effective method for controlling combustion phasing.

One of the major advantages of using reinducted exhaust for HCCI is the amount of sensible energy available in the exhaust that can be used as the thermal energy source needed to initiate combustion in HCCI. Shaver et al. [37] developed a physics-based model of a single-cylinder reinduction HCCI engine for control. However, one of the major challenges with reinduction HCCI is the cylinder-to-cylinder coupling, which occurs when exhaust from different cylinders mixes in the exhaust manifold and is then reinducted into the cylinders. This mixing couples the contents from one cylinder to the contents of the other cylinders. Kulkarni et al. [21] developed a model

and control strategies to handle the cylinder-to-cylinder coupling issues associated with exhaust reinduction HCCI, but exhaust recompression HCCI avoids these issues altogether.

Exhaust Recompression

Exhaust recompression HCCI, outlined in Section 1.2, also utilizes the sensible energy present in exhaust to help initiate combustion on the following engine cycle. However, instead of expelling the exhaust from the cylinder only to reaspirate it, the desired quantity of exhaust remains in the cylinder and is compressed and expanded prior to the intake valve opening. Kang and Druzhinina [18] demonstrated a control algorithm for an engine running exhaust recompression HCCI that used external exhaust gas recirculation (EGR), and Ravi et al. [32] developed a model for cycle-to-cycle control of a multi-cylinder recompression HCCI engine.

Multiple Injections

Song and Edwards [38] illustrated the effectiveness of using pilot injection to affect combustion timing in recompression HCCI. The pilot injections induce recompression reactions during the recompression portion of the cycle, when the elevated in-cylinder pressures and temperatures during recompression allow fuel to react with oxygen remaining in the cylinder after main combustion. Their experimental results showed that using a small pilot injection with controlled phasing resulted in a wider range of combustion timings than the range of combustion timings achieved by changing the ratio between the fuel in the pilot injection and the amount of fuel in the main injection.

Ravi et al. [33] utilized pilot injection timing to control combustion phasing on a multi-cylinder engine. Their experimental results highlighted that pilot injection timing control is a suitable high-bandwidth control input capable of making cycle-to-cycle changes in combustion timing.

1.3.2 Understanding Cyclic Variations in HCCI

In their attempts to model the cycle-to-cycle variations in HCCI, researchers have developed both empirically-identified and physically based models of the HCCI combustion process. Ghazimirsaied et al. [9] generated an auto-regressive, time-series model of combustion timing that incorporated conditions with significant cycle-to-cycle variations. Their model predicted combustion timing from one engine cycle to the next, but did not provide much physical insight into the source of the fluctuations in combustion timing.

Thinking about the different energy storage mechanisms in the cylinder provides a physical, intuitive way to think about the cyclic variations in HCCI. The two ways energy is stored in the cylinder are as chemical potential energy, in the bonds of fuel and oxygen, and as sensible energy, in the temperature of the charge. The different physical modeling approaches to investigating these cyclic variations and reducing them with control have relied upon either the chemical link between cycles, the thermal link between cycles, or both.

Kang et al. [19],[17] and Liao et al. [24] both captured the characteristics of highly oscillatory HCCI conditions through a thermal mechanism in models that assumed complete combustion of the fuel in the cylinder. Kang [17] graphically illustrated the oscillatory dynamics at certain HCCI operating conditions by manipulating the inputs air-fuel ratio, intake temperature, fueling rate, and external EGR. Their model showed that as either air-fuel ratio increased, or intake temperature decreased, or fueling rate decreased, or external EGR decreased while holding all of the other inputs constant, the dynamics of temperature at intake valve closing became oscillatory.

Liao et al. [24] used a physically-based, switching linear model to parse HCCI operating conditions into three regions; the three regions were based on the dynamics observed at different operating conditions. That model contained two states, temperature and oxygen concentration, and the model observed that the in-cylinder temperature dynamics changed as a function of combustion timing throughout the HCCI operating range. That model formed the basis for an explicit model predictive controller that altered exhaust valve closing timing in order to improve the dynamics

at highly oscillatory operating conditions. [48] The key aspect of both of these thermal models is that they predict combustion timing entirely from physical principles and not from empirically-derived models, making them very transparent.

Hellström and Stefanopoulou [12] captured the oscillatory dynamics of HCCI by modeling the amount of unburned fuel remaining in the cylinder after combustion. The modeling approach incorporates an empirically-derived fit between combustion timing and combustion efficiency during the main combustion event [26], and is consistent with the primary explanation for oscillations identified by Koopmans et al. [20]. However, the opacity of the combustion efficiency function is a significant drawback to this particular modeling approach because it makes no attempt to explain the physical reasons behind the change in combustion efficiency as a function of combustion timing. It is reasonable to expect that the physical link between combustion timing and combustion efficiency relies at least somewhat on the thermal characteristics inside the cylinder: the combustion timing and the volume at combustion are linked through the geometric properties of the cylinder, and the volume at combustion and the in-cylinder temperature at the start of combustion are inversely proportional to one another. Thus, the black-box nature of these models ignores the likely role that thermal dynamics play in inducing cyclic variations in HCCI.

Shahbakhti and Koch [36] developed a physical model for predicting HCCI combustion timing using both chemical and thermal mechanisms for linking cycles after testing more than 400 steady-state operating conditions on two different engines [35]. However, they did not publish a detailed investigation of how their model predicts combustion timing at operating conditions with high cyclic variability, so they do not discuss the relative contributions of thermal dynamics and chemical dynamics in driving cyclic variations in HCCI.

The models in this dissertation rely upon the thermal coupling from one engine cycle to the next to explain the oscillations that occur at certain HCCI operating conditions. The transparency afforded by the physical relationships provides insight into the oscillations and how to manipulate exhaust valve timing, pilot injection timing, and fuel quantity so as to reduce the oscillations.

1.4 Dissertation Contributions

This dissertation makes three contributions in order to make HCCI a more viable technology.

1. Root locus analysis describes the control challenges associated with using three different inputs to control HCCI combustion timing

    - Linearizing a physical, nonlinear, discrete-time model of an HCCI engine cycle yields three separate single-input, single-output systems, each corresponding to a physical input to the system, that are each analyzed on root loci.
    - The physical basis for the model allows for strong intuition about why the dynamics at any given operating condition behave as they do, especially regarding conditions with high levels of cyclic variability.
    - The classical control framework provides a clear description of how the dynamics at different operating conditions change from one condition to another, and it makes simple control development straightforward.

2. Control algorithms based upon the root locus analysis demonstrate the ability to improve the dynamics at HCCI operating conditions.

    - Three different inputs control combustion timing: exhaust valve timing, pilot fuel injection timing, and main fuel injection mass. The exhaust valve timing input relies on a proportional controller to affect combustion timing, while the pilot fuel injection timing and main fuel injection mass strategies rely upon lag compensators to affect combustion timing.
    - The simple control algorithms presented in this dissertation could be easily implemented on any embedded processor that would run an HCCI engine in a production vehicle.
    - Direct fuel injection systems like the one that produced the pilot fuel injection timing results and the main fuel injection mass results are available

on production vehicles, meaning that the results could be adapted to work on a relatively short time scale.

3. A flexible, multi-cylinder engine designed specifically for cycle-to-cycle HCCI control provides an excellent testbed for developing models and controllers that can improve HCCI.

   - The engine features a multi-cylinder variable valve actuation system, which allows for each pair of intake valves and exhaust valves on each cylinder to be opened independently of the intake valves and exhaust valves on the other cylinders and the engine crank position.
   - The direct-injection gasoline system provides a production grade actuator for controlling HCCI combustion. Similarly, in-cylinder pressure sensors and wide-band oxygen sensors on each cylinder provide information critical for controlling HCCI combustion on a cycle-to-cycle basis.

1.5 Dissertation Outline

This dissertation is structured into six chapters, and the five remaining ones are outlined as follows.

Chapter 2 describes the multi-cylinder HCCI engine. It highlights the actuators and sensors that make the engine well-suited for performing cycle-to-cycle control experiments. The chapter then provides background on the base engine design, and it provides information on the entire suite of actuators and sensors with which the engine is equipped that enable model calibration and experimental validation of control algorithms.

Chapter 3 covers the single-zone, four-state, nonlinear combustion model developed by Ravi et al. [32]. The model forms the basis from which the control approaches presented in the subsequent chapters are designed. The chapter then illustrates how the model is able to capture oscillatory operating conditions, and it concludes by comparing the three proposed actuators on the basis of how easily each actuator is

physically implemented against how easily the control problem associated with each actuator is solved.

Chapter 4 studies the control problem of reducing combustion instability using exhaust valve closing timing as the control input. The chapter presents a linearized version of the nonlinear model utilizing the EVC input, and illustrates that with the EVC input, the oscillations in certain HCCI operating conditions can be represented as a negative real-axis pole where one engine cycle is modeled as a discrete-time system. Then the chapter considers the logistical challenges of implementing such a controller in a passenger car. Finally the chapter presents a control design and exhibits how that controller decreases oscillations in combustion timing in both simulation on the nonlinear model and experimentally on the engine.

Chapter 5 compares the pilot injection timing and main injection mass methods for reducing combustion instability to each other and to the EVC timing input. The chapter is similar in structure to Chapter 4 in that it presents the linearization, control design, simulation validation, and experimental validation of the controllers for both the pilot injection timing input and the main injection fuel mass input. It then concludes with a brief discussion of the merits and drawbacks of each of the three inputs: exhaust valve closing timing, pilot fuel injection timing, and main fuel injection mass for reducing combustion instability in HCCI.

Finally, Chapter 6 provides some conclusions about the research and gives direction for potential future study.

Chapter 2

Stanford Multi-cylinder HCCI Engine

The Stanford multi-cylinder engine is a four cylinder, General Motors ECOTEC engine outfitted to run homogeneous charge compression ignition combustion. This chapter covers three topics regarding the engine's design. First, it describes the engine's actuator and sensor suite that is designed specifically for cycle-to-cycle HCCI control. Second, it discusses the engine's internal cylinder geometry and provides details about that geometry which are important for interpreting control results. Finally, it summarizes the remaining actuators and sensors on the engine that are essential for its operation and for modeling its characteristics.

2.1 Engine Overview

The engine, pictured in Figure 2.1, features an electro-hydraulic variable valve actuator (VVA) system that allows for the actuation of the intake and exhaust valves of each cylinder without the use of a mechanical cam. The valves in one cylinder can be opened and closed independently of crank position or valve events occurring in other cylinders. Additionally, the VVA system provides an actuator that can create drastically different valve profiles on subsequent engine cycles by permitting changes in valve duration and lift from one engine cycle to the next. Thus, the VVA is a

powerful control knob for cycle-to-cycle HCCI engine operation.

Each cylinder houses its own direct fuel injector. The direct fuel injection system enables fuel to be delivered to each cylinder more flexibly than an intake-based fuel system by allowing for multiple fuel injections per engine cycle, a technique critical to some of the results in this thesis that simply cannot be obtained with a port fuel injection system. Thus, the direct injection system provides a second, powerful control knob for cycle-to-cycle HCCI engine operation.

All four cylinders are equipped with in-cylinder pressure sensors, which allow for measuring cylinder pressure throughout the engine cycle and then calculating combustion phasing based on the cylinder pressure measurements. The cylinder pressure sensor provides the source of cycle-to-cycle information used by the control algorithms in this thesis and is the primary high-bandwidth sensor the engine features.

Finally, each exhaust port has a wide-band oxygen sensor that measures the composition of the exhaust leaving the cylinder at a high bandwidth. Although the cylinder-individual oxygen sensors are not used in this work, the engine has the capability to provide cycle-to-cycle information about the post-combustion composition of gases in the cylinder.

2.2 Engine Block and Cylinder Head Design

General Motors Corporation furnished the engine block for the Stanford Multi-cylinder HCCI engine. It is a Mule 1 HCCI test engine from GM's research facility in Warren, MI, with a 2.2 liter displacement and a 12:1 geometric compression ratio. Table 2.1 lists several important geometric parameters of the cylinders in the engine.

Figure 2.2 illustrates a schematic of one cylinder of the engine. The illustration shows fuel being injected into the cylinder while the piston is at bottom dead center. (Figure 2.3 shows the geometry of the piston crown.) The injector features a 60° spray pattern into the cylinder, which is important for determining when fuel injections could possibly come into contact with the piston crown or cylinder walls and negatively impact engine emissions. The cylinder geometry and the injector spray

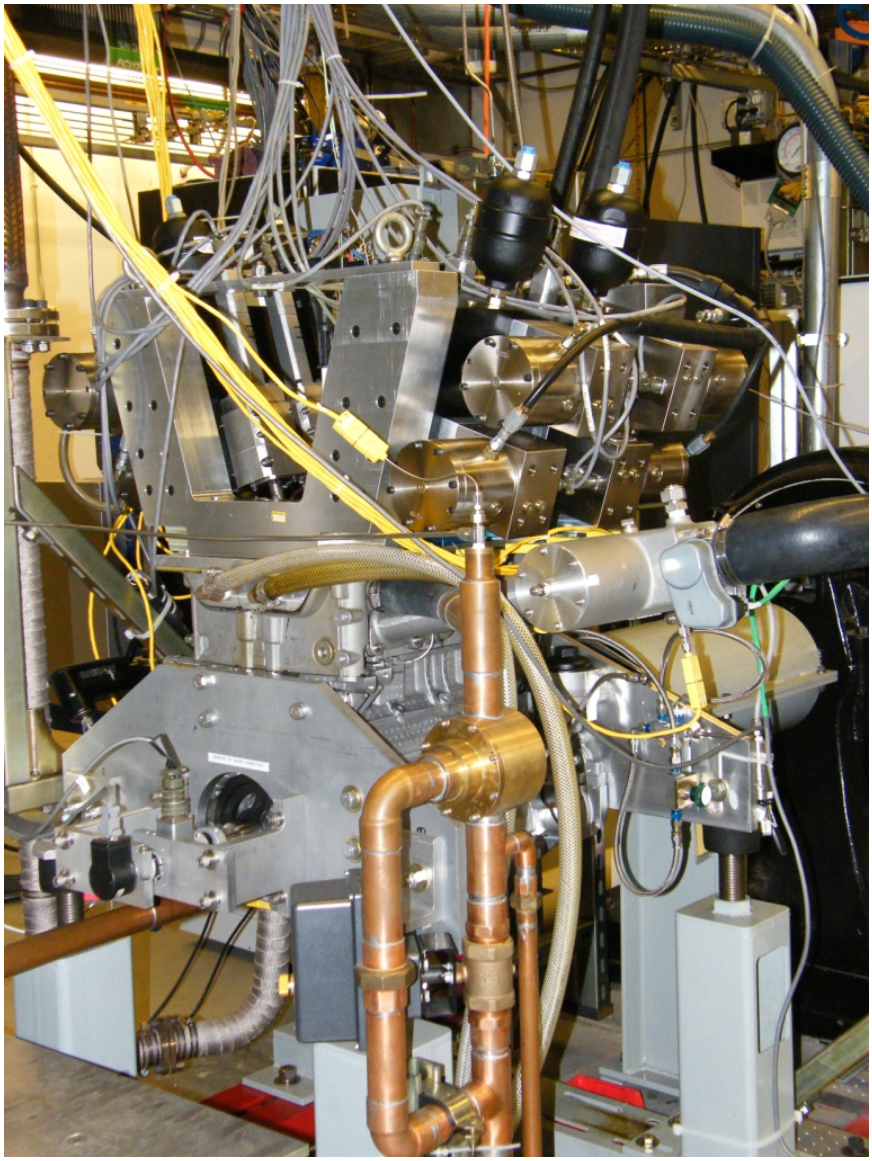

Figure 2.1: Stanford Multi-cylinder HCCI Engine

Table 2.1: Engine geometric and fuel system characteristics

Parameter	Value
Bore	86 mm
Stroke	94.6 mm
Compression Ratio	12:1
Valve Angle	18°
Injector Spray Angle	60°
Number of Holes on Injector	8
Injector Hole Diameter	0.370 mm
Fuel Injection Pressure	12.4 MPa

angle indicate that fuel would contact the cylinder walls after the piston travels approximately 61.3 mm of its stroke from top to bottom dead center. Figure 2.4 shows the piston position during the intake stroke as a function of the engine crank angle. The figure also calls out the piston height at which gasoline would impinge upon the cylinder wall, h_{imp}.

Figure 2.5 depicts the valve profile used for both the intake and exhaust valves. In both cases, the valve profile has a maximum lift of 4 mm and a duration of 120 CAD. The duration of 120 CAD allows the engine to close its exhaust valves early and open its intake valves late while still maintaining typical exhaust valve opening and intake valve closing timings. The early exhaust valve closing and late intake valve opening allow the exhaust recompression event to occur. The 4 mm maximum valve lift has two key features. First, it allows for mechanical stops to be set on the valve actuator system mentioned in 2.3.1 that prevent a valve-piston interference. Second, due to the relatively slow engine speeds at which the engine is designed to run (< 2500 RPM), the 4 mm lift is still sufficient to allow for the cylinder contents to exit the cylinder and fresh charge to enter the cylinder.

2.3 Engine Actuators

The Stanford Multi-Cylinder HCCI engine features two groups of actuators. The first group of actuators is used for controlling HCCI in each cylinder on a cycle-to-cycle

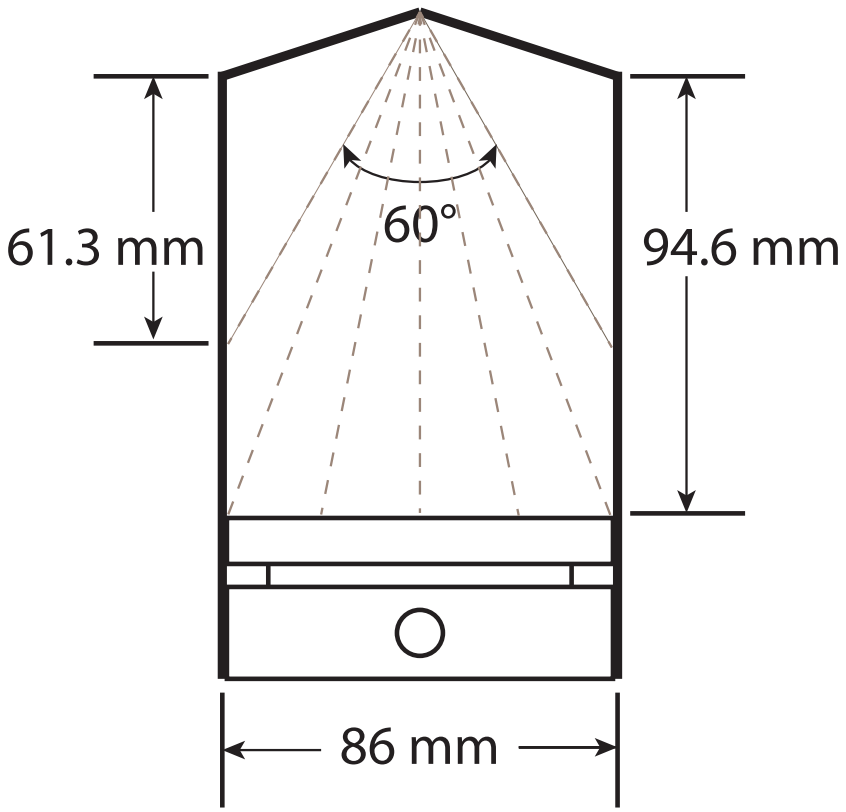

Figure 2.2: Cylinder with piston at bottom dead center illustrating fuel spray

Figure 2.3: Piston crown in Stanford multi-cylinder HCCI engine

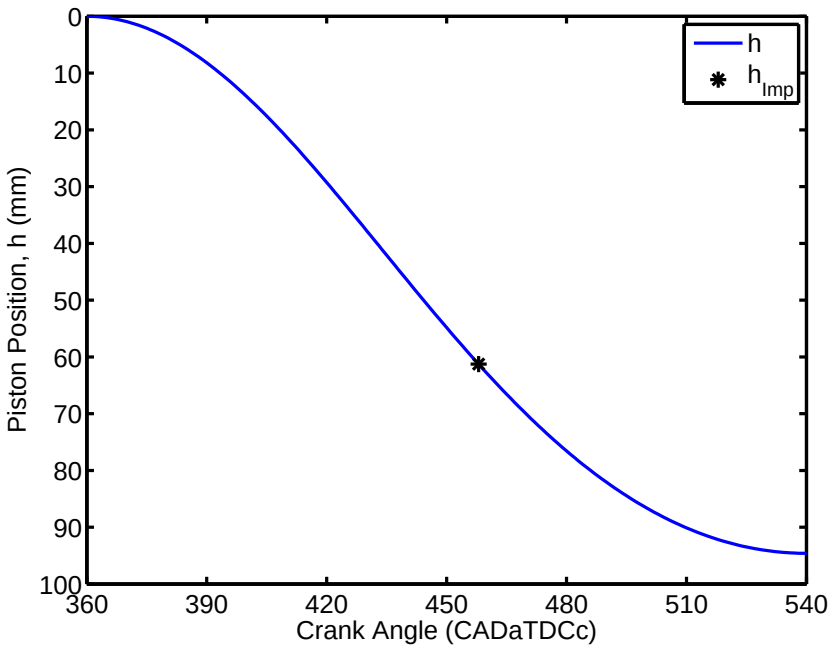

Figure 2.4: Piston position during intake stroke

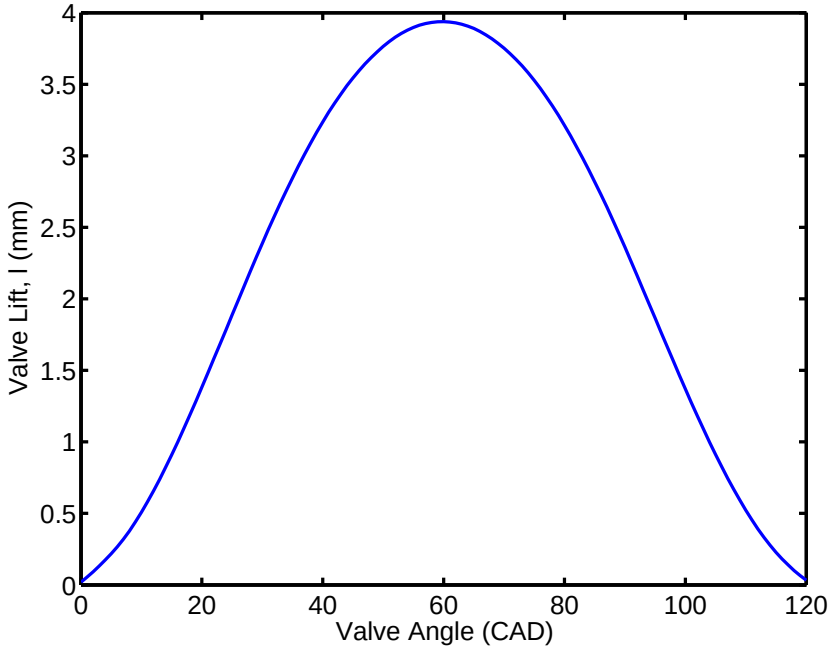

Figure 2.5: Valve lift versus valve duration

basis and consists of the VVA system and the fuel injection system. The second group of actuators is critical for engine function, but is not used for controlling HCCI on a cycle-to-cycle basis. The second group consists of the ignition system, the intake throttle, and the coolant temperature control system.

2.3.1 Actuators for Cycle-to-Cycle Control

Variable Valve Actuation System

The variable valve actuation system opens and closes the intake and exhaust valves on each cylinder instead of a mechanical cam and lifter system. Each cylinder has one pair of intake valves and one pair of exhaust valves; eight separate actuator systems control the position of the full valvetrain: one system for each pair of valves.

In each system, an amplifier sends a signal to a voice coil that moves a spool valve back and forth. The spool valve directs hydraulic oil supplied by an external pump onto either side of a piston connected to a rod that drives the intake or exhaust valves. A linear variable differential transformer (LVDT) measures the position of the piston and gives feedback to a control algorithm [22, 23] that controls the valve lift. Figure 2.6 shows a diagram of one of the VVA system for one pair of valves, and Figure 2.7 shows a picture of the entire system.

The valve system provides significantly greater flexibility than mechanical cams in two key ways. First, it allows each cylinder to have different valve timings than the other cylinders. Second, it enables changes in valve profile and timing to happen from one cycle to the next with fewer constraints than production variable valve lift and variable valve timing systems.

Fuel Injection System

A Bosch HDEV 1.2 common rail fuel injection system supplies gasoline directly to each cylinder of the multi-cylinder engine. The direct injection system enables multiple fuel injections per engine cycle, which would not be possible with a port fuel injection system. Additionally, the direct fuel injection system eliminates the fuel

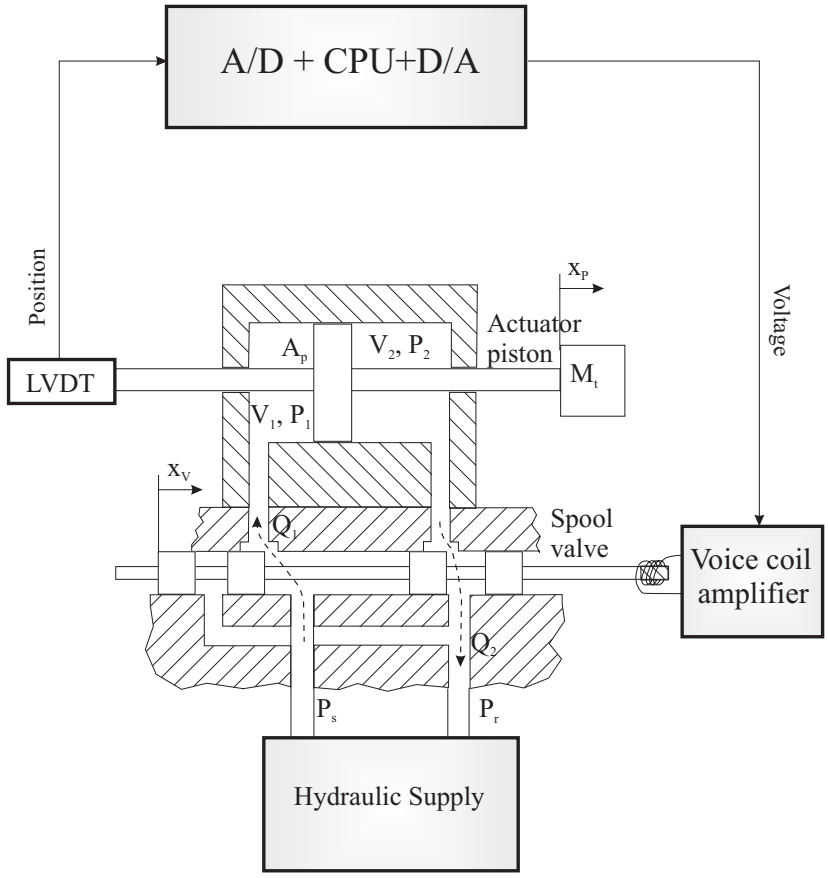

Figure 2.6: Schematic illustrating VVA system for one pair of valves

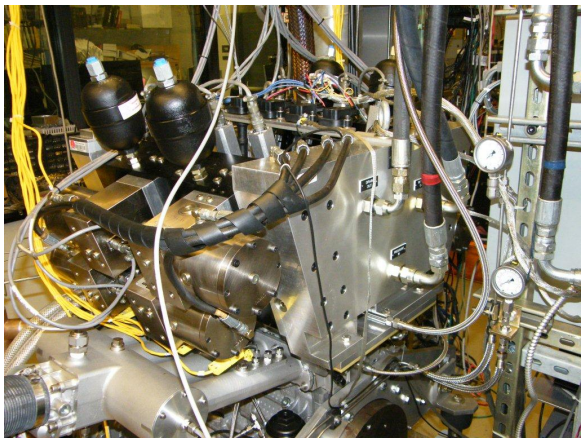

Figure 2.7: Picture of the valve system

mass transport delay arising from injecting fuel into the intake manifold with port fuel injection systems. [40]

The amount of fuel that can be injected in any given injection event is either 1 mg or 6 mg and more. Figure 2.8 illustrates the calibrations for the four injectors over the full range desired injection quantities, and Figures 2.10, 2.11, 2.12, and 2.13 illustrate the calibration for each individual injector along with the 90% confidence interval for each calibration. The fuel injectors feature a nonlinearity between the commanded pulse width and the resulting fuel mass injected for commanded fuel quantities between approximately 2 mg and 6 mg, illustrated in detail in Figure 2.9. Additionally, the injectors suffer repeatability issues for commands in that range, meaning that the nonlinearity for each injector cannot simply be inverted in order to obtain the proper injector command.

2.3.2 Additional Engine Actuators

Ignition System

A Bosch ignition system provides spark to each cylinder. The ignition system is critical for SI operation, and SI operation at startup supplies the hot exhaust necessary to transition to HCCI operating mode.

Intake Throttle

A production GM throttle body from a 2006 Chevrolet Cobalt controls the intake manifold pressure for the multi-cylinder engine. Throttling the intake manifold pressure results in smoother performance in both SI and HCCI combustion modes. In HCCI combustion mode, the intake manifold pressure is held at 97.5 kPaa. Throttling the intake during HCCI operation provides two benefits: it reduces pulsations in the intake system, and it reduces the audible noise produced by the engine. The main drawback to throttling during HCCI operation is that throttling introduces a loss of efficiency. A PI control algorithm adjusts the throttle valve position based on feedback from the throttle position sensor integrated into the throttle assembly. Figure 2.14 illustrates the intake throttle mounted to the intake manifold of the engine.

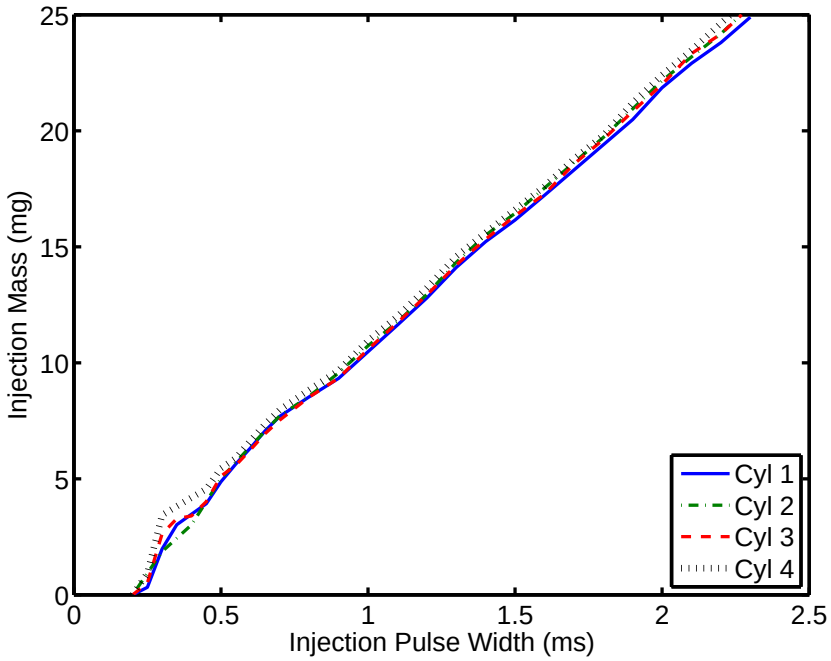

Figure 2.8: Fuel injector calibration curves

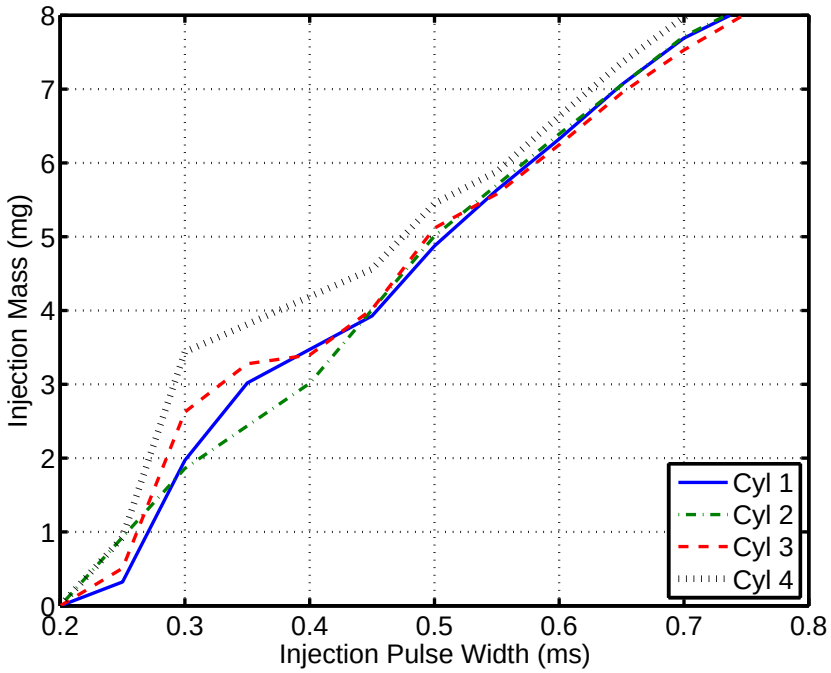

Figure 2.9: Zoomed view of fuel injector calibration curves

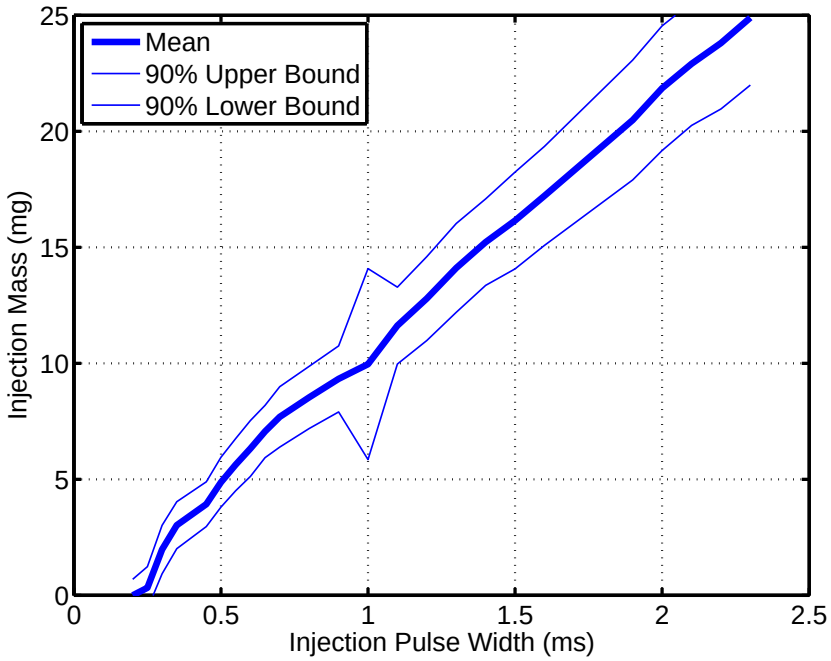

Figure 2.10: Fuel injector calibration curve for cylinder 1 showing 90% confidence interval

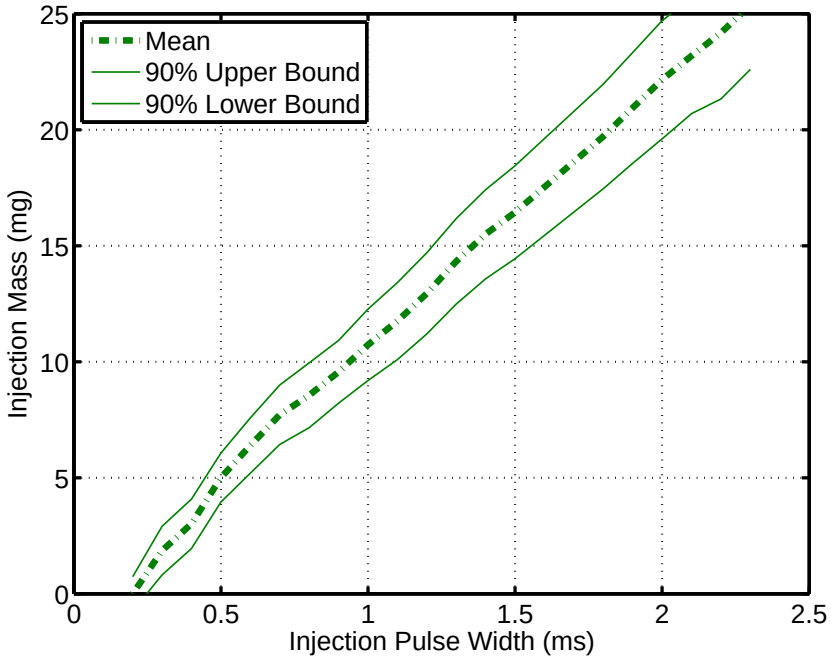

Figure 2.11: Fuel injector calibration curve for cylinder 2 showing 90% confidence interval

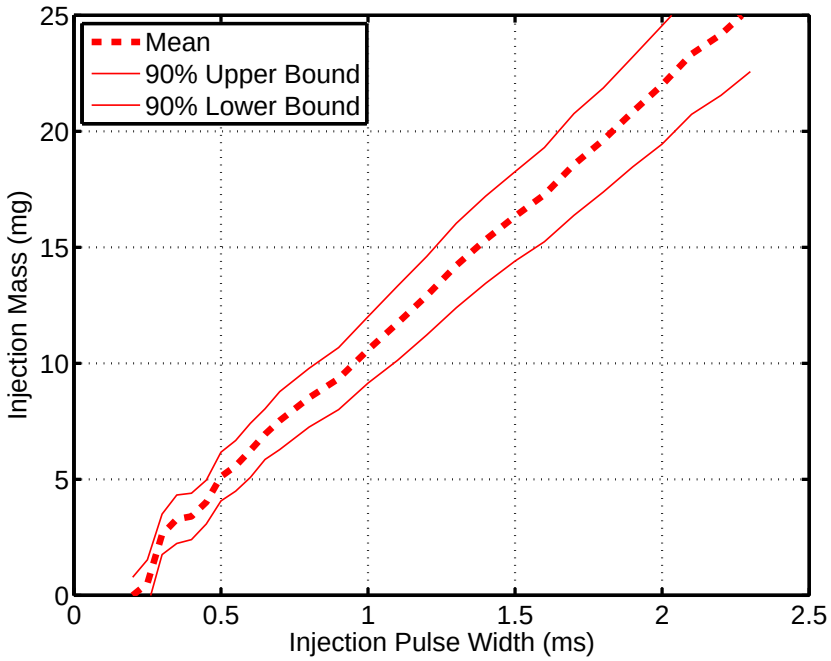

Figure 2.12: Fuel injector calibration curve for cylinder 3 showing 90% confidence interval

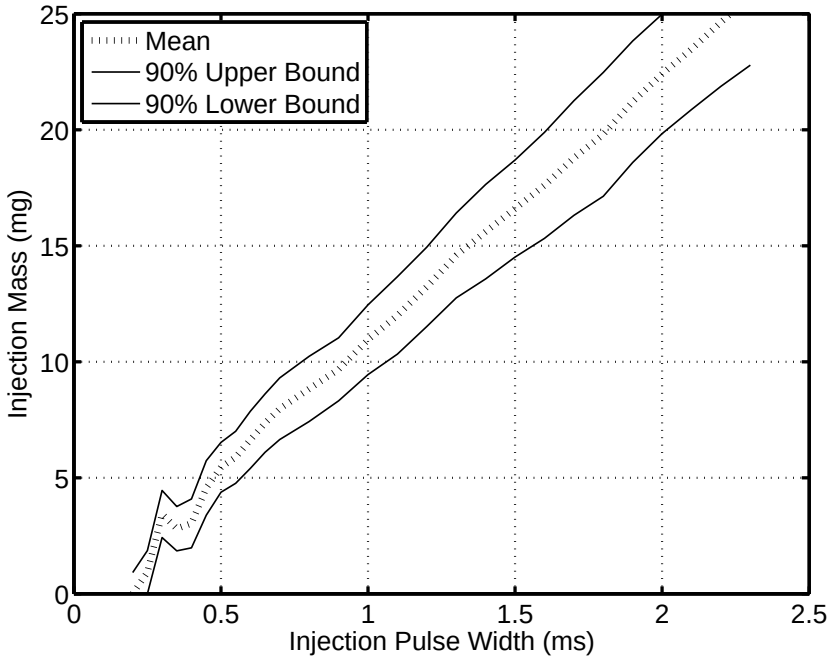

Figure 2.13: Fuel injector calibration curve for cylinder 4 showing 90% confidence interval

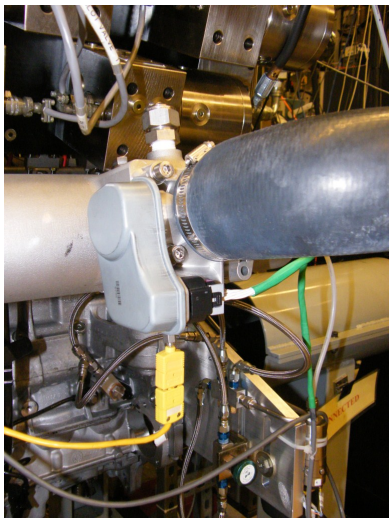

Figure 2.14: Picture of the intake throttle and intake manifold

Engine Coolant Temperature Control Valve and System

The engine coolant control system, shown in Figure 2.15, regulates the engine inlet coolant temperature to a user-defined value that can be changed while the engine operates. The cooling system operates by adjusting the mixture of hot and cold engine coolant entering a large tank. A butterfly valve, driven by a DC motor, controls the flow of engine coolant through a water-to-water heat exchanger that allows energy to be transferred from the engine coolant to the building's process cooling water system. Hot coolant bypasses the heat exchanger in a pipe smaller in diameter than the pipe through the heat exchanger, meaning the coolant valve has sufficient actuator authority to cool the engine if necessary. The two streams join together downstream of the heat exchanger and mix prior to entering the tank.

A bang-bang controller adjusts the butterfly valve position based on the sign of the difference between the measured tank inlet temperature and the desired engine coolant temperature. If the mixture is too hot, the controller opens the butterfly valve slightly, while if the mixture is too cold, the controller closes the valve slightly.

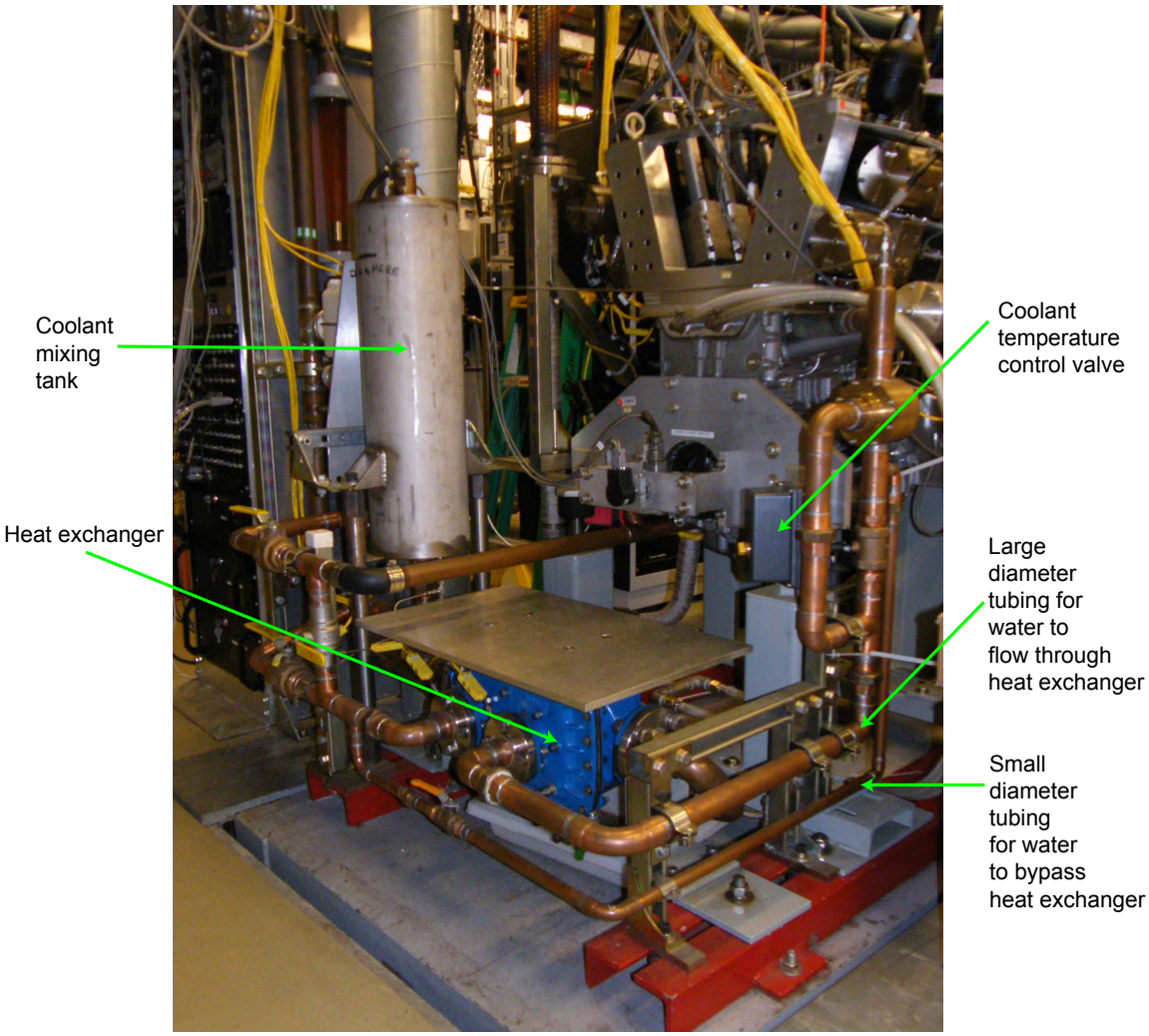

Figure 2.15: Picture of the engine cooling system

The tank's natural dynamics act as a low-pass filter and smooth out the temperature fluctuations in the tank inlet stream, providing coolant at a specified temperature to the engine. This cooling system provides an extra degree of freedom for testing HCCI conditions relative to conventional thermostat-controlled cooling systems because it allows for user-specified coolant temperatures as opposed to a single coolant temperature determined by hardware design.

2.4 Engine Sensors

Similar to the two groups of actuators, the Stanford Multi-Cylinder HCCI engine features two sets of sensors. The first set of sensors provides data for controlling HCCI in each cylinder on a cycle-to-cycle basis, and it consists of the in-cylinder pressure sensors, the exhaust-port-mounted, wide-band oxygen sensors and the engine crank encoder. The second set of sensors is critical for engine function, but is not used for controlling HCCI on a cycle-to-cycle basis. The engine's exhaust-manifold-mounted oxygen sensor, static pressure sensors, flow meters, and thermocouples comprise the second set of sensors.

2.4.1 Sensors for Cycle-to-Cycle Control

In-cylinder Pressure Sensors

A Kistler 6125B piezo-electric pressure transducer produces cylinder pressure data in each cylinder of the HCCI engine. A modified Rassweiler–Withrow algorithm [29] converts the pressure data into combustion timing data, and integrating the pressure signal with respect to engine volume yields the work being done by the cylinder. The combustion timing data is the sole source of information used by the controllers presented in Chapters 4 and 5.

Exhaust Runner Oxygen Sensors

Each of the four exhaust runners on the Stanford multi-cylinder HCCI engine holds a Bosch LSU 4.9 wide-band oxygen sensor. The sensors provide information about

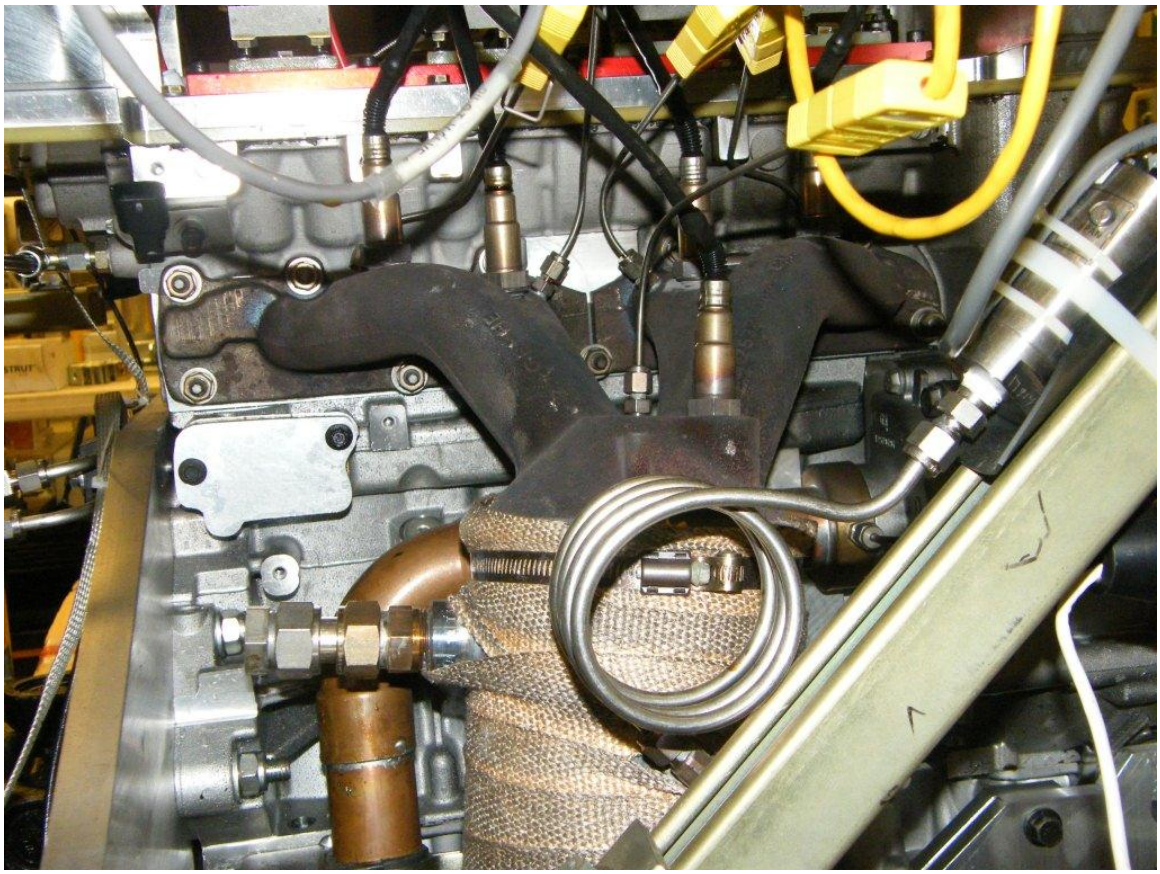

Figure 2.16: Picture of the exhaust manifold showing all oxygen sensors.

the oxygen content of the exhaust stream flowing through the runner past the sensor, and each sensor can be used in control schemes to provide feedback for improving the estimated amount of oxygen in the cylinder during recompression [30]. Additionally, the sensors can be used to control the air-fuel ratio in each cylinder, which is beneficial for controlling engine emissions. Figure 2.16 depicts the exhaust manifold and illustrates the oxygen sensors in each exhaust runner.

Encoders

Two encoders affixed to the crankshaft on the front of the multi-cylinder engine measure the crankshaft's position. The encoders measure 4096 counts per revolution and

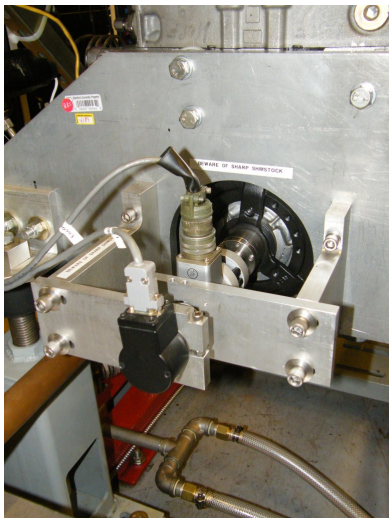

Figure 2.17: Picture of encoders mounted to the engine

send full quadrature signals, consisting of two signals, A and B, their complements, $\tilde{A}$ and $\tilde{B}$, and an index pulse and its complement, Z and $\tilde{Z}$, to each of the three target computers running the engine described in Section 2.5. Figure 2.17 depicts the encoders mounted to the engine.

The crank position data are critically important to the engine's operation because all of the cycle-to-cycle inputs rely on being timed properly to be effective. Thus, without knowledge of the engine position, the VVA system, the fuel injection system, and the ignition system would all be ineffective. Additionally, the encoder signal is used in conjunction with the in-cylinder pressure signals to calculate the combustion timing and work output signals, which are used for control of the engine.

2.4.2 Additional Engine Sensors

Exhaust Manifold Oxygen Sensor

A fifth Bosch LSU 4.9 wide-band oxygen sensor, mounted in the exhaust manifold, provides feedback about the air-fuel ratio for the whole engine. This sensor displays information on the host computer useful for operating the engine during an experiment. Figure 2.16 shows the exhaust manifold and illustrates the exhaust manifold

oxygen sensor in addition to the oxygen sensors in each exhaust runner.

Static Pressure Sensors

Four GP50 211 series static pressure sensors yield information about the pressure in the intake manifold, the exhaust manifold, the fuel system, and the ambient pressure. The information from each sensor provides a record of conditions under which any experiment operated.

Additionally, the host computer displays the intake manifold pressure sensor values, and those values allow the operator to adjust the desired throttle position in order to maintain the desired intake manifold pressure. The fuel pressure sensor readings displayed on the host computer also give the operator knowledge of the how closely the fuel system is operating to its desired pressure of 12 MPa.

Airflow Sensors

Three separate airflow sensors – an AVL research-grade anemometer, a Bosch production-grade anemometer, and a laminar flow element – all measure the rate of air flowing through the engine. The airflow measurements provide critical information for tuning engine models and for monitoring engine operation. Figure 2.18 shows the AVL and Bosch airflow sensors.

Fuel Flow Sensor

A Max Model 213-513 positive displacement fuel flow meter, depicted in Figure 2.19, measures the flow of gasoline delivered to the engine. The fuel flow sensor provides data for calibrating the fuel injector pulse widths and for confirming the quantity of fuel delivered to the engine during a particular experiment. Downstream of the meter, an orifice and a hydraulic bladder accumulator serve to dampen the pulsations in the fuel system resulting from the discrete fuel injection events that occur into the cylinders and cause pressure fluctuations in the engine fuel rail and its supply tubing.

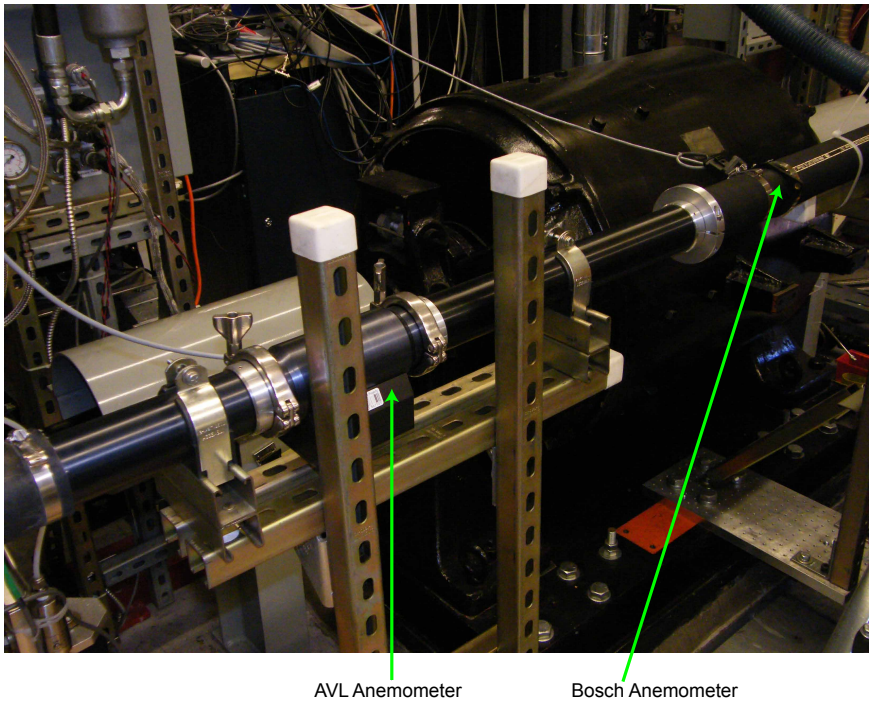

Figure 2.18: Picture of both anemometers

Figure 2.19: Picture of the gasoline fuel flow meter

Temperature Sensors

Twenty-six Omega Engineering K-type thermocouples measure temperatures throughout the intake, exhaust, cooling, and oiling systems in the multi-cylinder engine. The coolant tank inlet temperature signal provides the source of feedback for controlling the engine coolant temperature, as mentioned in Section 2.3.2. Many of the other temperature signals are displayed by the host computer in the control room for the operator's benefit; all 26 signals are recorded for analysis if necessary. Table 2.2 lists the locations of all the thermocouples installed on the engine.

2.5 Engine Computer Architecture

The complexity of the multi-cylinder engine requires four personal computers to control and monitor the engine while it operates. Three of the computers interact with the engine on a real-time basis running Mathworks' xPC operating system as xPC targets, while the fourth computer provides the interface through which the operator interacts with the three target computers.

2.5.1 Engine Control Unit

The engine control unit, or ECU, functions as the primary real-time computer controlling the multi-cylinder engine. It executes the control algorithms for the engine and collects all cycle-to-cycle measurements from the cylinder pressure sensors and the runner-mounted oxygen sensors. By running at a sampling rate of 10 kHz, the ECU collects cylinder pressure data from the engine every 1.08 crank angle degrees when the engine speed equals 1800 RPM.

The ECU drives all of the actuators with the exception of the valves. It determines fuel injection quantity and timing, determines spark timing and controls the ignition coils. It also controls the throttle and coolant valves, calculates intake and exhaust valve timings and sends those valve timings to the valve control unit via CAN. An NI-6602 PCI card runs the fuel injectors with counter pins that operate using an 80 MHz clock, providing the resolution needed for fuel injector pulse widths.

Table 2.2: Engine thermocouple locations

System	Location
Intake	Intake Runner, Cylinder 1
Intake	Intake Runner, Cylinder 2
Intake	Intake Runner, Cylinder 3
Intake	Intake Runner, Cylinder 4
Intake	Intake Manifold
Intake	Air Filter
Exhaust	Exhaust Runner, Cylinder 1
Exhaust	Exhaust Runner, Cylinder 2
Exhaust	Exhaust Runner, Cylinder 3
Exhaust	Exhaust Runner, Cylinder 4
Exhaust	Exhaust Manifold
Cooling	Engine Inlet
Cooling	Engine Outlet
Cooling	Heat Exchanger Inlet
Cooling	Heat Exchanger Outlet
Cooling	Tank Inlet
Cooling	Tank Outlet
Cooling	Tank Bypass
Oiling	Oil Pan
Cylinder Head	Cylinder Wall, Cylinder 1
Cylinder Head	Cylinder Wall, Cylinder 2
Cylinder Head	Cylinder Wall, Cylinder 3
Cylinder Head	Cylinder Wall, Cylinder 4
Process Cooling Water	Heat Exchanger Inlet
Process Cooling Water	Heat Exchanger Outlet

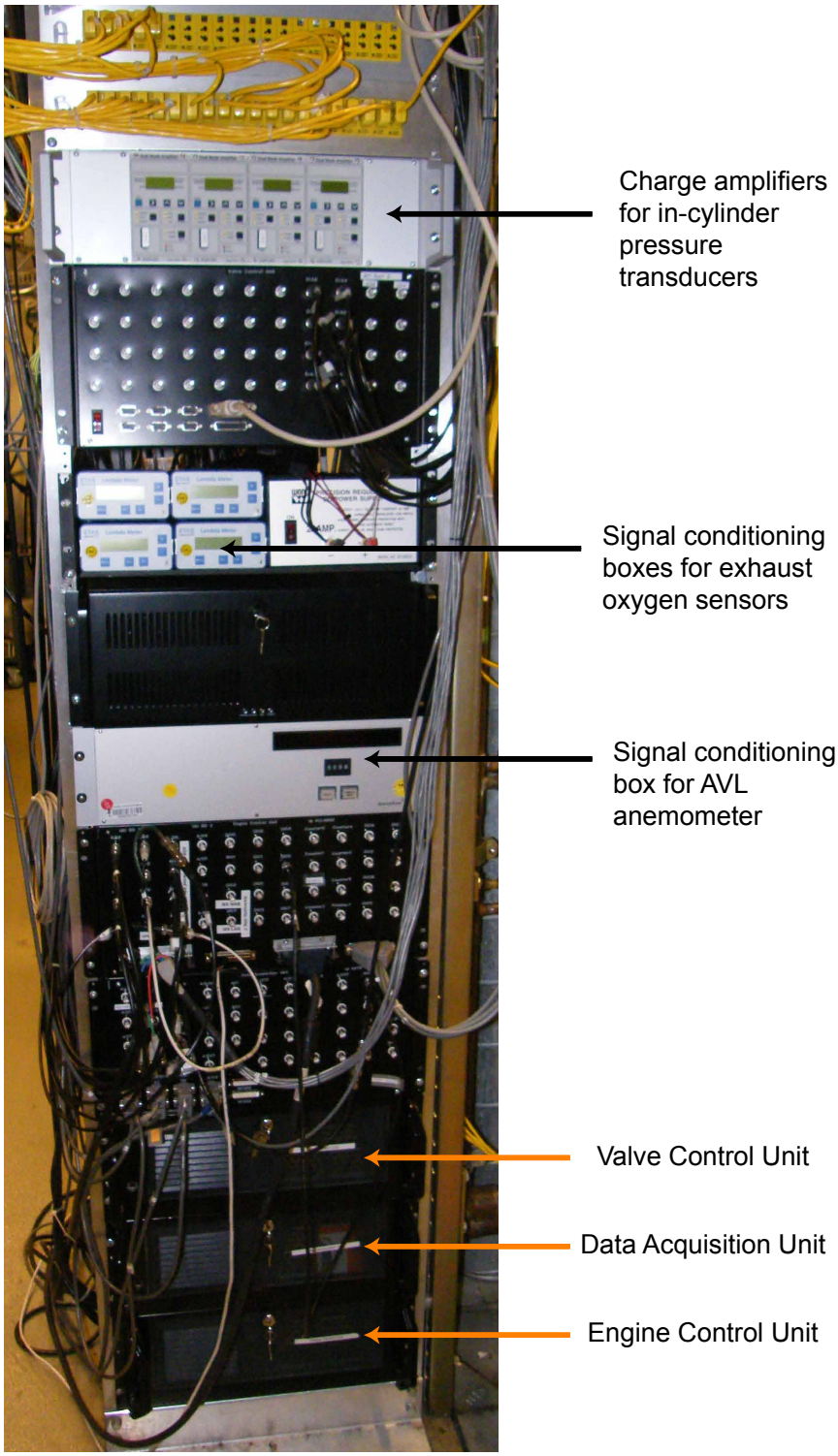

Figure 2.20: Picture of engine electronics rack

2.5.2 Valve Control Unit

The valve control unit, or VCU, controls the VVA system. It measures the engine position and the valve actuator positions of the eight valve systems, executes the control algorithms for each valve system, and sends the appropriate drive signals to the VVA system to drive the valves.

2.5.3 Data Acquisition Unit

The data acquisition unit, or DAU, measures engine position and all the additional sensors' information mentioned in Section 2.4.2. It also sends the coolant tank inlet temperature to the ECU over an ethernet connection to control the coolant temperature and works to align the clocks on the ECU and DAU for data analysis.

2.5.4 Host Computer

The final computer, the host, performs three major functions. It allows the operator the ability to adjust engine parameters while operating the engine such as spark timing, valve timing, throttle position, fueling rate, control gains, and so forth, by providing a Simulink model to interface to the targets and an ethernet connection to communicate with them. It also displays data being collected by the targets on monitors in the control room so that the operator can be aware of the engine's state. Finally, it provides a mechanism for programming the target computers.

Chapter 3

A Simple Model of HCCI as a Dynamic System

Understanding the dynamics of HCCI is critically necessary for improving them. This chapter covers a simple, physical model of one cylinder of the engine in Chapter 2. First, the chapter describes the distinct physical processes that combine together to form a discrete-time, nonlinear model of one HCCI engine cycle. Next, it covers the model's structure and discusses the choices of system states, inputs, and output. Then, the model shows that it captures oscillatory dynamics at certain HCCI operating conditions. Finally, it discusses the advantages and disadvantages of each actuation strategy, giving an overview of the material discusses in greater detail in the following two chapters.

3.1 Model Processes

The nonlinear model represents an HCCI engine cycle according to eight distinct, nonlinear processes. Each of these processes explains the evolution of the volume, pressure, temperature, and composition of the charge contained in the cylinder through simplified analytical models.

The model starts at the state angle $\theta_{s,k} = 60$ CADbTDCc (Crank Angle Degrees before Top Dead Center combustion) on cycle k with temperature $T_{s,k}$, volume $V_{s,k}$,

oxygen concentration $[O_2]_{s,k}$, and pressure $P_{s,k}$; $P_{s,k}$ is a function of intake manifold pressure and the intake valve closing angle, $\theta_{IVC,k}$. Using the ideal gas law, the total number of moles, $n_{tot,s,k}$, in the cylinder can be found. Additionally, the number of moles of oxygen present in the cylinder, $n_{O_2,s,k}$, can be determined from the oxygen concentration.

$$n_{tot,s,k} = \frac{P_{s,k}V_{s,k}}{R_u T_{s,k}} \tag{3.1}$$

$$n_{O_2,s,k} = [O_2]_{s,k}V_{s,k} \tag{3.2}$$

The following processes form the cycle:

1. *Compression:* Compression is modeled polytropically from the state angle, $\theta_{s,k}$, to the angle of the start of combustion, $\theta_{SOC,k}$. Equation (3.3) determines the cylinder temperature at the start of combustion, while equation (3.4) determines cylinder pressure at the start of combustion. As with any polytropic process, some heat transfer occurs between the charge and the cylinder wall, but the polytropic exponent accounts for that heat transfer. Additionally, it is assumed that no flow into or out of the cylinder occurs and that the composition of the cylinder constituents remains constant during the compression process.

$$T_{SOC,k} = T_{s,k}\left(\frac{V_{s,k}}{V_{SOC,k}}\right)^{\kappa_{cmp}-1} \tag{3.3}$$

$$P_{SOC,k} = P_{s,k}\left(\frac{V_{s,k}}{V_{SOC,k}}\right)^{\kappa_{cmp}} \tag{3.4}$$

   The polytropic exponent κ_{cmp} and all the other polytropic exponents in the model are obtained by fitting the model to experimental pressure traces.

2. *Combustion Phasing Determination:* Combustion phasing is determined at the start of compression by using an integrated global Arrhenius reaction rate model [37, 32]. The global Arrhenius reaction rate equation is given by equation (3.5):

$$RR \quad = A_{th} e^{\frac{E_a}{R_u T}} [f]^a [O_2]^b \tag{3.5}$$

where A_{th} is the pre-exponential factor, a property specific to the fuel used, E_a is the activation energy, also specific to the fuel used, R_u is the universal gas constant, T is the bulk mixture temperature, $[f]$ is the fuel concentration, and $[O_2]$ is the oxygen concentration present. The exponents a and b are also properties of the fuel used. The equation can then be integrated as in equation (3.6):

$$K_{th} \quad = \int RRdt \quad = \int_{\theta_{s,k}}^{\theta_{SOC,k}} A_{th} e^{\frac{E_a}{R_u T}} [f]^a [O_2]^b \frac{1}{\omega} d\theta \tag{3.6}$$

where ω is the engine speed and K_{th} is the Arrhenius threshold. The only changes to each term in the integrand over the interval $[\theta_s, \theta_{SOC}]$ are caused by the changing volume of the cylinder, which is deterministic. Therefore, the entire integral can be represented explicitly by the following map:

$$\theta_{SOC,k} = g([O_2]_{s,k}, T_{s,k}, [f]_{s,k}) \tag{3.7}$$

Figure 3.1 illustrates a three-dimensional version of that map. In that map, the output combustion timing is shown as a function of the oxygen and temperature states while fuel concentration is held constant. The model assumes a constant combustion duration, so there is a simple constant difference between $\theta_{SOC,k}$ and $\theta_{50,k}$.

All of the inputs to equation (3.7) are known at the start of compression and thus combustion phasing can be determined at the start of the compression process.

3. *Combustion:* Combustion is modeled as a two-step process that occurs over a constant crank angle duration. First, reactants undergo a polytropic process from the start of combustion, $\theta_{SOC,k}$, to the end of combustion, $\theta_{EOC,k}$. Then, at the end of combustion angle, the fuel reacts with the air and converts completely to products while energy is released into the mixture. This two-step combustion

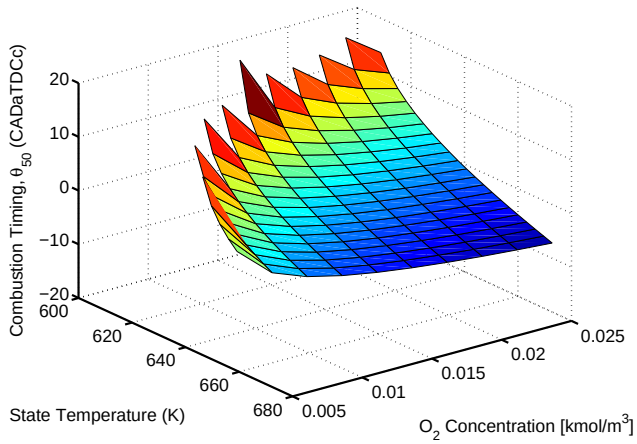

Figure 3.1: Combustion timing map showing θ_{50} dependence upon oxygen and temperature states

model allows for the amount of heat transfer taking place during combustion to be a function of the combustion phasing because different start of combustion and end of combustion angles result in different amounts of heat transfer during the polytropic process. Equation (3.8) determines the intermediate-step cylinder temperature, $T_{EOC',k}$, at the end of combustion angle; equation (3.9) determines the cylinder pressure, $P_{EOC',k}$ at $\theta_{EOC,k}$.

$$T_{EOC',k} = T_{SOC,k} \left(\frac{V_{SOC,k}}{V_{EOC,k}} \right)^{(\kappa_{cmb}-1)} \tag{3.8}$$

$$P_{EOC',k} = P_{SOC,k} \left(\frac{V_{SOC,k}}{V_{EOC,k}} \right)^{\kappa_{cmb}} \tag{3.9}$$

The stoichiometric equation for the combustion reaction of gasoline and dry air is given by equation (3.10). The fuel is modeled as the hypothetical molecule C_7H_{13} because both its carbon-to-hydrogen ratio and its molecular weight are similar to gasoline's.

$$C_7H_{13} + 10.25O_2 + 38.54N_2 \rightarrow 7CO_2 + 6.5H_2O + 38.54N_2 \tag{3.10}$$

The model assumes that the engine operates at a lean condition, so there will be some O_2 remaining after combustion. Equation (3.11) calculates the number of moles of oxygen remaining in the cylinder after combustion, $n_{O_2,EOC,k}$.

$$n_{O_2,EOC,k} = n_{O_2,s,k} - 10.25 n_{f,k} \tag{3.11}$$

The total number of moles of products of combustion are then calculated as $n_{O_2,s,k} - 10.25 n_{f,k} + 7 n_{f,k} + 6.5 n_{f,k} = n_{O_2,s,k} + 3.25 n_{f,k}$.

A first-law analysis determines the temperature of the mixture at the end of combustion by modeling the energy release as a heat addition process:

$$U_{EOC,k} - U_{EOC',k} = Q_{comb} - W \tag{3.12}$$

The process is assumed to occur at constant volume and therefore $W = 0$. Additionally, Q_{comb} can be split into two terms, Q_{er} and Q_w, which are the heat transfer due to energy release and the heat transfer from the charge to the wall respectively. Additionally, the total energy release is taken to be the product of $\bar{u}_{LHV,f}$, the lower heating value of the fuel on an internal energy basis, and $n_{f,k}$, the number of moles of fuel present in the cylinder; this relation is shown in equation (3.13).

$$Q_{er} = n_{f,k} \bar{u}_{LHV,f} \tag{3.13}$$

The heat transfer from the charge to the wall, Q_w, is simply taken to be a fraction, denoted by the parameter ϵ, scaled by the lower heating value of the fuel. The parameter ϵ results from calibration of the model. Equation (3.14) shows the method for determining Q_w.

$$Q_w = \epsilon n_{f,k} \bar{u}_{LHV,f} \tag{3.14}$$

The model captures heat transfer to the cylinder wall during combustion through

two different pathways: first, through the polytropic process, and second, through the lumped heat transfer during the instantaneous energy release. One drawback to this approach is the complexity in calculating the amount of heat transfer taking place during combustion. Another drawback is that the model likely understates the changes in the quantity of heat transfer taking place as a function of combustion timing.

By substituting equations (3.13) and (3.14) into equation (3.12) and combining common terms, the first law can be rewritten as in equation (3.15).

$$U_{EOC,k} - U_{EOC',k} = (1-\epsilon) n_{f,k} \bar{u}_{LHV} \tag{3.15}$$

Equation (3.15) can be further simplified by assuming that O_2, N_2, CO_2, and H_2O all have an identical, molar constant specific heat, $\bar{C}_v$. Substituting for $U_{EOC'}$ and U_{EOC} results in equation (3.16); in the equation $n_{gases,EOC'} = n_{O_2,EOC'} + n_{N_2,EOC'} + n_{CO_2,EOC'} + n_{H_2O,EOC'}$.

$$\begin{aligned} &\bar{C}_v(n_{gases,EOC'} + 3.25 n_{f,k})(T_{EOC,k} - T_{ref}) \\ &-(\bar{C}_{v,f} n_{f,k} + \bar{C}_v n_{gases,EOC'})(T_{EOC',k} - T_{ref}) \\ &= (1-\epsilon) n_f \bar{u}_{LHV} \end{aligned} \tag{3.16}$$

Equation (3.16) can then be rearranged to yield an equation for $T_{EOC,k}$. Additionally, the post-combustion pressure, $P_{EOC,k}$, is calculated according to equation (3.17) by using the ideal gas law. A simplification in this equation assumes that the number of moles in the cylinder after combustion is equal to the number of moles in the cylinder prior to combustion; this assumption is valid due to the high amounts of nitrogen and exhaust from the previous engine cycle present in the cylinder.

$$P_{EOC,k} = P_{EOC',k} \left(\frac{T_{EOC,k}}{T_{EOC',k}} \right) \tag{3.17}$$

4. *Expansion:* In the model, expansion occurs polytropically from the end of combustion, $\theta_{EOC,k}$, to the angle of exhaust valve opening, $\theta_{EVO,k}$. The equations that determine the in-cylinder temperature and pressure at $\theta_{EVO,k}$ are identical to equations (3.3) and (3.4); the only differences are the different start and end angles.

$$T_{EVO,k} = T_{EOC,k} \left(\frac{V_{EOC,k}}{V_{EVO,k}} \right)^{(\kappa_{exp}-1)} \tag{3.18}$$

$$P_{EVO,k} = P_{EOC,k} \left(\frac{V_{EOC,k}}{V_{EVO,k}} \right)^{\kappa_{exp}} \tag{3.19}$$

5. *Exhaust:* The exhaust process occurs polytropically from exhaust valve opening, $\theta_{EVO,k}$, to the angle of exhaust valve closing, $\theta_{EVC,k}$. The model assumes the exhaust manifold is at atmospheric pressure; thus, equation (3.20) provides $T_{EVC,k}$.

$$T_{EVC,k} = T_{EVO,k} \left(\frac{P_{exh}}{P_{EVO,k}} \right)^{\frac{\kappa_{exh}-1}{\kappa_{exh}}} \tag{3.20}$$

The fraction of retained exhaust, β, results from applying the ideal gas law to the start and end points of the exhaust process.

$$\beta = \frac{n_{EVC,k}}{n_{EVO,k}} = \frac{P_{exh} V_{EVC,k} T_{EVO,k}}{P_{EVO,k} V_{EVO,k} T_{EVC,k}} \tag{3.21}$$

Assuming the fraction of oxygen present in the cylinder at $\theta_{EVC,k}$ is equal to the fraction of oxygen in the cylinder at $\theta_{EVO,k}$, the number of moles of oxygen remaining in the cylinder at $\theta_{EVC,k}$ is calculated in equation (3.22).

$$n_{O_2,EVC,k} = \beta n_{O_2,EOC,k} = \beta \left([O_2]_{s,k} - 10.25[f]_{s,k} \right) V_{s,k} \tag{3.22}$$

6. *Recompression:* The recompression process is modeled as the compression and expansion of retained exhaust gases between exhaust valve closing, $\theta_{EVC,k}$, and

the angle of intake valve opening, $\theta_{IVO,k}$; the model therefore assumes that no gases flow into or out of the cylinder during recompression. Fuel injection occurs instantaneously immediately prior to intake valve opening, so the model assumes no reactions take place with the fuel during recompression. The fuel enters the cylinder as a liquid that vaporizes instantly upon injection.

$$U_{IVO,k} - U_{EVC,k} = -hA_{avg}(T_{avg} - T_w)\Delta t_{recomp} - n_{f,inj,k}\bar{h}_{fg,f} \tag{3.23}$$

The first law of thermodynamics calculates the internal energy at intake valve opening, $U_{IVO,k}$. The model assumes that the intake valve opening and exhaust valve closing angles are roughly symmetric about gas exchange top center, so the work term is omitted. A lumped heat transfer model transfers some energy from the retained exhaust to the cylinder walls. The heat transfer model uses an approximation of the average cylinder temperature, T_{avg}, which calculates the average cylinder temperature assuming an isentropic compression and expansion process. Additionally, the elapsed time of recompression, Δt_{recomp}, is calculated from knowledge of the exhaust valve closing, the intake valve opening, and the engine speed. From equation (3.23), the temperature at intake valve opening, $T_{IVO,k}$, can be obtained.

7. *Intake:* Fresh air at atmospheric temperature and intake manifold pressure pressure enters the cylinder between the angles of intake valve opening and closing. The model then assumes the air mixes instantaneously with the retained exhaust from the previous engine cycle at intake valve closing. The model assumes the pressure in the cylinder at $\theta_{IVC,k}$ is the same pressure as the intake manifold.

   The model applies the first law to the problem of filling the cylinder assuming that the properties of the intake manifold are constant throughout the filling process that kinetic and potential energy terms are negligible. Equation (3.24) shows the first law for filling the cylinder assuming no heat transfer to the cylinder walls where $\bar{h}_{int}$ is the enthalpy of the air in the intake manifold and

$n_{a,k}$ is the number of moles of air inducted into the cylinder.

$$\bar{h}_{int} n_{a,k} = \bar{u}_{IVC,k} n_{IVC,k} - \bar{u}_{IVO,k} n_{IVO,k} \tag{3.24}$$

Additionally, the ideal gas law is applied at $\theta_{IVC,k}$. Together with the molar balance equation and the first law, $T_{IVC,k}$ and $n_{IVC,k}$ can be solved.

$$T_{IVC,k} = \frac{P_{IVC,k} V_{IVC,k}}{n_{IVC,k} R_u} \tag{3.25}$$

$$n_{IVC,k} = n_{IVO,k} + n_{a,k} \tag{3.26}$$

8. *Compression:* Finally, a polytropic compression process occurs from intake valve closing, θ_{IVC}, to the state angle of the subsequent cycle, $\theta_{s,k+1}$.

$$T_{s,k+1} = T_{IVC,k} \left(\frac{V_{IVC,k}}{V_{s,k+1}} \right)^{\kappa_{cmp}-1} \tag{3.27}$$

$$P_{s,k+1} = P_{IVC,k} \left(\frac{V_{IVC,k}}{V_{s,k+1}} \right)^{\kappa_{cmp}} \tag{3.28}$$

3.2 Model Structure

The previous eight processes form a discrete-time representation of a HCCI engine cycle. However, in order to study that model from a dynamic systems perspective, it is critical to define system states and consider the inputs and outputs of interest of the system. This section covers the structure of the model, explaining its most important features and assumptions.

3.2.1 Model States

Defining the system state requires some consideration. The full thermodynamic state of the cylinder contents would be two independent properties, such as temperature,

specific volume, and pressure, along with the concentrations of all species present in the cylinder. Even simply considering only the concentrations of the major species of fuel, oxygen, nitrogen, carbon dioxide, and water vapor results in seven different states.

From a dynamic systems perspective, the system's states are the information needed to reconstruct the system's configuration at any point in time. Often, the system's states typically correspond to its modes of energy storage. A mass-spring-damper system stores potential energy in the compression or elongation of the spring and stores kinetic energy in the velocity of the mass; each energy storage mode corresponds to a system state: the two states are the displacement of the mass (and therefore also the spring) and the velocity of the mass. In an RLC circuit, the two system states are the charge stored on the capacitor and the current flowing through the inductor. The concept even extends to fields like vehicle dynamics, where the three states are the lateral velocity of the vehicle and the longitudinal velocity of the vehicle, which store translational kinetic energy, and the yaw rate of the vehicle, which stores rotational kinetic energy.

In the cylinder, the charge of fuel and air stores both sensible energy and chemical energy. The in-cylinder charge temperature state captures the system's sensible energy, while the molecular bonds in the fuel and oxygen store the system's potential energy. Two different states account for chemical energy storage: the oxygen concentration state and the fuel concentration state. The chemical energy storage in both the oxygen and the fuel concentrations is fairly straightforward. In both cases, the covalent bonds of O_2 molecules and fuel molecules contain energy that can be released when the fuel and oxygen react with one another.

A fourth state, the integrated Arrhenius state, captures both sensible and chemical energy changes within the cylinder that occur when fuel from pilot injections is exposed to elevated temperatures and pressures during recompression. Pilot injections induce two major effects on the cylinder charge: charge cooling and fuel reactions. Charge cooling occurs when the fuel injected into the cylinder vaporizes, cooling the mixture and reducing the sensible energy present in the cylinder. The fuel reactions

that occur in the cylinder are a combination of endothermic and exothermic reactions that both absorb and release sensible energy, changing the amount of sensible energy present in the charge. The reactions also alter the chemical composition of the mixture through some combination of breaking down into smaller fuel molecules and becoming H_2 and CO; these different molecules have different ignition characteristics and are generally more easily ignited than gasoline. The Arrhenius threshold state captures the effect that pilot injection timing has on the system, combining the charge cooling and fuel reactions effects into a single state representing the propensity of the mixture to autoignite based upon when the pilot injection occurred.

The model's states are:

1. Oxygen concentration, $[O_2]_{s,k}$
2. Temperature, $T_{s,k}$
3. Fuel concentration, $[f]_{s,k}$
4. Arrhenius state, $K_{th,k}$

The states are defined at the angle 60 CADbTDCC, and this definition has two advantages. First, it results in system definition in which the outputs depend only upon the states and not upon the inputs, meaning the model has no feedthrough matrix. Second, it means that the the volume at which the state angle occurs does not change from one cycle to the next, as it might if the angle of intake valve closing or exhaust valve closing defined the state angle. This fixed angle removes any changes to the cylinder states caused by changes in the volume of the state angle.

The model assumes that all of the fuel burns completely each engine cycle and leaves no unburned residual fuel in the cylinder. This assumption dictates then that both the fuel concentration and the Arrhenius threshold states will have no dependence upon their previous values; they will only depend upon inputs. However, relaxing the complete combustion assumption would result in one (or both) of these states depending upon their values from previous cycles. Adding a combustion model that would allow for fuel residuals to remain in the exhaust would perhaps improve the accuracy of the model, but could potentially sacrifice some of its transparency.

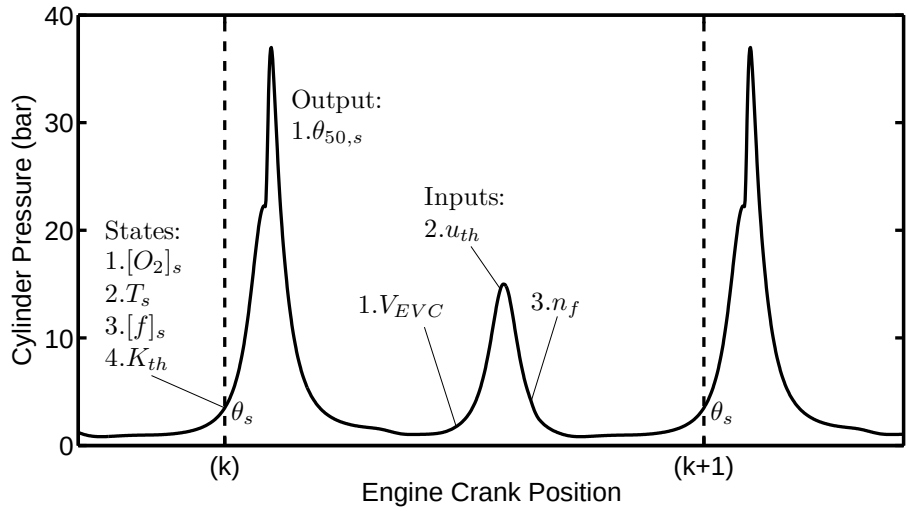

Figure 3.2: Engine model shown on an in-cylinder pressure trace

3.2.2 Model Output

Predicting combustion timing in HCCI engines is important because it is critically important to avoid misfires. Hence, the model's output is the crank angle at which 50% of the fuel mass in the cylinder burns, $\theta_{50,k}$. The angle of 50% fuel mass burned makes a superior metric for combustion timing as compared to the location of peak pressure or the start of combustion angle, θ_{SOC}, because the location of peak pressure can sometimes occur prior to combustion for cycles with very late combustion events, while the start of combustion angle can be similar for many combustion events that have different durations. [2, 1]

The model's output is:

1. Crank angle of 50% fuel mass burn, $\theta_{50,k}$.

3.2.3 Model Inputs

Three different inputs alter the states of the system: exhaust valve closing timing, $\theta_{EVC,k}$, the number of moles of fuel injected, $n_{f,inj,k}$, and the pilot injection timing, $\theta_{inj,pilot,k}$. However, in the case of both the exhaust valve timing and the pilot injection

timing, significant input non-linearities exist that make it more challenging to use those two inputs with linear control algorithms.

In the case of the exhaust valve timing input, replacing the exhaust valve closing timing with the volume at exhaust valve closing removes the geometric nonlinearity that results from the slider-crank relationship between crank angle and cylinder volume. The relationships between the volume of exhaust retained in the cylinder and the in-cylinder temperature and oxygen concentration are more linear than the relationships between the angle of exhaust valve closing and the in-cylinder temperature and oxygen concentration, so changing the input improves the linearity of the model and makes it more suited to linear control strategies.

The relationship between pilot injection timing and combustion timing is nonlinear, but it can be broken into a static, nonlinear relationship between pilot injection timing and Arrhenius threshold and a nearly-linear relationship between Arrhenius threshold and combustion timing that contains the system dynamics; this relationship is explained further in Section 5.1.1. Thus, modeling the pilot injection input as an Arrhenius threshold input instead of an angle improves the model's linearity.

The model's inputs are:

1. Volume at exhaust valve closure, $V_{EVC,k}$
2. Number of moles of fuel injected, $n_{f,inj,k}$
3. Arrhenius input, $u_{th,k}$

Figure 3.2 illustrates the model with all four states and all three inputs.

The combination of the physical steps in Section 3.1 leads to a nonlinear model for the whole engine cycle that captures cycle-to-cycle coupling in the form of a discrete-time dynamic system:

$$\begin{aligned} x_{k+1} &= F\left(x_k, u_k\right) \\ y_k &= H\left(x_k\right) \end{aligned} \tag{3.29}$$

where x_k is the system state, y_k is the system output, and u_k is the system input.

Table 3.1: Simulation conditions

Condition	Value
Compression ratio	12:1
Engine speed	1800 RPM
Fuel mass	10 mg/cylinder/cycle
Fuel end-of-injection timing	420 CADaTDCc
Exhaust valve opening	θ_{EVC} - 140
Intake valve opening	433 CADaTDCc
Intake valve closing	573 CADaTDCc

3.3 Nonlinear Control Model Time-Domain Behavior

Figure 3.3 shows the time-based response of the nonlinear model as the engine model receives different exhaust valve closing commands, and Table 3.1 shows the other simulation conditions. The exhaust valve timing changes between $\theta_{EVC} = 287$ CADaTDCc, $\theta_{EVC} = 292$ CADaTDCc, and $\theta_{EVC} = 297$ CADaTDCc throughout the simulation. For the cases run with $\theta_{EVC} = 287$ CADaTDCc and $\theta_{EVC} = 292$ CADaTDCc, the θ_{50} response is well-damped and responds quickly to changes in exhaust valve timing. However, for the case with $\theta_{EVC} = 297$ CADaTDCc, the θ_{50} response oscillates about the equilibrium combustion phasing before finally settling to it. The model clearly suggests that the system dynamics change as exhaust valve timing changes and combustion phasing shifts later.

One key difference exists between the nonlinear model and the experimental engine. The model is deterministic and is not subjected to continued perturbations the way the engine is. One example of a perturbation arises from air flow: for a given set of valve timings, the air flow into and out of the cylinder is not the same from one cycle to the next on the experimental engine. These perturbations continually excite the oscillatory dynamics of the system and cause the observed variations in combustion timing. The model does not include these perturbations by design and thus does not show the continued oscillations in combustion timing that the experimental data show.

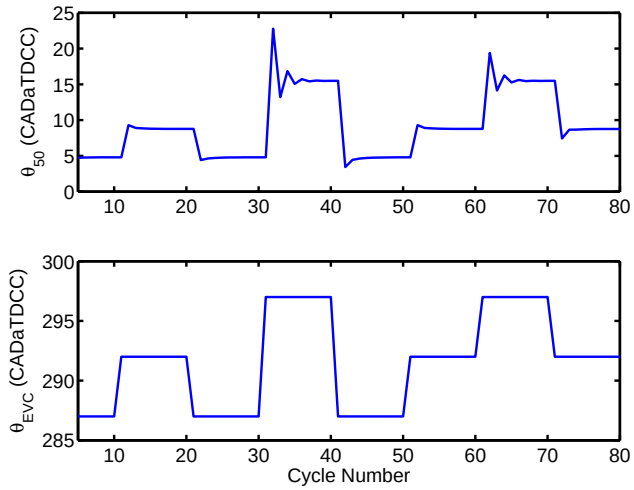

Figure 3.3: θ_{50} response of the model to a series of exhaust valve timing step changes

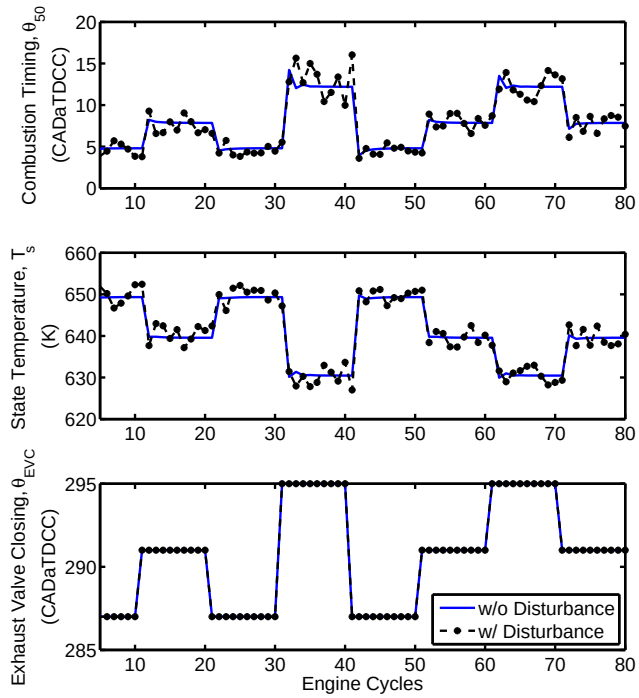

Figure 3.4: θ_{50} response of the model to a series of exhaust valve timing step changes with a disturbance added to temperature signal

However, simulating a disturbance on the temperature signal, which could be caused by variations in airflow, illustrates the changing dynamics between the operating conditions. While the oscillations in state temperature have the same magnitude regardless of the valve timing, the oscillations in combustion timing are larger for the conditions with late exhaust valve timings. Thus, the model predicts that the cyclic variation grows larger as the mean combustion timing moves later.

3.4 Controllability versus Ease of Implementation Tradeoffs

As chapters 4 and 5 will show, each of the three inputs, exhaust valve closing timing, $\theta_{EVC,k}$, pilot injection timing, $\theta_{inj,pilot,k}$, and fuel quantity, $n_{f,inj,k}$, face significant tradeoffs with respect to controllability and implementability, which Table 3.2 displays. When only one of the three inputs changes on a cycle-to-cycle basis and the other two inputs are held constant, some of the states do not change either. The exhaust valve timing input does not affect either the fuel concentration state or the Arrhenius state, so the control problem using the exhaust valve timing input reduces to a two state problem. Similarly, the pilot injection timing input does not affect the fuel concentration state, so the control problem associated with the pilot injection timing input reduces to a three state problem. Finally, since the fuel quantity input does not affect the Arrhenius state, the control problem associated with the fuel quantity input reduces to a three-state problem.

The exhaust valve closing input is the easiest control problem to solve because it involves controlling only a two-state system with one negative-real-axis eigenvalue and a simple geometric input nonlinearity. As the results in Chapter 4 will show, a proportional controller sufficiently reduces the oscillations in combustion timing and in indicated mean effective pressure at a late-phasing operating condition.

However, the technology needed to implement individual cylinder exhaust valve timing control is significantly more difficult to package into an automobile than the

Table 3.2: Implementation and Control Challenges for the Three Actuation Technologies Studied

Input	Ease of Implementing	States	Control Challenge	Ease of Control
Exhaust valve closing	Difficult	Oxygen conc. Temperature	Geometric input non-linearity	Easy
Pilot injection timing	Easy	Oxygen conc. Temperature Arrhenius thrsh.	Non-obvious input non-linearity	Moderate
Fuel injection quantity	Easy	Oxygen con. Temperature Fuel conc.	Non-minimum phase input, Linked to work	Difficult

direct fuel injection technology required to implement the two different fuel injection-based technologies. Instead, technologies that increase the bandwidth of cam phasers have the promise to make this valve control strategy implementable. [14]

Chapter 5 demonstrates that the pilot injection timing control input problem is moderately difficult to solve. The control problem itself is straightforward: it involves controlling a three-state system instead of a two-state system that also includes one negative real axis eigenvalue. A lag compensator sufficiently reduces the cyclic oscillations in combustion timing by moving that pole into the right half complex plane. However, the authority of pilot injection timing to control combustion timing at high loads may be limited. The pilot injection timing input relies on the presence of significant amounts of exhaust residual in the cylinder during recompression HCCI to change the fuel's properties. The effectiveness of the input may diminish at high loads when the quantity of exhaust residual decreases and the fuel spends less time exposed to elevated temperatures and pressures, since less exhaust is needed to initiate combustion at high loads.

From an implementation standpoint, pilot injection timing control is easily achieved in currently-available hardware since it relies on a direct injection fuel injector and system for its implementation.

Chapter 5 also illustrates that the fuel mass control problem is the most difficult of the three to solve because of a non-minimum phase relationship between the fuel mass input and the combustion timing output. Additionally, the non-minimum phase nature of the input is complicated by the fact that it is unclear how much charge cooling occurs in the cylinder; this uncertainty manifests itself as uncertainty in the location of the non-minimum phase zero. Again, a lag compensator moves the negative real axis pole into the right half plane while being robust to different assumptions about charge cooling.

Fortunately, the fuel mass implementation uses the same currently-available fuel injection hardware as the pilot injection timing input. Therefore, it is straightforward to implement in a vehicle.

Chapter 4

Combustion Instability as a Negative Eigenvalue

This chapter shows how the exhaust valve closing input can be used to reduce oscillations at certain HCCI operating conditions. First, it describes the linearized control model structure, which follows from the nonlinear model in the previous chapter. Second, it linearizes the model at two different operating conditions and compares the dynamics at the two conditions. Then, through a root locus analysis it explains the control design process that reduces the oscillations at late-phasing conditions. Finally, it validates that control design experimentally on the test engine.

4.1 Linear Control Model

The nonlinear model can be numerically linearized about an operating point to yield a linear, state-space, discrete-time model of the form

$$\begin{aligned} x_{k+1} &= Ax_k + Bu_k \\ y_k &= Cx_k \end{aligned} \tag{4.1}$$

where $A \in \mathbb{R}^{4\times4}$ is the system matrix, $B \in \mathbb{R}^{4\times3}$ is the input matrix, and $C \in \mathbb{R}^{1\times4}$ is the output matrix. The system state, x_k, input, u_k, and output, y_k, are all normalized by the steady-state equilibrium condition about which the system is linearized and

valid. Thus, the state of the linearized model is

$$x_k = \left[\frac{[O_2]_k - [O_2]_{ss}}{[O_2]_{ss}}, \ \frac{T_k - T_{ss}}{T_{ss}}, \ \frac{[f]_k - [f]_{ss}}{[f]_{ss}}, \ \frac{K_{th,k} - K_{th,ss}}{K_{th,ss}} \right]^T$$

where $[O_2]_k$ is the oxygen concentration on cycle k and $[O_2]_{ss}$ is the steady-state oxygen concentration, T_k is the state temperature on cycle k and T_{ss} is the steady-state state temperature, $[f]_k$ is the fuel concentration on cycle k and $[f]_{ss}$ is the steady-state fuel concentration, and $K_{th,_k}$ is the Arrhenius threshold state on cycle k and $K_{th,ss}$ is the steady-state Arrhenius threshold state.

The input of the linearized model is

$$u_k = \left[\frac{V_{EVC,k} - V_{EVC,ss}}{V_{EVC,ss}}, \ \frac{n_{f,k} - n_{f,ss}}{n_{f,ss}}, \ \frac{u_{th,k} - u_{th,ss}}{u_{th,ss}} \right]^T$$

where $V_{EVC,k}$ is the volume at exhaust valve closing on cycle k and $V_{EVC,ss}$ is the steady-state volume at exhaust valve closing, $n_{f,k}$ is the number of moles of fuel injected on cycle k and $n_{f,ss}$ is the steady-state number of moles of fuel injected, and $u_{th,_k}$ is the Arrhenius threshold input on cycle k and $u_{th,ss}$ is the steady-state Arrhenius threshold input.

The output of the linearized model is

$$y_k = \frac{\theta_{50,k} - \theta_{50,ss}}{\theta_{50,ss}}$$

where $\theta_{50,k}$ is the combustion timing on cycle k and $\theta_{50,ss}$ is the steady-state combustion timing.

In equation (4.1), the system matrix, A, captures the cycle-to-cycle coupling of the system and thus contains any changes in system dynamics between nominal and late-phasing HCCI operating conditions.

The combustion phasing on any given cycle can be calculated by combining the two equations in equation (4.1). If the input to the system is the equilibrium valve timing, then $u = 0$ and the phasing is simply a function of the initial condition:

$$y_k \quad = CA^k x_0 \tag{4.2}$$

The system matrix, A, can be decomposed into its eigenvalues and eigenvectors such that

$$A \quad = \lambda_1 v_1 {w_1}^T + \lambda_2 v_2 {w_2}^T + \lambda_3 v_3 {w_3}^T + \lambda_4 v_4 {w_4}^T \tag{4.3}$$

where λ_1, λ_2, λ_3, and λ_4 are the eigenvalues of A; v_1, v_2, v_3, and v_4 are eigenvectors such that $Av_i = v_i\lambda_i$; and ${w_1}^T$, ${w_2}^T$, ${w_3}^T$, and ${w_4}^T$ are eigenvectors such that ${w_i}^T A = \lambda_i {w_i}^T$. Equations (4.2) and (4.3) can be combined to show how the eigenvalues influence the combustion timing on cycle k for a given initial condition.

$$y_k \quad = C({\lambda_1}^k v_1 {w_1}^T + {\lambda_2}^k v_2 {w_2}^T + {\lambda_3}^k v_3 {w_3}^T + {\lambda_4}^k v_4 {w_4}^T)x_0 \tag{4.4}$$

Equation (4.4) shows that the combustion phasing is a function of the eigenvalues and that they therefore govern the unforced response of the system. If any eigenvalue has a magnitude of greater than one, the response will grow indefinitely; this would result in a loss of combustion on the engine. If all four eigenvalues have magnitude of less than one, the system will naturally decay to the steady-state operating condition. If all four eigenvalues' real parts have a positive sign, the system will naturally decay smoothly to the steady-state condition; however, if one eigenvalue's real part has a negative sign, the response will oscillate about the equilibrium on a cycle-by-cycle basis while decaying to the steady-state condition.

4.2 Nominal vs. Late Phasing Region Linearizations

In this section, the linearization of the nonlinear model at a nominal-phasing point is compared to the linearization at a late-phasing point. The rest of this chapter only considers the exhaust valve closing input; hence, the model states and input reduce to

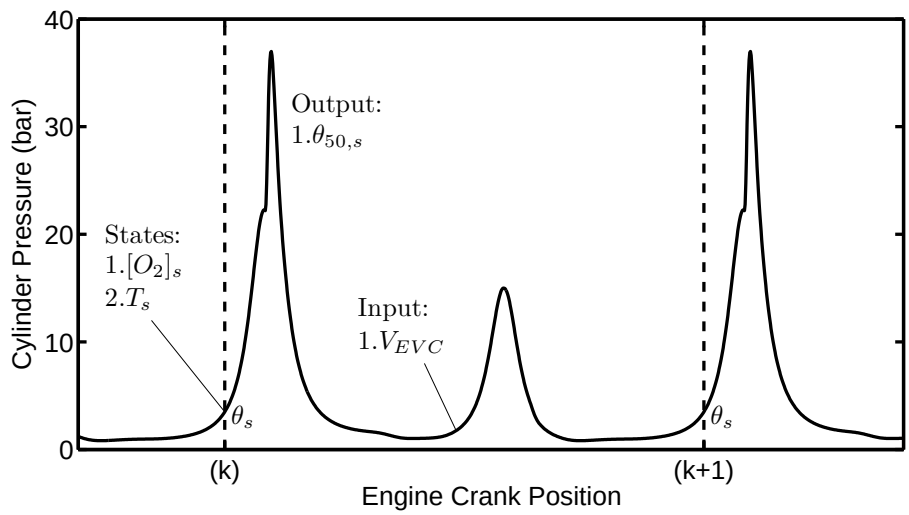

Figure 4.1: Reduced model showing the exhaust valve closing model with the volume at exhaust valve closing input

$$x_k = \left[\frac{[O_2]_k - [O_2]_{ss}}{[O_2]_{ss}}, \ \frac{T_k - T_{ss}}{T_{ss}} \right]^T$$

$$u_k = \frac{V_{EVC,k} - V_{EVC,ss}}{V_{EVC,ss}}$$

while the output remains the same. Accordingly, $A \in \mathbb{R}^{2\times 2}$ is the reduced system matrix, $B \in \mathbb{R}^{2\times 1}$ is the reduced input matrix, and $C \in \mathbb{R}^{1\times 2}$ is the reduced output matrix. Figure 4.1 illustrates the reduced model.

4.2.1 Nominal Phasing Region Linearization

Linearizing the model about a point with an exhaust valve closure of $\theta_{EVC} = 287$ CADaTDCc and a combustion phasing of $\theta_{50} = 5$ CADaTDCc yields the following linear system matrices:

$$A_{nominal,valve} = \begin{bmatrix} 0.53 & 0.24 \\ -0.0067 & 0.022 \end{bmatrix} \quad B_{nominal,valve} = \begin{bmatrix} -1.54 \\ 0.46 \end{bmatrix}$$
$$C_{nominal,valve} = \begin{bmatrix} -0.022 & -0.62 \end{bmatrix} \tag{4.5}$$

The state temperature of any engine cycle operating near the nominal operating condition is largely independent of the state temperature from the previous cycle, which can be seen from the circled $(2, 2)$ entry of $A_{nominal,valve}$. Furthermore, comparing $A_{nominal,valve}(2, 2)$ to $B_{nominal,valve}(2)$ shows that the state temperature on cycle $k + 1$ is significantly more dependent upon the exhaust valve timing on cycle k than on the state temperature on cycle k.

The state temperature's independence from the previous state temperature can also be seen from the the poles of the nominal system, which are the eigenvalues of the matrix $A_{nominal,valve}$, and are located at

$$\lambda_{nominal,valve} = \begin{bmatrix} 0.53 \\ 0.025 \end{bmatrix}.$$

The nominal system is stable because it meets the discrete-time stability criteria, $||\lambda_i|| < 1$ for all i. Thus, any deviations in state temperature will naturally decay away over time provided the system is not continually excited. The eigenvalues suggest that the nominal system responds smoothly to excitations, similar to a first-order system, because both eigenvalues are real and positive as suggested by equation (4.4).

4.2.2 Late Phasing Region Linearization

Linearizing the model about a point with an exhaust valve closure of $\theta_{EVC} = 294$ CADaTDCc yields a point with an estimated combustion phasing of $\theta_{50} = 12$ CADaTDCc and the following linear system matrices:

$$A_{late,valve} = \begin{bmatrix} 0.45 & -0.17 \\ -0.022 & \text{-0.32} \end{bmatrix} \quad B_{late,valve} = \begin{bmatrix} -1.05 \\ 0.41 \end{bmatrix}$$
$$C_{late,valve} = \begin{bmatrix} -0.082 & -2.09 \end{bmatrix} \tag{4.6}$$

In the late-phasing system, the state temperature on one engine cycle significantly influences the state temperature on the following engine cycle, which can be seen from the circled $(2, 2)$ entry of $A_{late,valve}$. Additionally, comparing $A_{late,valve}(2, 2)$ to $B_{late,valve}(2)$ shows that the state temperature on cycle $k + 1$ depends significantly upon both the exhaust valve timing on cycle k and the state temperature on cycle k.

In the late system, the state temperature's dependence on the previous state temperature can also be seen from the poles of the system, which are the eigenvalues of the matrix $A_{late,valve}$ and are located at

$$\lambda_{late,valve} = \begin{bmatrix} 0.45 \\ -0.32 \end{bmatrix}.$$

Again, the late-phasing system is stable. However, the second eigenvalue has a value of $\lambda = -0.32$, indicating that the state temperature on any cycle somewhat strongly depends on the state temperature of the previous cycle. The eigenvalue also shows that the late-phasing system will have an oscillatory transient response to any input as it approaches its steady-state value because the second eigenvalue is negative in sign. The oscillatory response of the late-phasing system contrasts with the smooth response of the nominal phasing system, and the different responses result from the different eigenvalue locations of the two systems.

4.3 Nominal Model and Late-Phasing Model Transfer Functions

The linear state-space systems described by equations (4.5) and (4.6) can also be combined to form a discrete-time transfer function representation according to the equation

$$G(z) \quad = C(zI - A)^{-1}B \ , \tag{4.7}$$

if $(zI - A)$ is an invertible matrix. When the state-space system for the nominal system is combined into a transfer function using equation (4.7), the result is

$$G_{nominal}(z) = -0.25\tfrac{(z-0.57)}{(z-0.53)(z-0.025)}. \tag{4.8}$$

The result from combining the late-phasing state-space system into a transfer function is

$$G_{late}(z) = -0.76\tfrac{(z-0.48)}{(z-0.45)(z+0.32)} \ . \tag{4.9}$$

In both transfer functions, the system poles for the nominal and late systems are simply the corresponding eigenvalues discussed in Section 4.2. Plotting the pulse response of each system helps illustrate this point. Figure (4.2) shows how both systems respond to a pulse input, pictured in the lowest plot. Upon reexamining equation (4.4), it is not surprising that the nominal system returns to the equilibrium value of 0 very quickly without oscillating because its dominant pole is located at $z = 0.025$. Alternatively, the late-phasing system oscillates as it returns to the equilibrium as expected due to its dominant pole location at $z = -0.32$.

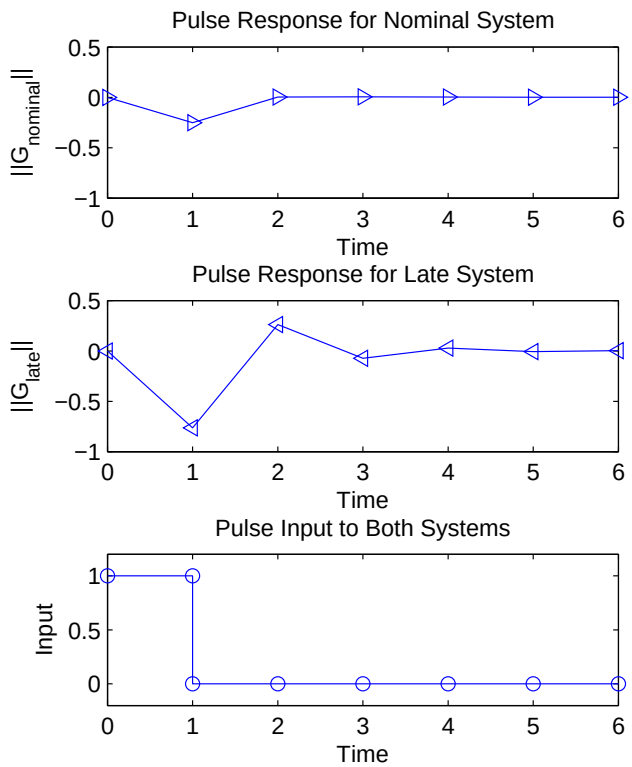

Figure 4.2: Pulse responses of nominal and late-phasing linearized systems

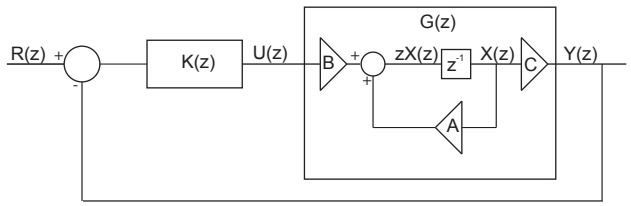

Figure 4.3: Block Diagram of closed-loop system showing plant and controller

4.4 Control Design that Remedies Combustion Instability

The dynamics of late-phasing HCCI can be improved with the use of feedback control by moving the system poles off of the negative real axis. Figure 4.3 shows a schematic of the system in closed-loop feedback. In the schematic, the system plant $G(z)$ is composed of the A, B, and C matrices from equations (4.1) and (4.7). The plant maps the system input, normalized volume at exhaust valve closing, $U(z)$, to the system output, normalized combustion timing, $Y(z)$. The compensator $K(z)$ calculates the desired exhaust valve closing volume based on the difference between the measured and desired combustion timings.

Figure 4.4 shows the root locus of the nominal system while Figure 4.5 shows the root locus of the late-phasing system. The root loci are simply plots of how each system's poles move in response to changes in a constant gain $K(z)$. On the root loci, the x characters represent the open-loop pole locations from equations (4.8) and (4.9) while the o characters represent the zero locations. The large circle in each figure is the unit circle, which shows the stability criterion for the system.

The root locus in Figure 4.5 illustrates that a simple proportional controller sufficiently improves the combustion phasing performance at the late phasing point. As the gain increases, the pole in the left-half plane moves to the right. At a gain of $K = 1.1$, the poles reach closed-loop locations specified by the squares ($\square$).

The controller changes the system dynamics relative to the open-loop case:

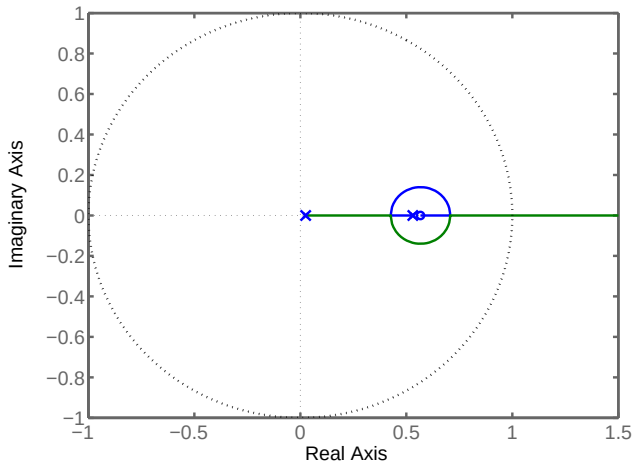

Figure 4.4: Root locus of a linearization at a nominal phasing condition

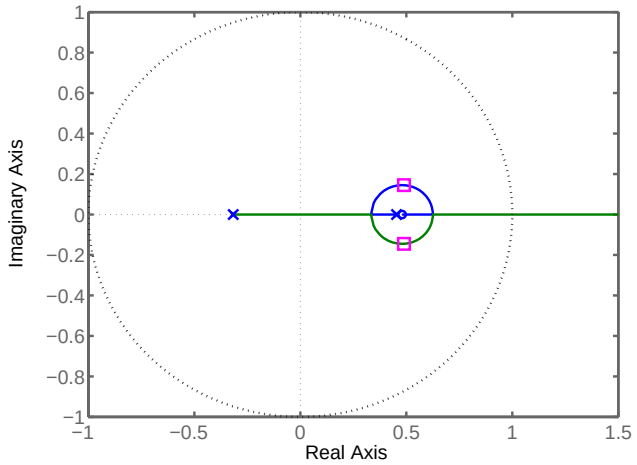

Figure 4.5: Root locus of linearization at a late phasing condition showing closed-loop pole locations

$$\begin{aligned} x_{k+1} &= Ax_k + Bu_k \\ &= Ax_k + B(-Ky_k) \\ &= (A - BKC)x_k \\ &= A_{cl}x_k \end{aligned} \tag{4.10}$$

where

$$A_{late,cl,valve} = \begin{bmatrix} 0.36 & -2.58 \\ 0.015 & 0.62 \end{bmatrix}$$

resulting in closed-loop pole locations of

$$\lambda_{late,cl,valve} = \begin{bmatrix} 0.49 + 0.14i \\ 0.49 - 0.14i \end{bmatrix}.$$

The controller successfully moves the pole on the negative real-axis into the right-half plane and thus eliminates the oscillations predicted by equation (4.4) that are driven by the negative real-axis pole. The proportional controller also succeeds in keeping both poles inside the unit circle, ensuring that the system is stable.

The proposed controller makes intuitive sense as well. If the measured combustion phasing on cycle k is later than the desired combustion phasing, the natural system dynamics dictate that combustion phasing on cycle $k+1$ would be earlier than desired on the following cycle. The controller responds by decreasing the volume at exhaust valve closing and retaining less exhaust. By retaining less exhaust in the cylinder, less sensible energy remains in the cylinder. If the same amounts of air and fuel are inducted into the cylinder, the controller counteracts the natural dynamics and causes combustion to occur later than in the open-loop case on cycle $k + 1$ because more compression will be necessary to achieve autoignition, reducing the change in combustion phasing from one cycle to the next and smoothing the response.

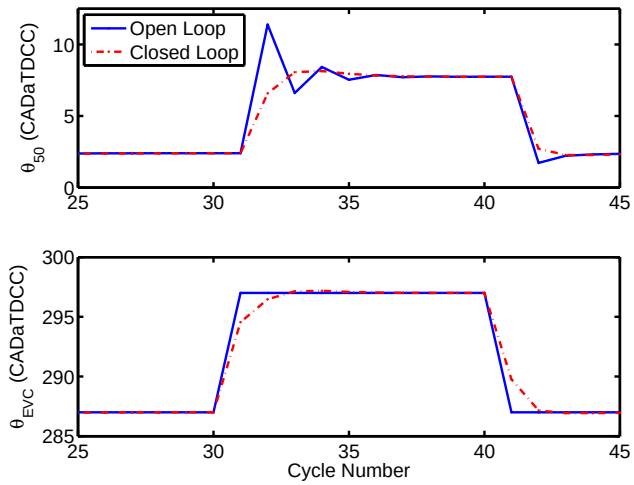

Figure 4.6: Closed-loop simulation of controller performance on nonlinear model

4.5 Controller Validation in Simulation

The controller eliminates the oscillations in combustion phasing simply by changing the exhaust valve timing closing. Figure 4.6 shows that the controller eliminates the oscillatory dynamics seen in the uncontrolled case through small changes in θ_{EVC}.

4.6 Experimental Results

The engine used in these experiments is the 2.2L, 16-valve, 4-cylinder General Motors ECOTEC engine discussed in Chapter 2. Tables 4.1 and 4.2 show the conditions under which the experiments were conducted. The engine speed, fuel mass, fuel injection timing, intake air temperature, and intake valve timing all remained constant during these experiments.

The experimental controller evaluation compares the results from two separate experiments. In the first experiment, the engine operated in an open-loop mode to collect data against which to compare the controller's performance. In the second experiment, the proportional controller altered the open-loop exhaust valve commands. The mean combustion timing of the late-phasing condition generated from the control

Table 4.1: Experimental conditions

Condition	Value
Engine speed	1800 RPM
Fuel mass	10 mg/cylinder/cycle
Fuel injection duration (for 10 mg)	10.3 CAD
Fuel end-of-injection timing	420 CADaTDCC
Intake valve opening	433 CADaTDCC
Intake valve closing	573 CADaTDCC

Table 4.2: Feedforward Exhaust Valve Commands

Condition	Nominal Case	Late Case
Exhaust valve opening	147 CADaTDCC	154 CADaTDCC
Exhaust valve closing	287 CADaTDCC	294 CADaTDCC

model served as the desired combustion phasing value for both conditions.

Figures 4.7, 4.8, 4.9, and 4.10 show the results of the two experiments described above in all four cylinders. Both open-loop and closed-loop data show the controller's ability to reduce variation in both θ_{50} and IMEP.

4.7 Discussion of Results

The simple proportional controller successfully reduces the variation in θ_{50} significantly by manipulating the exhaust valve closing angle over a range of approximately 3 CAD. Some oscillations in θ_{50} still exist even in closed-loop operation, but these are the result of disturbances to airflow and other parameters. Furthermore, by changing the underlying system dynamics, these disturbances cause oscillations of much smaller magnitudes.

Cylinders 1, 3, and 4 all operate in the late-phasing region with an open-loop exhaust valve timing of 293 CADaTDCC. However, cylinder 2 operates in the nominal region with that exhaust valve timing, and the closed-loop results show what happens when the late-phasing controller is applied to a nominal-phasing system. Yun et al. [50] noted the cylinder-to-cylinder differences in θ_{50} on GM ECOTEC HCCI engines,

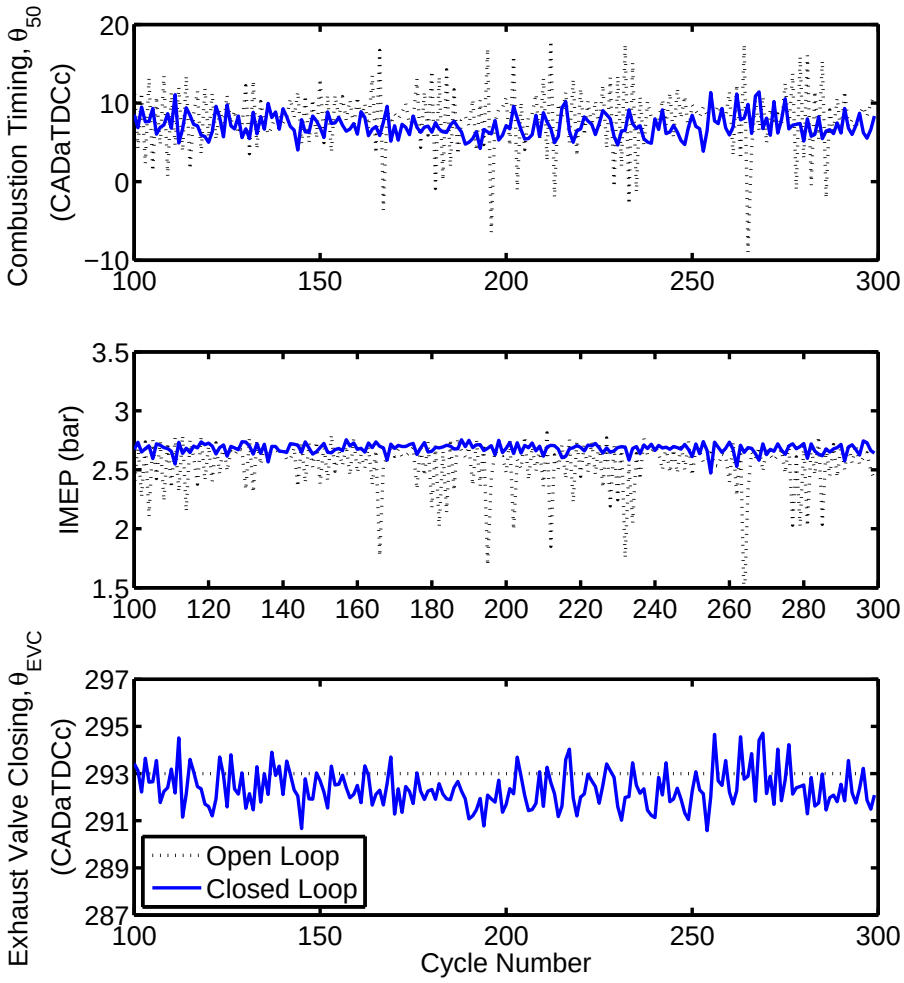

Figure 4.7: Closed-loop vs. open-loop θ_{50} and IMEP responses on cylinder 1

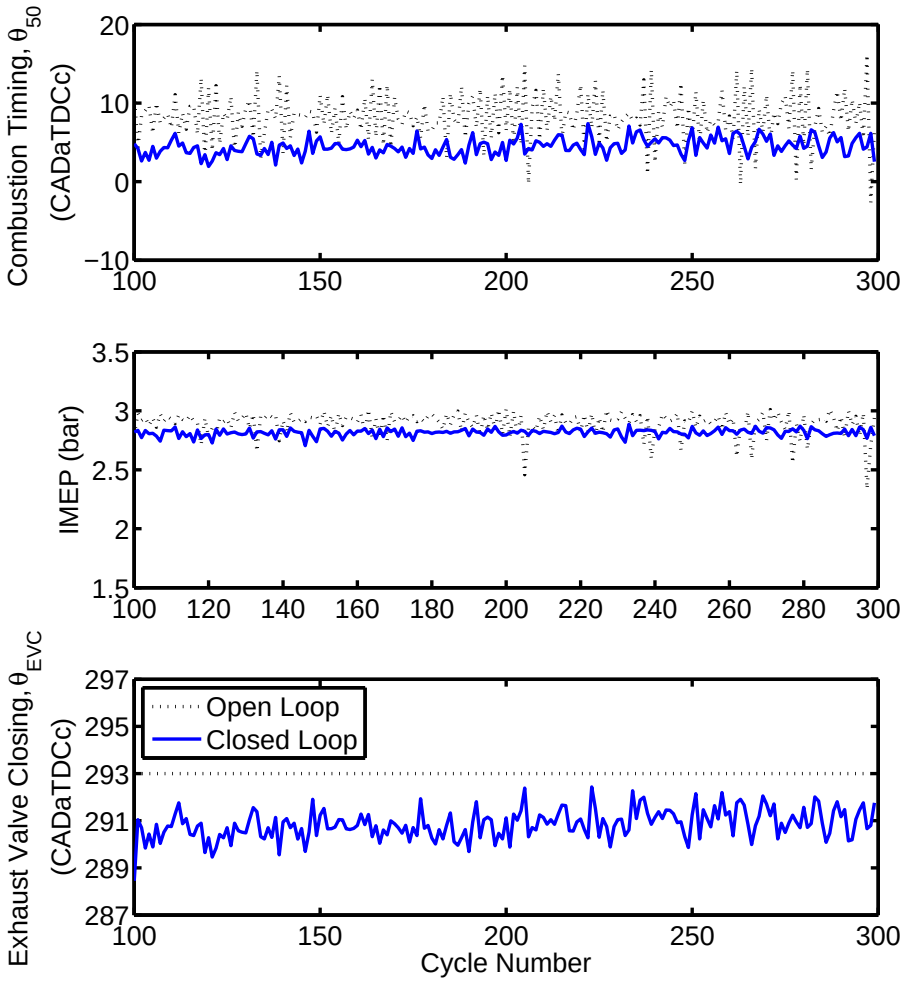

Figure 4.8: Closed-loop vs. open-loop θ_{50} and IMEP responses on cylinder 2

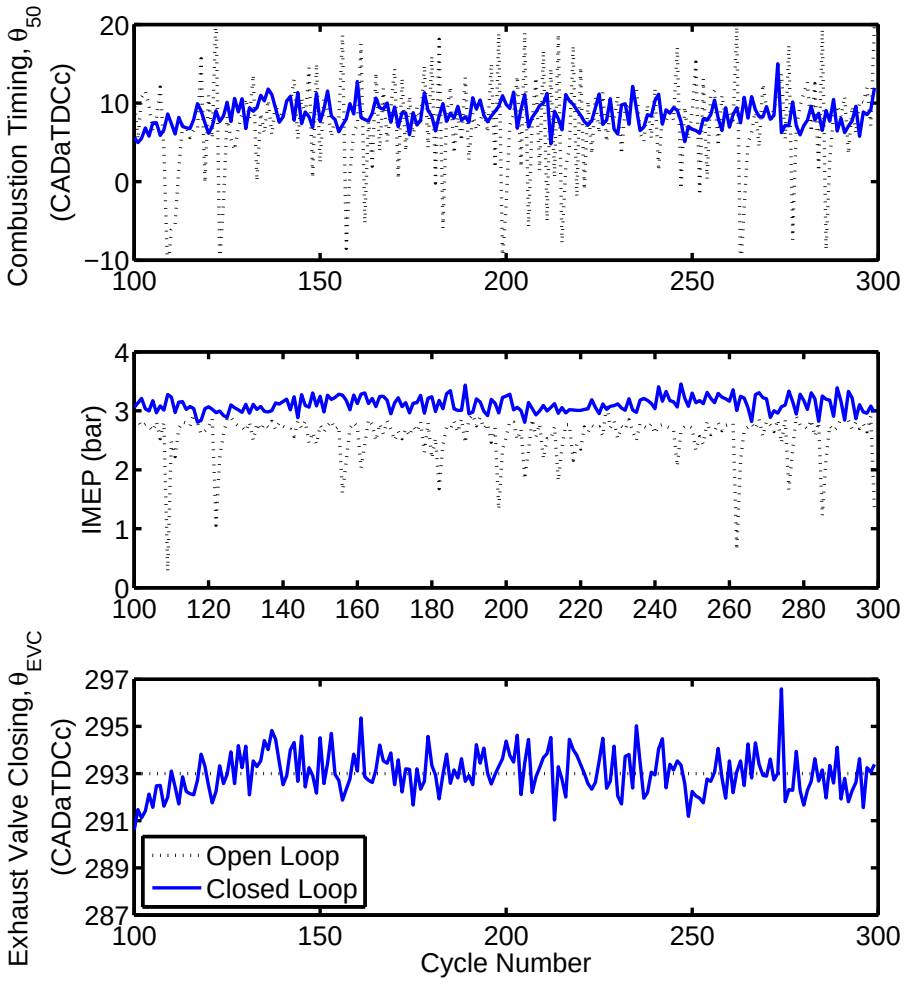

Figure 4.9: Closed-loop vs. open-loop θ_{50} and IMEP responses on cylinder 3

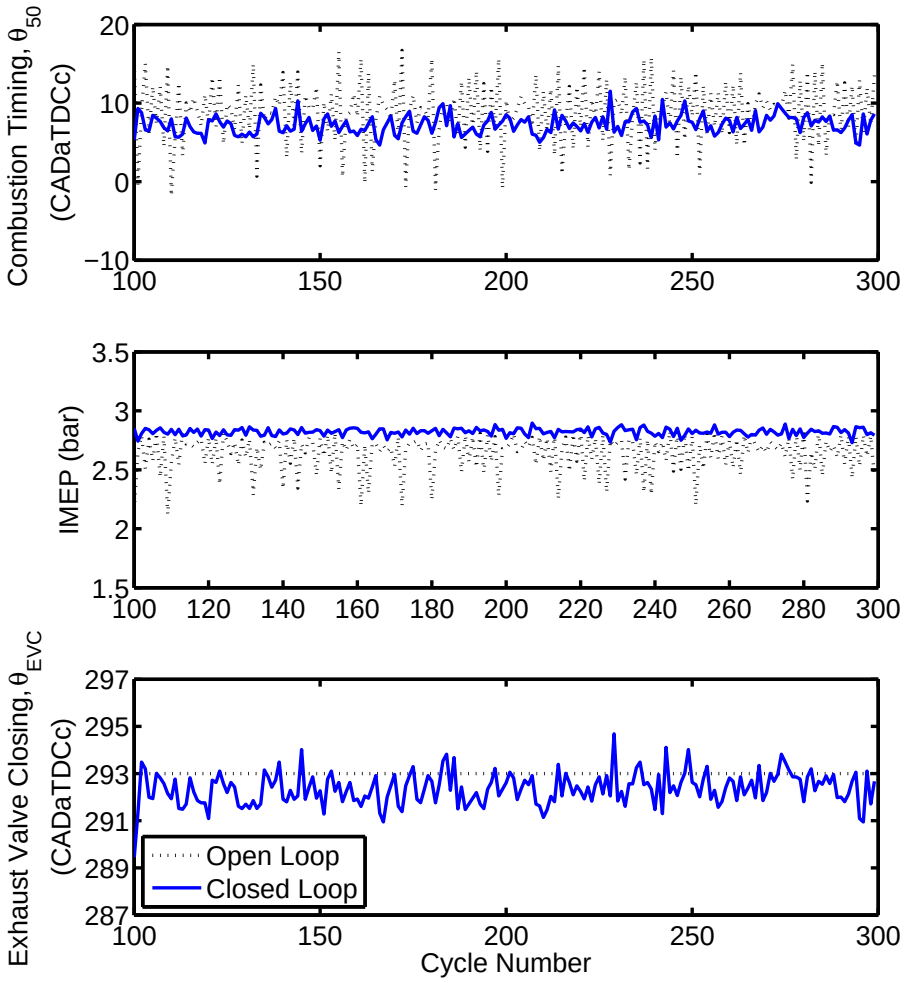

Figure 4.10: Closed-loop vs. open-loop θ_{50} and IMEP responses on cylinder 4

Table 4.3: IMEP Coefficient of Variation Reduction

Cylinder No.	Open Loop CoV	Closed Loop CoV
1	9.76 %	1.60 %
2	3.73 %	1.07 %
3	14.9 %	4.21 %
4	6.29 %	1.08 %

and found that cylinder 2 consistently had an earlier combustion timing than the other three cylinders; these results demonstrate that trend as well. In the cylinder 2 closed-loop results, the late-phasing controller holds the valve timing early because it expects that an early combustion timing will be followed by a late combustion timing, and the controller anticipates that it will need to retain extra exhaust to prevent that late combustion timing. However, because the cylinder is actually operating in the nominal phasing region, there are no oscillatory temperature dynamics present in the cylinder, so the combustion timing on the following cycle is early again, and the pattern repeats itself. The control gain is not large enough to make the nominal system unstable, so the cylinder will continue to function.

The controller is also successful at reducing the variation in IMEP through the same actions. Even though the controller did not act upon any explicit information about IMEP, it reduced the coefficient of variation in IMEP on all four cylinders by the amounts shown in Table 4.3. Considering that a CoV of 5% is the typical threshold for acceptable operating conditions, the controller effectively turned an undesirable operating condition into a very desirable one.

Additionally, more results from cylinder 4 show the controller's effectiveness further. Figure 4.11 shows another data set from cylinder 4 in which the controller reduced the coefficient of variation in IMEP from from 13.1% to 4.37% when switched on at cycle 129.

The controller's effectiveness demonstrates that the linearized control model sufficiently captures the dynamics of HCCI at late-phasing conditions as represented by the pole on the negative real-axis. This insight validates the physical modeling process used to capture the dynamics and design the controller, and it allows the

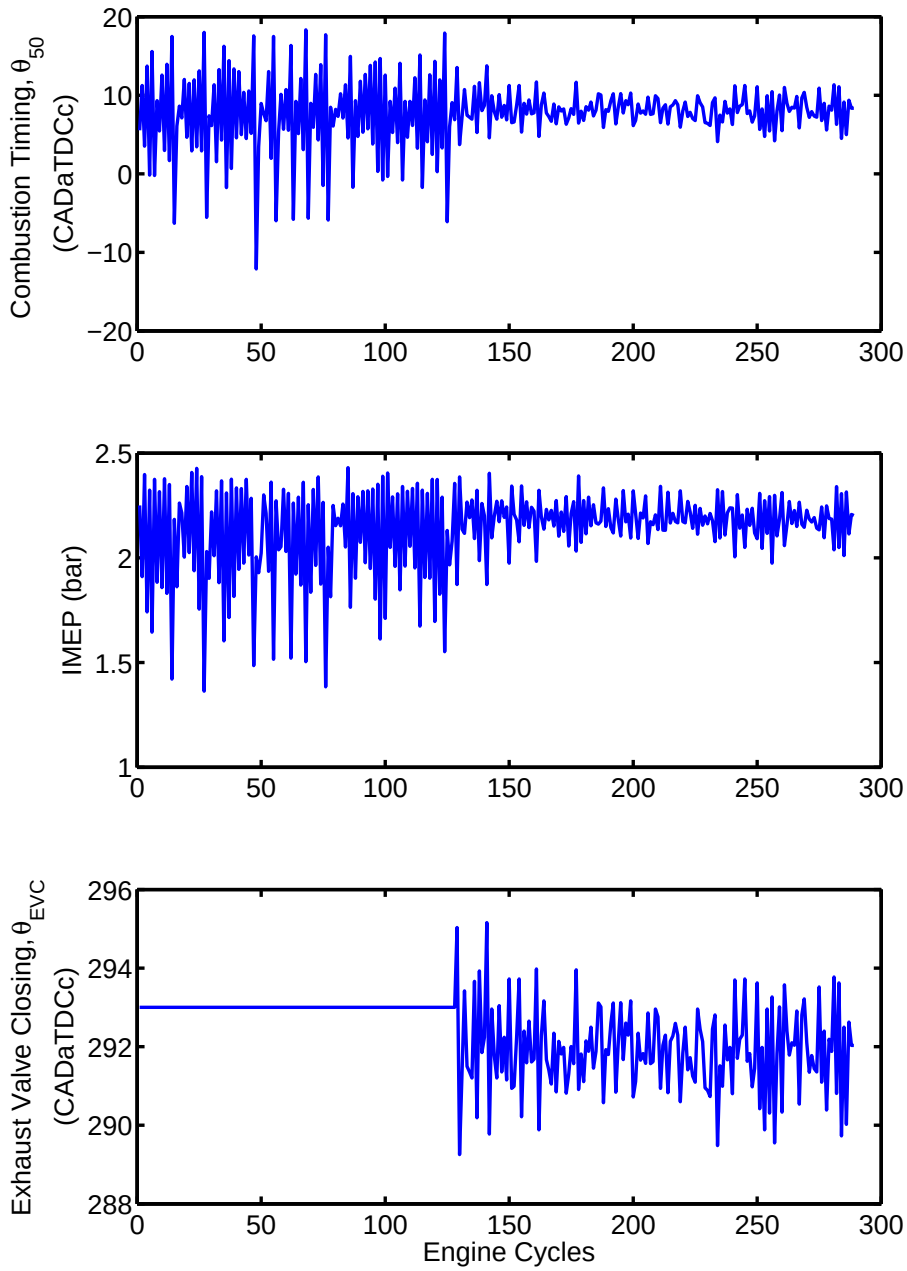

Figure 4.11: Second data set comparing closed-loop vs. open-loop θ_{50} and IMEP responses on cylinder 4

process to be used for other late-phasing conditions at higher loads, expanding the viable region of HCCI operation.

The valve control result also allows for other inputs, such as fuel mass or fuel injection timing [15, 16], to be considered for reducing the variance in combustion at these previously undesirable operating conditions. The underlying oscillatory dynamics of late-phasing HCCI conditions are not a result of the input choice; instead, the dynamics are determined by the relationship between the pre-combustion temperature and oxygen concentration from one engine cycle to the next as illustrated by the eigenvalue decompositions. Therefore, other inputs can also be employed to reduce the cyclic oscillations characteristic of late-phasing HCCI. These other methods are discussed further in Chapter 5.

Chapter 5

Comparing Actuators for Controlling HCCI

The previous chapter focused on modeling combustion instability as a negative real axis pole in a discrete-time system and manipulating that pole location with closed-loop exhaust valve timing control. This chapter focuses on controlling combustion timing with two different fuel injection strategies: changing the pilot injection timing and changing the main injection fuel quantity. The interest in the fuel control strategies arises from the hardware used to implement them. While the valve control strategy relies upon an expensive valve system that is difficult to implement in a production setting, the fuel strategies both rely on a relatively inexpensive and currently mass-produced direct fuel injection system to control HCCI combustion timing. The chapter ends by comparing the three control strategies to one another.

5.1 Pilot Injection Timing Input as Input

Song and Edwards [38] demonstrated that pilot injection timing, $\theta_{inj,pilot}$, can be an effective method for controlling combustion timing in recompression HCCI. A pilot injection strategy for HCCI requires injecting the fuel into the cylinder in two different injection events. The pilot event, which occurs first, is an injection of fuel that occurs during exhaust recompression; in this work it is always a 1 mg injection. The main

injection event, which occurs second, sees the rest of the fuel injected into the cylinder during the intake stroke. The fuel injected during the pilot event reacts with the hot exhaust during the recompression event and advances combustion timing as explained in Section 5.1.1. By altering the residence time in which the fuel is exposed to the hot exhaust, combustion timing can be affected.

5.1.1 Modeling Pilot Injection as an Arrhenius Threshold Change

Ravi et al. [31] successfully implemented a controller using pilot injection timing as an input to control combustion timing on a cycle-to-cycle basis in the nominal phasing region. Combustion timing control is achieved by injecting fuel into a mixture of retained exhaust gases; these gases are then recompressed and expanded prior to mixing with fresh air upon intake valve opening. Altering the timing of this pilot injection allows for control of combustion phasing.

Exposing the fuel to the elevated temperatures and pressures of the gases in the cylinder during recompression leads to one of three effects. First, the fuel evaporates upon entry in the cylinder, causing the retained exhaust charge to cool. This charge cooling has the effect of moving the ignition timing later. Second, the fuel molecules break down into smaller carbon-chain molecules in a process known as pyrolysis. Pyrolysis leads to two counteracting effects: the process of breaking down the fuel molecules is endothermic, causing the charge temperature to drop further. However, the smaller fuel molecules have a shorter ignition delay, which leads to advanced ignition timing; this shortened ignition delay typically more than offsets the endothermic reactions required to break down the fuel molecules. Finally, if enough oxygen is present in the cylinder, fuel reforming can occur, and CO and H_2 can be produced. Reforming also advances combustion timing.

The relationship between combustion timing and pilot injection timing is highly nonlinear. Figure 5.1 illustrates the relationship with experimental data. The conditions for the experiments are shown in Table 5.1. The relationship can be broken into three separate relationships:

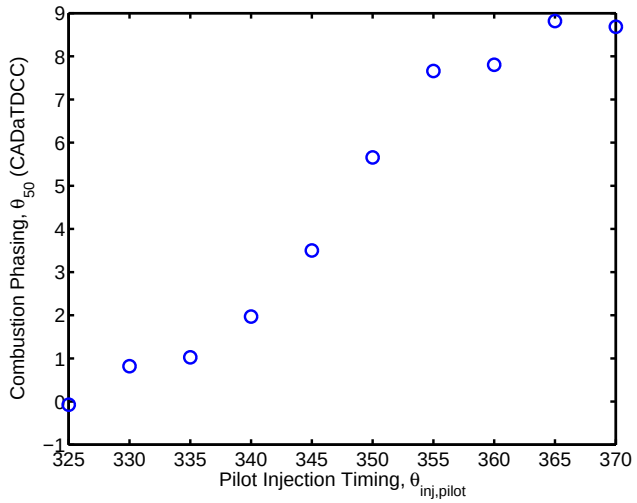

Figure 5.1: Relationship between combustion timing and pilot injection timing

Table 5.1: Pilot injection timing sweep experimental conditions

Condition	Value
Engine speed	1800 RPM
Intake valve opening	433 CADaTDCc
Intake valve closing	573 CADaTDCc
Exhaust valve opening	156 CADaTDCc
Exhaust valve closing	296 CADaTDCc
Main injection fuel mass	9 mg/cylinder/cycle
Pilot injection fuel mass	1 mg/cylinder/cycle
Main injection timing	420 CADaTDCc

$$\begin{aligned} t_{res} &= f_1\left(\theta_{inj,pilot}\right) \\ K_{th} &= f_2\left(t_{res}\right) \\ \theta_{50} &= f_3\left(K_{th}\right) \end{aligned} \tag{5.1}$$

where t_{res} is the residence time for the fuel in the cylinder during recompression. In the first relationship, residence time and injection timing are related through engine speed, ω, by equation 5.2:

$$t_{res} = \frac{\theta_{inj,main} - \theta_{inj,pilot}}{\omega} \tag{5.2}$$

where $\theta_{inj,main}$ is the fixed end-of-injection timing for the main fuel injection event, $\theta_{inj,main} = 420$ CADaTDCc, and $\theta_{inj,pilot}$ is the end-of-injection timing for the pilot injection.

The relationship $\theta_{50} = f_3(K_{th})$ is then determined by finding the input Arrhenius thresholds K_{th} that correspond to the experimentally obtained combustion timings through simulation. Figure 5.2 shows the relationship between the Arrhenius threshold and combustion timing. The relationship is well approximated by a linear function and therefore allows for a linear controller to be designed that manipulates K_{th} in order to achieve a desired θ_{50}.

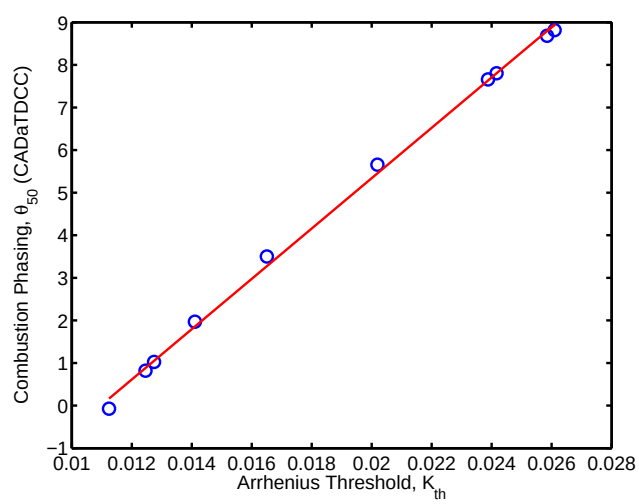

Figure 5.2: Relationship between combustion timing and Arrhenius threshold

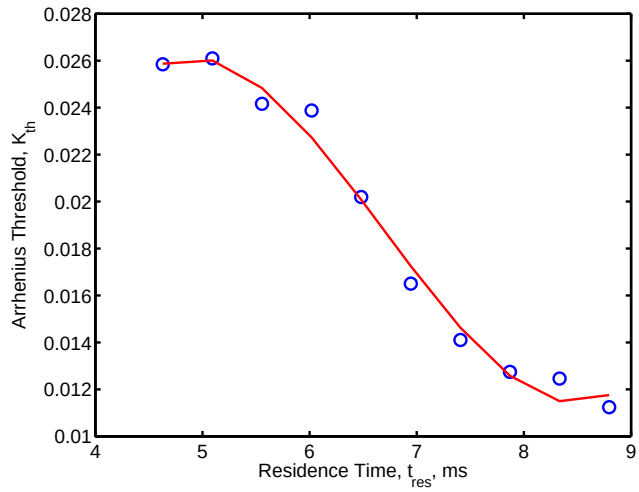

Figure 5.3: Relationship between Arrhenius threshold and fuel residence time during recompression

The final step is to determine the relationship between in-cylinder residence time and Arrhenius threshold. Figure 5.3 illustrates the dependence of Arrhenius threshold upon residence time, t_{res}. The nonlinear relationship between t_{res} and K_{th} effectively isolates the input nonlinearity associated with $\theta_{inj,pilot}$ into a steady-state relationship because the system dynamics can be modeled as occurring in the relationship between K_{th} and θ_{50}. The model incorporates the relationship as a polynomial fit to the experimental data presented in Figure 5.3.

Changing the Arrhenius threshold can be thought of as simply shifting the combustion timing map from equation 3.7 vertically. Decreasing the Arrhenius threshold advances combustion timing, while increasing the threshold retards combustion timing. Figures 5.4 and 5.5 illustrate two different Arrhenius threshold conditions and show different combustion timings for the same oxygen and temperature states. There is some change of shape between the two maps, but the primary difference between them is their vertical position.

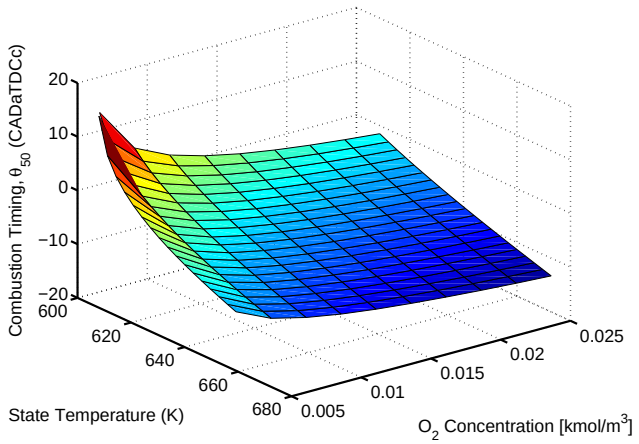

Figure 5.4: θ_{50} map showing an early pilot injection

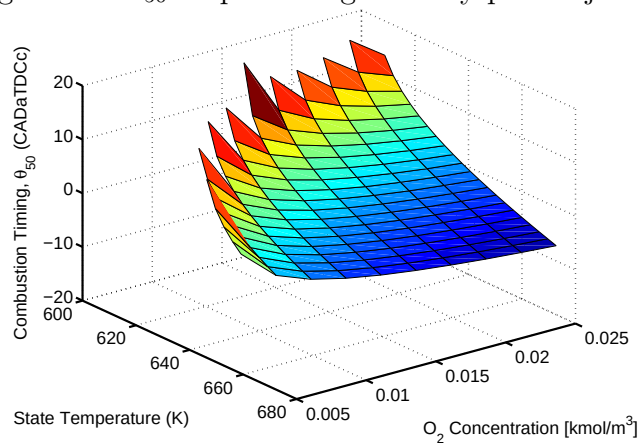

Figure 5.5: θ_{50} map showing a late pilot injection

5.1.2 Linearized Pilot Injection Model

Reducing the linearized control model from Section 4.1 simplifies the pilot injection control problem. Throughout this section, the model's state, x_k, and input, u_k, are defined as

$$x_k = \left[\frac{[O_2]_k - [O_2]_{ss}}{[O_2]_{ss}}, \ \frac{T_k - T_{ss}}{T_{ss}} \ \frac{K_{th,k} - K_{th,ss}}{K_{th,ss}} \right]^T$$

$$u_k = \frac{u_{th,k} - u_{th,ss}}{u_{th,ss}}$$

Fittingly, $A \in \mathbb{R}^{3\times3}$ is the reduced system matrix, $B \in \mathbb{R}^{3\times1}$ is the reduced input matrix, and $C \in \mathbb{R}^{1\times3}$ is the reduced output matrix. Figure 5.6 depicts the reduced model. The Arrhenius state, K_{th}, is equal to the Arrhenius input, u_{th}, ($K_{th,k+1} = u_{th,k}$) because the model assumes complete combustion. If the model assumed that smaller fuel molecules such as methane or ethane were present in the cylinder after combustion and before pilot injection occurred, then instead of only being a function of the Arrhenius input, the Arrhenius state would be a function of the previous state values and the Arrhenius input. ($K_{th,k+1} \neq u_{th,k}$; $K_{th,k+1} = f([O_2]_k, T_k, K_{th,k}, u_{th,k})$)

A linearization of the nonlinear model at a nominal operating condition with $\theta_{50} = 5$ CADaTDCc yields the state-space system shown by the system of equations in equation 5.3.

$$A_{nominal,pilot} = \begin{bmatrix} 0.53 & 0.27 & 0.022 \\ -0.0060 & 0.037 & 0.012 \\ 0 & 0 & 0 \end{bmatrix} \quad B_{nominal,pilot} = \begin{bmatrix} 0 \\ 0 \\ 1 \end{bmatrix}$$
$$C_{nominal,pilot} = \begin{bmatrix} -0.020 & -0.58 & 0.039 \end{bmatrix} \tag{5.3}$$

Similar to the exhaust valve input case illustrated by equation 4.5, the circled $A_{nominal,pilot}(2,2)$ entry is positive and nearly zero, indicating that the relationship between temperature on one cycle and the next is not oscillatory. Additionally, the

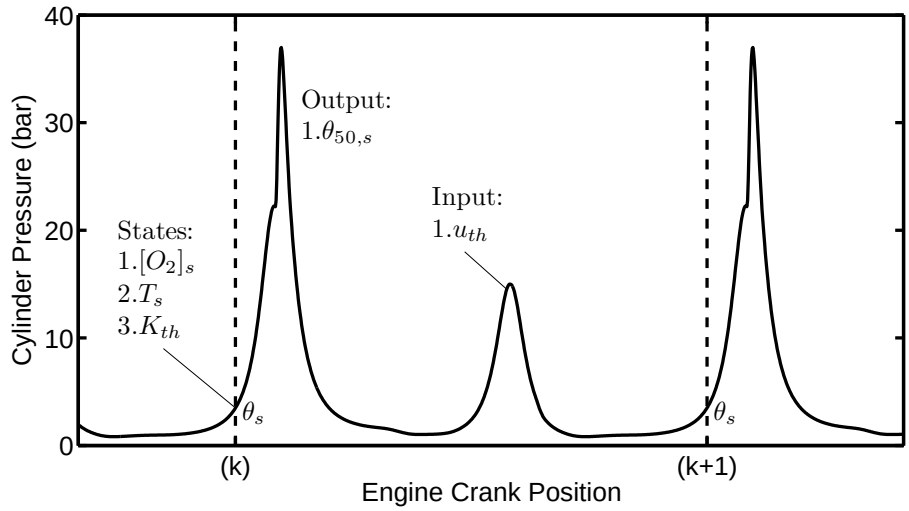

Figure 5.6: Reduced model showing the pilot injection model with the Arrhenius threshold input

third row of $A_{nominal,pilot}$ is all zeros because of the complete combustion assumption. Changing that assumption would result in non-zero entries in the third row, since in that case the states from the current engine cycle would influence the Arrhenius state on the following cycle. The nominal phasing system of equations can be combined into a transfer function relating the input, u_{th} to the output, θ_{50}, shown in equation 5.4.

$$G_{nominal,pilot}(z) \quad = 0.039\frac{(z-0.55)(z-0.21)}{z(z-0.54)(z-0.040)} \tag{5.4}$$

Meanwhile, a linearization of the nonlinear model at a late operating condition with $\theta_{50} = 11$ CADaTDCc yields the state-space system shown by the system of equations in equation 5.5.

$$A_{late,pilot} = \begin{bmatrix} 0.50 & 0.088 & 0.032 \\ -0.011 & \text{-0.10} & 0.022 \\ 0 & 0 & 0 \end{bmatrix} \quad B_{late,pilot} = \begin{bmatrix} 0 \\ 0 \\ 1 \end{bmatrix}$$

$$C_{late,pilot} = \begin{bmatrix} -0.036 & -1.04 & 0.069 \end{bmatrix} \tag{5.5}$$

As in the exhaust valve input case, the circled $A_{late,pilot}(2,2)$ is less than zero, indicating an oscillatory relationship between the state temperature on one engine cycle and the next. Again, the late-phasing system of equations can be combined to form a transfer function, shown in equation 5.6.

$$G_{late,pilot}(z) \quad = 0.069\tfrac{(z-0.51)(z-0.22)}{z(z-0.49)(z+0.10)} \tag{5.6}$$

As with the valve input linearizations in equations 4.8 and 4.9, the key difference between the two transfer functions is the location of the last pole. In the nominal case, all three poles are nonnegative at locations $z = 0.54, z = .04$, and $z = 0$. In the late-phasing case, one of the poles is negative; there, the pole locations are at $z = .49, z = 0$, and $z = -0.10$. This negative pole again drives the oscillations seen at late conditions.

Figures 5.7 and 5.8 illustrate root loci of the two pilot injection models. Figure 5.7 shows the nominal system while Figure 5.8 shows the late-phasing system.

5.1.3 Pilot Injection Control Design

The control design objective for the late-phasing model is to reduce the oscillations in combustion timing. According to the linearized model, moving the negative real axis pole into the right half plane should reduce the oscillations observed at late-phasing operating conditions.

A lag compensator design with a negative gain, shown in equation 5.7, reduces the oscillatory nature of the operating condition. The zero of the lag compensator cancels the time delay pole at $z = 0$. The negative gain then moves the left half plane pole

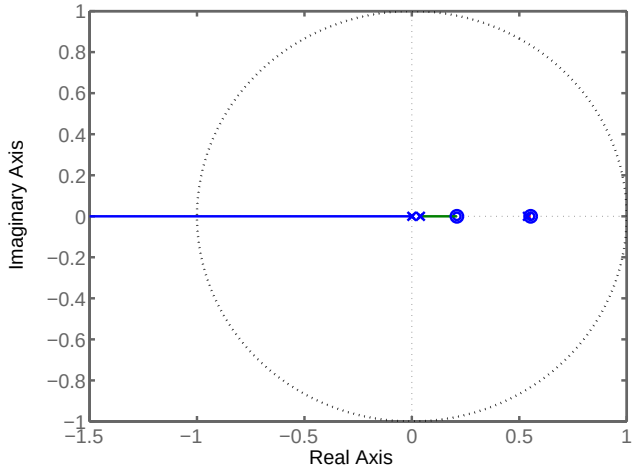

Figure 5.7: Root locus of nominal linearization

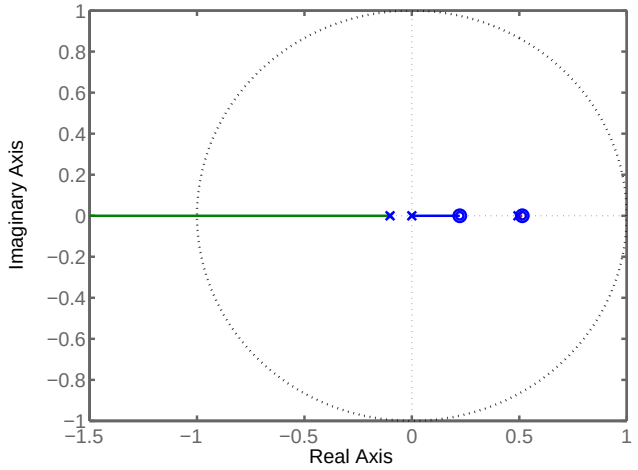

Figure 5.8: Root locus of late-phasing linearization

into the right-half plane. The compensator also moves the pole located at $z = 0.49$ to the left, improving the response time of system. It accomplishes this while keeping all the closed-loop poles inside the unit circle and therefore not inducing any stability concerns. Figure 5.9 illustrates the compensator, and Figure 5.10 shows a close-up view of the compensator.

$$K_{late,pilot}(z) = -6\frac{(z)}{(z-0.25)} \tag{5.7}$$

5.1.4 Pilot Injection Control Results

The controller successfully reduces the magnitude of the oscillations in θ_{50}. Figure 5.11 shows the performance of the controller operating on the research engine. The controller is switched on at cycle 206; the reduction in the peak-to-peak oscillations is apparent. The controller reduces the standard deviation of θ_{50} from 6.23 CAD to 1.78 CAD. The controller also manages to reduce the cycle-to-cycle variations in IMEP even though that is not an explicit goal of the controller; it reduces the coefficient of variation in IMEP from 14.9% to 6.46%.

5.2 Main Fuel Injection Quantity as an Input

The fuel quantity input has two distinct effects on combustion timing: charge cooling, in which fuel injected into the cylinder evaporates and cools the charge, acting to retard combustion timing, and energy release, in which the additional fuel injected releases more energy into the exhaust, acting to advance combustion timing. The two different effects result in the fuel injection quantity input having a non-minimum phase nature, and that non-minimum phase nature creates one of two primary challenge surrounding its use as a suitable input for controlling combustion phasing. As the quantity of fuel injected into the cylinder changes, the amount of charge cooling that takes place in the cylinder changes and affects the combustion phasing by changing the temperature of the cylinder contents prior to combustion on the following cycle. Unfortunately, the quantity of charge cooling resulting from a given mass

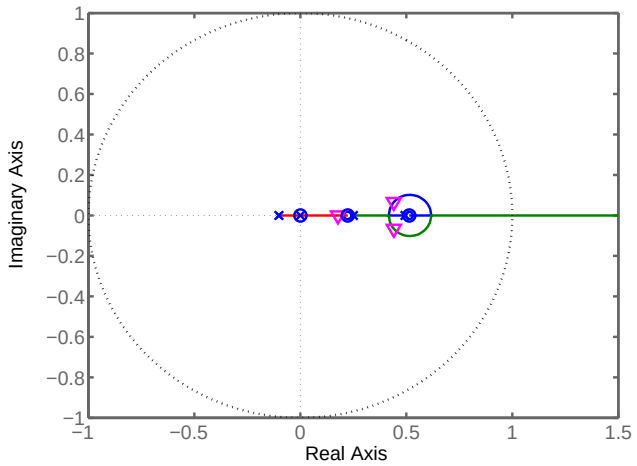

Figure 5.9: Root locus of late-phasing linearization showing closed loop pole locations

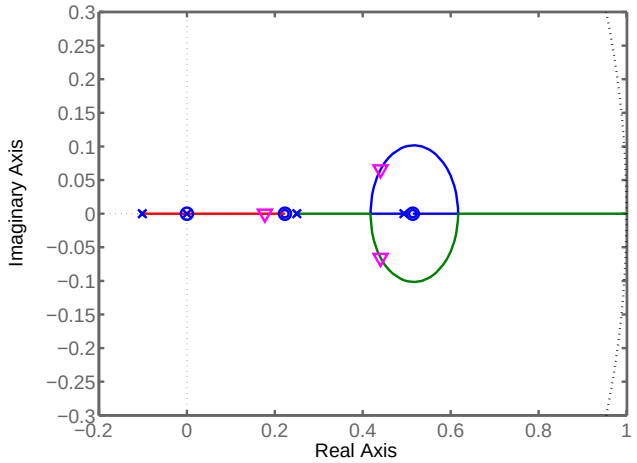

Figure 5.10: Zoomed root locus of late-phasing linearization showing closed loop pole locations

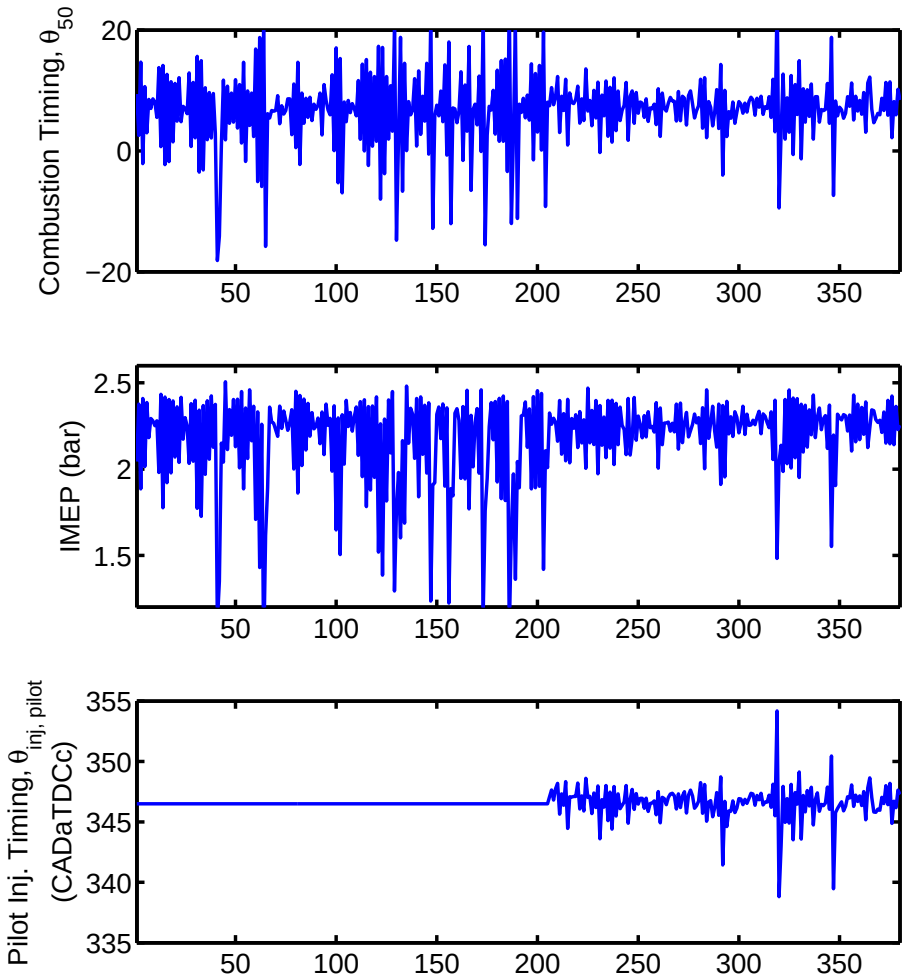

Figure 5.11: Experimental results showing reductions in both combustion timing variation and IMEP variation using pilot injection timing control

of fuel injected is difficult to capture in a simple, control-oriented model. Thus, any controller seeking to use fuel quantity inputs to control combustion phasing must be robust to different assumptions about the extent of charge cooling that takes place in the cylinder as a result of changes in the fuel injection quantity.

The second primary challenge with using fuel quantity to control combustion timing is that fuel is directly tied to the work output of the engine. Thus, any changes to fuel mass intended to change θ_{50} would also change work and IMEP.

5.2.1 Linearized Main Fuel Injection Quantity Model

Similar to both the valve control problem and the pilot injection control problem, reducing the linearized control model simplifies the fuel quantity control problem. Throughout this section, the model's state, x_k, and input, u_k, are defined as

$$x_k = \left[\frac{[O_2]_k - [O_2]_{ss}}{[O_2]_{ss}}, \ \frac{T_k - T_{ss}}{T_{ss}} \ \frac{[f]_k - [f]_{ss}}{[f]_{ss}} \right]^T$$

$$u_k = \frac{n_{f,k} - n_{f,ss}}{n_{f,ss}}$$

Again, $A \in \mathbb{R}^{3\times3}$ is the reduced system matrix, $B \in \mathbb{R}^{3\times1}$ is the reduced input matrix, and $C \in \mathbb{R}^{1\times3}$ is the reduced output matrix. Figure 5.12 illustrates the reduced model.

A linearization of the nonlinear model at a late operating condition with a $\theta_{50} =$ 13 CADaTDCc yields the state-space system shown by the system of equations in equation 5.8.

$$A_{late,qty,full\ cc} = \begin{bmatrix} 0.44 & -0.053 & -0.15 \\ -0.014 & \text{-0.26} & 0.051 \\ 0 & 0 & 0 \end{bmatrix} \quad B_{late,qty,full\ cc} = \begin{bmatrix} 0.031 \\ -0.022 \\ 1 \end{bmatrix}$$

$$C_{late,qty,full\ cc} = \begin{bmatrix} -0.061 & -1.70 & 0.013 \end{bmatrix} \tag{5.8}$$

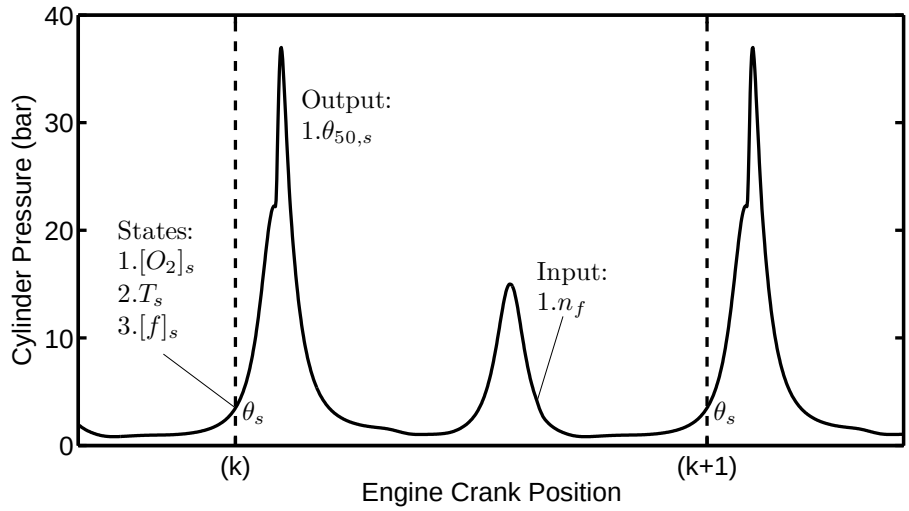

Figure 5.12: Reduced model showing the fuel quantity model with the number of moles of fuel input

Similar to both the exhaust valve closing and pilot injection input cases, the circled $A_{late,qty,full\ cc}(2,2)$ entry indicates that the relationship between state temperature on one cycle and the following one is oscillatory. The state-space system can be combined into a transfer function that shows the pole and zero locations of the linearized system.

$$G(z)_{late,qty,full\ cc} = 0.048\frac{(z-0.49)(z-1.51)}{z(z-0.44)(z+0.26)} \tag{5.9}$$

The transfer function mapping the fuel quantity input to the combustion timing output has two zeros and three poles. Similar to the exhaust valve and pilot injection cases, one of the poles lies on the negative real axis, which leads to oscillations in the system output. This open-loop pole location explains how the model is able to capture the oscillatory dynamics of the late phasing condition.

Additionally, the transfer function has a negative DC gain, meaning that a step increase in the quantity of fuel injected into the cylinder will result in an earlier combustion timing after the system dynamics settle. The negative DC gain aligns well with physical intuition about the problem: by adding more fuel to the system, more energy is released during combustion, resulting in hotter retained exhaust and

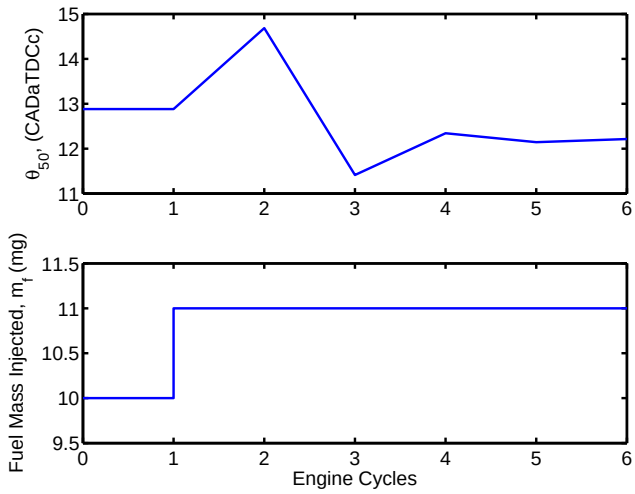

Figure 5.13: Simulation showing a the effect of a step change in fuel quantity on combustion timing

a higher state temperature on the subsequent cycle. This higher state temperature initiates combustion earlier and leads to advanced combustion timings.

Finally, one of the zeros is a non-minimum phase zero, located at $z = 1.51$, to the right of $z = 1$. The non-minimum phase zero causes the system's response to move in the opposite direction of the steady-state response on the first cycle and then to move in the direction of the steady-state response on subsequent cycles. This means that a step increase in fuel quantity on cycle k will first lead to a later combustion phasing on cycle $k + 1$ before leading to earlier phasings on cycle $k + 2$ and all subsequent cycles. The non-minimum phase behavior results from additional charge cooling of the retained exhaust, which occurs due to the increased fuel quantity injected in the cylinder. The charge cooling occurring on cycle k results in a lower state temperature and a later combustion phasing on cycle $k + 1$.

Figure 5.13 shows the response of the linearized model to a 10 % step increase in fuel quantity. The non-minimum phase behavior, negative DC gain, and oscillatory behavior are all visible in the output's response.

5.2.2 Examination of Charge Cooling

Roelle et al. [34] illustrated the non-minimum phase relationship between fuel quantity and combustion phasing. However, their model showed a smaller impact of charge cooling on the combustion phasing on cycle $k+1$ for a step change in fuel quantity on cycle k than this model shows. Specifically, for a given change in injected fuel mass, this model predicts that combustion timing shifts later on the first cycle following the fueling change than the model in Roelle et al. [34] predicts. Although both models are based on gasoline, the differences between them arise from different assumptions about the enthalpy of vaporization and the enthalpy-temperature relationship of the gasoline.

Figure 5.14 shows experimental results of charge cooling from the engine. The asterisk symbols show the effect of main fuel mass injected upon cycle k against the combustion phasing from cycle $k+1$, the immediately subsequent combustion event, and a dashed trend line shows a linear fit of that data. As the model predicts, the line slopes positively, indicating that as injected fuel quantity increases, charge cooling increases and combustion phasing retards on the following cycle. The plus-sign symbols illustrate the effect of mass of fuel injected on cycle k upon the combustion phasing from cycle $k+2$, and a solid trend line shows the linear fit of the data. Again, as the model predicts, the solid line slopes negatively, indicating that as injected fuel quantity increases, energy release increases and combustion timing advances on subsequent cycles.

The slopes of the trend lines in Figure 5.14 illustrate the impact the fueling change has on the engine on average. The dashed line, representing the change occurring to combustion timing on the combustion event immediately following the fueling change, has a slope of 0.45, indicating that on average combustion timing retards by roughly one-half of one degree in the engine on the cycle following a 1 mg fueling increase from 10 mg to 11 mg. The solid line, representing the change occurring to combustion timing on the second combustion event following the fueling change, has a slope of -1.91, indicating that on average combustion timing advances by roughly two degrees ahead of the pre-fueling increase combustion timing in the engine on the second cycle following the fueling change.

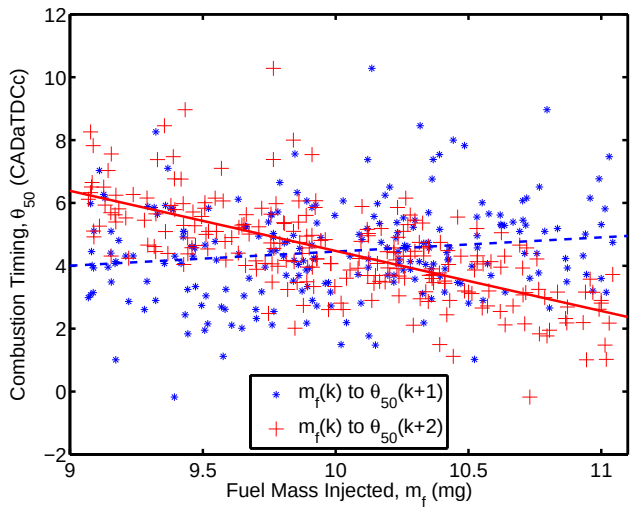

Figure 5.14: Experimental results showing the effect of fuel mass injected on cycle k on combustion phasing on cycle $k+1$ and combustion phasing on cycle $k+2$

The experimentally-obtained numbers differ from the values predicted by the model. The model predicts that combustion retards by 4.31 CAD on the cycle after the 1 mg fueling increase, which is basically an order of magnitude greater than the 0.45 CAD change observed on the engine for the same fueling change. Thus, the disagreement indicates that the model predicts about ten times the amount of combustion timing change that the engine exhibits. The model also predicts that the combustion timing advances by 1.30 CAD beyond the pre-fueling increase combustion timing on the second cycle after combustion, which is relatively similar to the 1.91 CAD advance observed on the engine. These numbers suggest that the model drastically overstates the amount of charge cooling that occurs due to fuel injection, but ultimately captures the total effect of fuel injection changes reasonably well.

The primary explanation for this overstatement is the difficulty in modeling the thermodynamic state of the fuel when it enters the cylinder. The model assumes that the fuel is some abstract approximation of gasoline, fully liquid, and at a temperature of 300 K when it leaves the fuel injector and enters the cylinder. The actual fuel differs in composition from the modeled fuel and is almost certainly warmer than 300 K when it leaves the fuel injector. These facts make it understandable that such

discrepancy between the model and experiment exist regarding the quantity of charge cooling taking place in cylinder. The facts also illustrate that considering models that include less charge cooling would be advantageous to effective control design.

One simple strategy to test the impact charge cooling has on fuel quantity as an input is to simply modify the linearized model to reduce its charge cooling characteristic and then design one controller that moves the system poles to desirable locations for both the reduced charge cooling model and the full charge cooling model. Physically, assuming that the fuel was warmer than 300 K and either had a lower enthalpy of vaporization or was partially vaporized at injection would reduce the amount of charge cooling associated with increases in fuel injection quantities. In the linearized model, the charge cooling reduction is accomplished by modifying the input matrix, $B_{late,qty,full\ cc}$, in equation 5.8 so that the effect of changing the amount of fuel injected on cycle k will have less impact on the phasing on cycle $k+1$. By setting $B_{late,qty,full\ cc}(2) = 0$, any changes in fuel quantity will not effect state temperature on the following cycle through the input; those changes will instead only effect state temperature through the fuel and oxygen states in the system dynamics. Thus, setting $B_{late,qty,full\ cc}(2) = 0$ establishes a lower bound on the amount of charge cooling in the system. Equation 5.10 shows the reduced charge cooling linear model, and it highlights the circled $B_{late,qty,reduced\ cc}(2)$ entry.

$$A_{late,qty,reduced\ cc} = \begin{bmatrix} 0.44 & -0.053 & -0.15 \\ -0.014 & \text{-0.26} & 0.051 \\ 0 & 0 & 0 \end{bmatrix} \quad B_{late,qty,reduced\ cc} = \begin{bmatrix} 0.031 \\ 0 \\ 1 \end{bmatrix}$$
$$C_{late,qty,reduced\ cc} = \begin{bmatrix} -0.061 & -1.70 & 0.013 \end{bmatrix} \tag{5.10}$$

Figure 5.15 compares the step responses of the full charge cooling linearized model, the reduced charge cooling linearized model, and an identified experimental model to each other. The only difference between the two linearized models results from the differing input matrices, which can be seen between cycles 1 and 2. The two systems follow parallel trajectories after the cycle 2 because they have the identical system

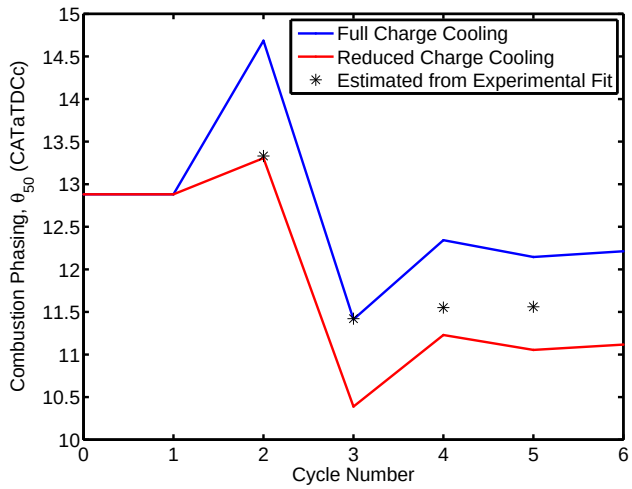

Figure 5.15: Plot showing simulations for both the full charge cooling model and the reduced charge cooling model. The two simulations bound the estimated experimental step response.

matrix, A.

Equation 5.11 shows the transfer function for the reduced charge cooling linearized system. Both the full charge cooling and reduced charge cooling systems have poles at $z = 0$, $z = 0.44$, and $z = -0.26$, and the full charge cooling system has a zero at $z = 0.49$ while the reduced charge cooling system has a zero at $z = 0.48$. The key difference between the two systems is the non-minimum phase zero location: in the full charge cooling system, the zero is located at $z = 1.51$, while in the reduced charge cooling system, the zero is located at $z = 6.57$. Thus, the different assumptions about charge cooling can be described simply as different zero locations.

$$G_{late,qty,reduced\ cc}(z) \quad = 0.011\frac{(z-0.48)(z-6.57)}{z(z-0.44)(z+0.26)} \tag{5.11}$$

The two different zero locations can be visualized in Figs. 5.16 and 5.17, which show the root loci for both systems.

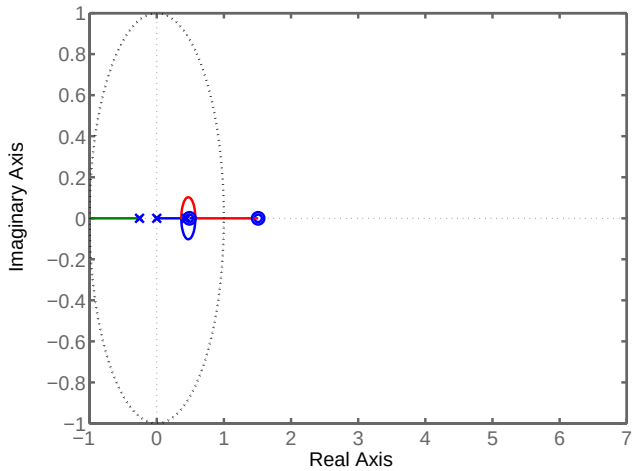

Figure 5.16: Root locus of linearized model with full charge cooling

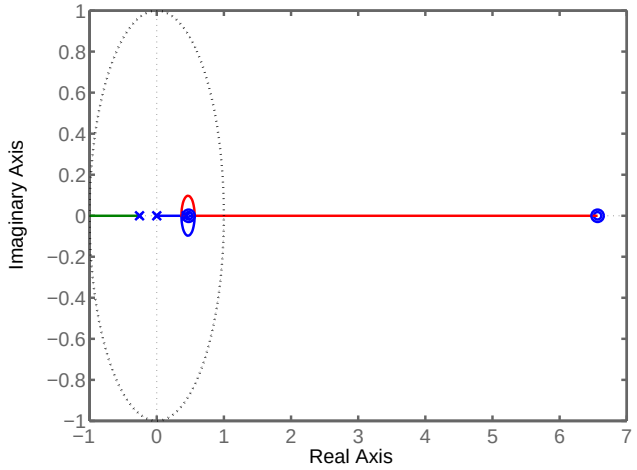

Figure 5.17: Root locus of linearized model with reduced charge cooling

5.2.3 Fuel Quantity Control Design

The controller for the late-phasing system needs to fulfill two goals: first, eliminate the cycle-to-cycle oscillations in θ_{50}, and second, be robust to model uncertainty regarding charge cooling. A lag compensator with a negative gain, shown in Eq. 5.12, meets both of these objectives.

$$K_{late,qty,both}(z) = -6\frac{z}{(z-0.7)} \tag{5.12}$$

The intuition behind the compensator is straightforward. The negative system gain moves the negative real axis pole back into the right-half plane in both discrete-time systems, removing the oscillating dynamics. The zero in the lag compensator is placed at the origin, canceling the open-loop pole at $z = 0$ in both systems. The compensator adds a pole at $z = 0.7$ to both systems, effectively filtering oscillations out of the system. The compensator accomplishes both its objectives while keeping all the closed-loop poles inside the unit circle and therefore not inducing any stability concerns.

Figure 5.18 shows a root locus illustrating the control design for the full charge cooling model, and Figure 5.19 shows a root locus for the reduced charge cooling model. The figures illustrate that the closed-loop poles for both systems lie at similar locations. In the full charge cooling system, the closed-loop pole locations occur at $z = 0.54$ and $z = 0.29 \pm 0.31i$, while in the reduced charge cooling system, the closed-loop pole locations occur at $z = 0.50$ and $z = 0.22 \pm 0.39i$.

5.2.4 Fuel Quantity Control Results and Discussion

The fuel quantity controller reduced the variation in combustion timing while effectively holding the mean main injection fuel mass constant. The standard deviation of combustion timing dropped from 4.94 CAD in open loop to 2.79 CAD in closed-loop. Again, it also reduced the coefficient of variation in IMEP from 9.96% in open loop to 5.80% in closed-loop, even though the controller did not explicitly act on any information about IMEP. Table 5.2 summarizes the IMEP improvements for the data presented in Figure 5.22.

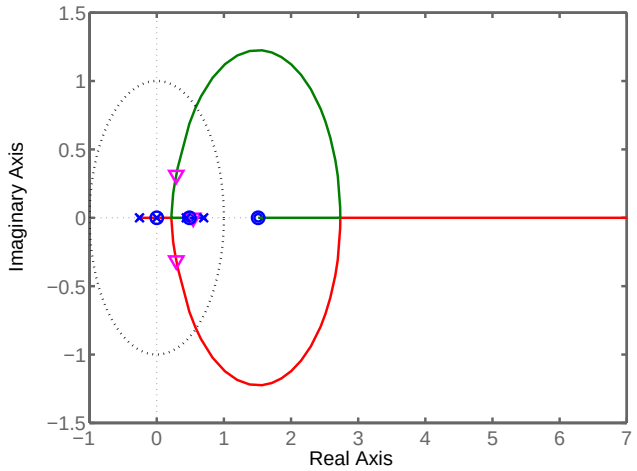

Figure 5.18: Root locus of linearized model with full charge cooling showing closed loop pole locations

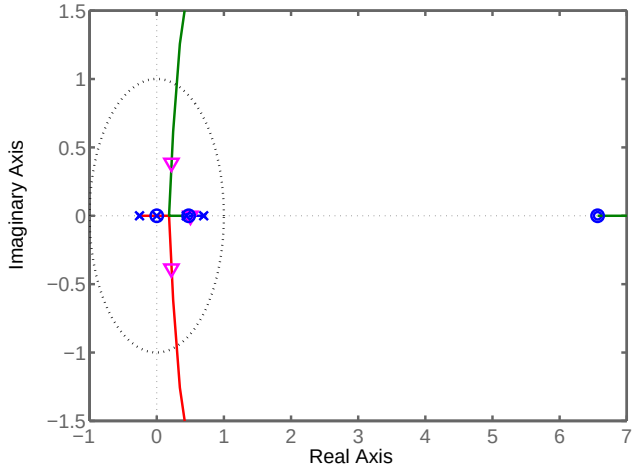

Figure 5.19: Root locus of linearized model with reduced charge cooling showing closed loop pole locations

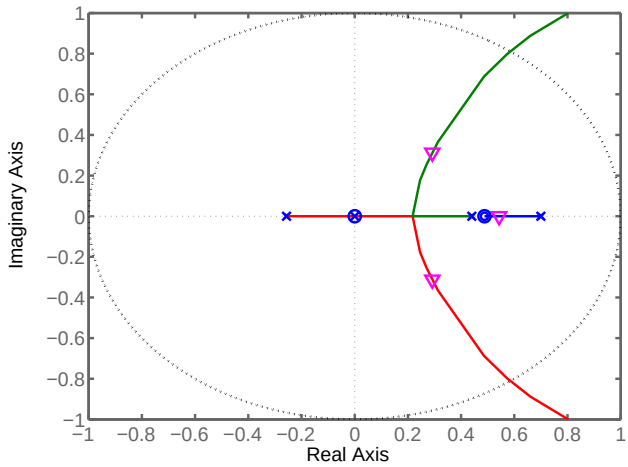

Figure 5.20: Zoomed root locus of linearized model with full charge cooling showing closed loop pole locations

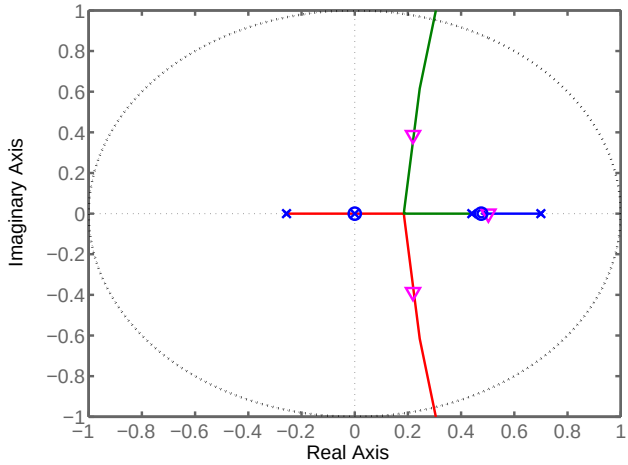

Figure 5.21: Zoomed root locus of linearized model with reduced charge cooling showing closed loop pole locations

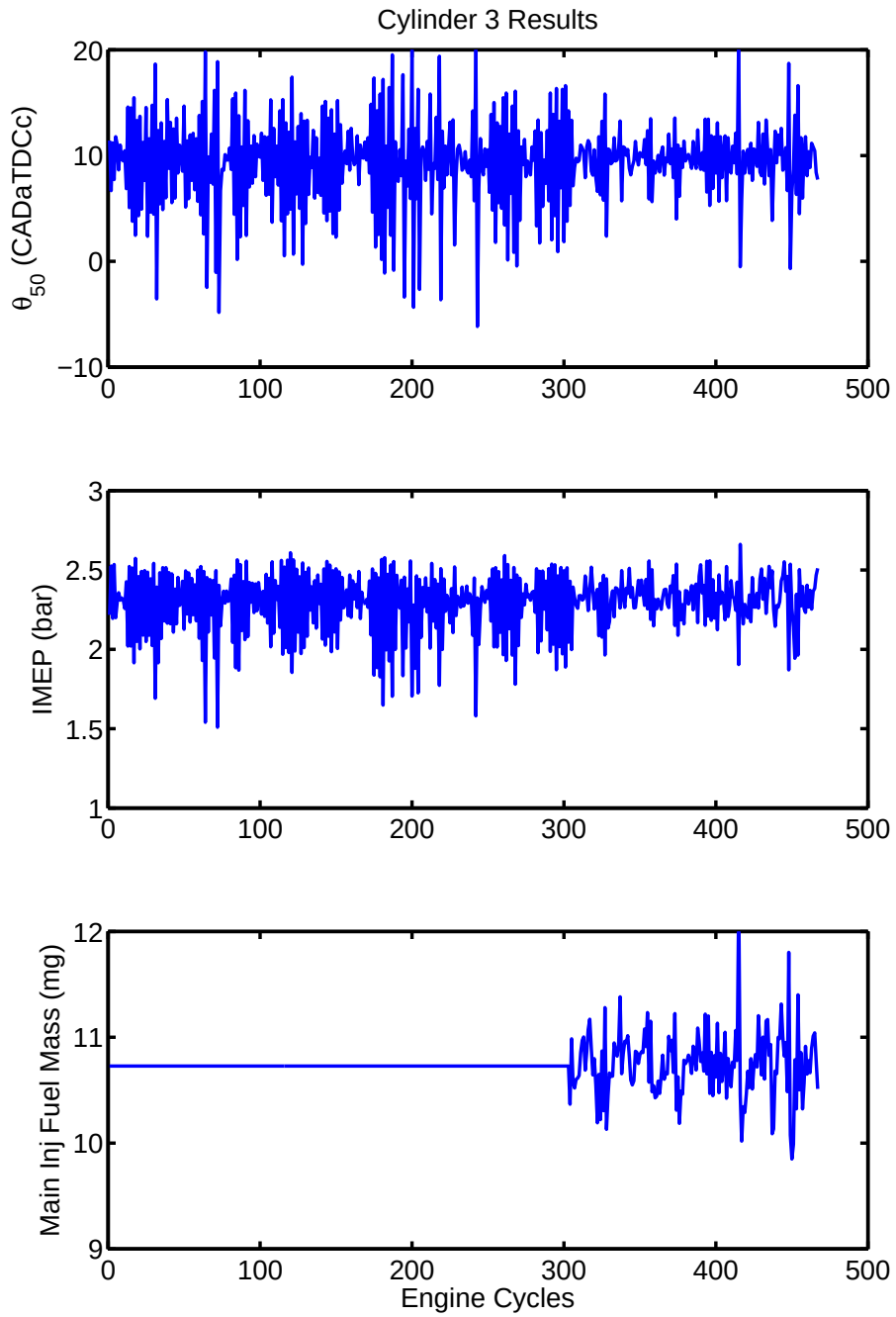

Figure 5.22: Closed-loop vs. open-loop θ_{50} and IMEP responses on cylinder 3

Table 5.2: Fuel Mass Control Results from Cylinder 3

Mean θ_{50}, OL (CADaTDCc)	9.14
Mean θ_{50}, CL (CADaTDCc)	9.62
Mean IMEP, OL (bar)	2.27
Mean IMEP, CL (bar)	2.32
IMEP CoV, OL (%)	9.96
IMEP CoV, CL (%)	5.80
Mean m_f, OL (mg)	10.730
Mean m_f, CL (mg)	10.745

5.3 Comparison of Three Inputs for Control

Two distinct comparisons between the models for each input yield insight into their differences. Comparing the characteristics of each linearized model allows for discussion of the differences between the dynamics of each system, while comparing the results from implementing each controller allows for discussion of each actuator's ability to improve HCCI dynamics.

5.3.1 Model Characteristic Comparison of Inputs

The four models of highly oscillatory operating conditions have several similarities with each other. They all have one negative pole, which roughly corresponds to the temperature state and describes the oscillatory dynamics observed at these operating conditions. They also all have one positive pole near $z = 0.5$, which roughly corresponds to the oxygen concentration state. The models also all have one zero near $z = 0.5$ that arises because combustion timing depends strongly upon temperature but weakly upon oxygen concentration. Thus, that zero blocks transmission of information about the oxygen concentration to combustion timing in all four models.

The models also have some significant differences between themselves. Three of the models have three states; the fourth, based on the exhaust valve closing timing input, has only two. The third pole, at $z = 0$ in all three cases, represents a fuel-related state: in the pilot injection timing input model, the third state is the Arrhenius threshold, while in the fuel injection quantity models, the third state is the quantity

Table 5.3: Pole and zero locations from all linearized models at highly oscillatory operating conditions

Input	p_1	p_2	p_3	z_1	z_2
Exhaust valve closing	-0.32	0.45	–	0.57	–
Pilot injection timing	-0.10	0.49	0	0.51	**0.22**
Fuel injection quantity, full charge cooling	-0.26	0.44	0	0.49	**1.51**
Fuel injection quantity, reduced charge cooling	-0.26	0.44	0	0.48	**6.57**

of fuel in the cylinder. In both of these cases, the poles occur at $z = 0$ because the models assume complete combustion of the fuel. Allowing for incomplete combustion would create nonzero values for those poles, and it would add a third state to the exhaust valve timing case also.

The other key difference between the models is the location of the second zero. The three models with three poles all possess a second zero. In the pilot injection input case, that zero occurs inside the unit circle, while in the fuel injection quantity case, that zero occurs outside the unit circle as a non-minimum phase zero. The root loci in Figures 5.8, 5.16, and 5.17 illustrate the different zero positions in an easy to visualize manner that cannot be easily replicated by state-space representations of each system. While the state-space representations of the systems in equations 5.5, 5.8, and 5.10 contain the same dynamics as the root loci representations, only the root loci systems show the key difference between the pilot injection and fuel quantity inputs as a zero location.

5.3.2 Experimental Results Comparison of Inputs

By comparing the distributions in cylinder pressure, IMEP, combustion timing, and input quantity, the three control inputs can be evaluated against one another to determine their effectiveness at reducing cyclic variations. Figures 5.23 and 5.24 illustrate the relationship between in-cylinder pressure and volume for all of the cycles corresponding to Figure 4.11 in a valve control experiment; Figure 5.23 plots the open-loop cases while Figure 5.24 plots the closed-loop cases. The two figures give a visual representation of the cylinder pressure trace distributions in both the open-loop and closed-loop cases. The open-loop case exhibits significant variations in the start of combustion and combustion duration, while the closed-loop case exhibits much smaller variations in both.

Figures 5.25 and 5.26 plot the relationship between in-cylinder pressure and volume in a pilot injection timing control experiment corresponding to cycles 1 to 213 in Figure 5.11 in open loop and closed-loop. Figure 5.26 shows that there is greater variation in cylinder pressure with the pilot injection timing controller than with the exhaust valve controller, illustrated by 5.24.

Figures 5.27 and 5.28 depict the pressure-volume relationship in a main fuel injection quantity control experiment for the data corresponding to cycles 141 through 467 in Figure 5.22. The range of the distribution of pressure traces in closed-loop using the fuel quantity controller is greater than the range pressure traces for either the valve control or pilot timing control problems.

Table 5.4 compares the effects each of the three inputs has on both combustion timing and IMEP. All three inputs reduce cyclic variations in both θ_{50} and IMEP, and all three inputs improve the efficiency of their respective operating conditions. However, the valve and pilot injection control schemes show greater effectiveness than the fuel mass scheme at improving combustion dynamics. Table 5.5 extends Table 3.2 to add the information about the effectiveness of each control strategy.

Two significant conclusions result from comparing the ease of implementing each actuator to the ease of the control problem and the effectiveness of each actuator of reducing cyclic variations. First, controllers seeking to reduce cyclic variations in HCCI combustion timing that manipulate exhaust valve timing and pilot injection

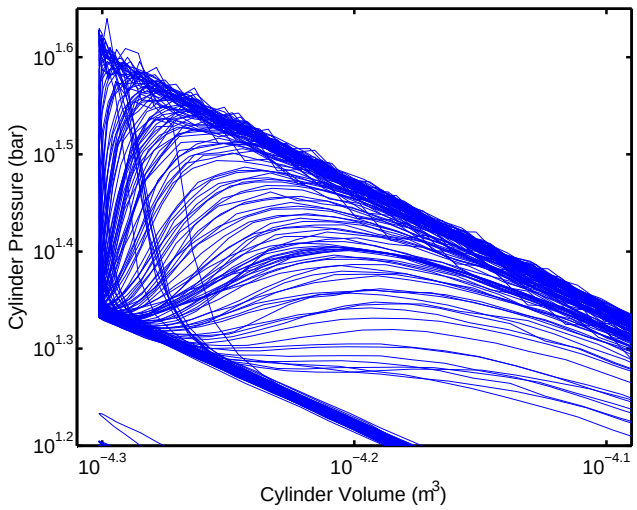

Figure 5.23: Logarithmic scale pressure vs. volume plot of cylinder 4 open-loop combustion data in valve control data set

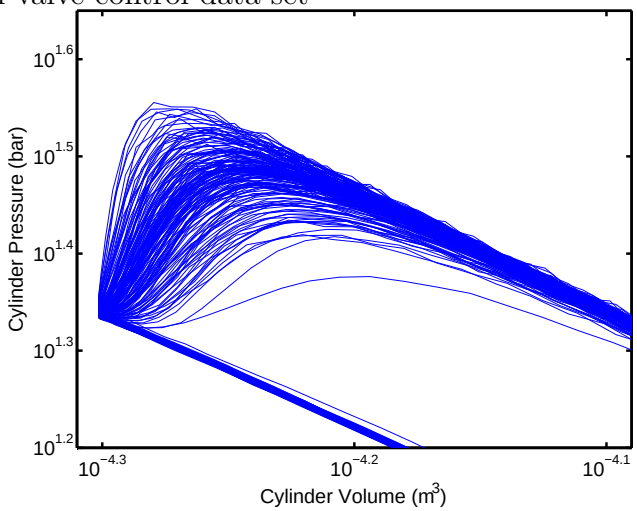

Figure 5.24: Logarithmic scale pressure vs. volume plot of cylinder 4 closed-loop combustion data in valve control data set

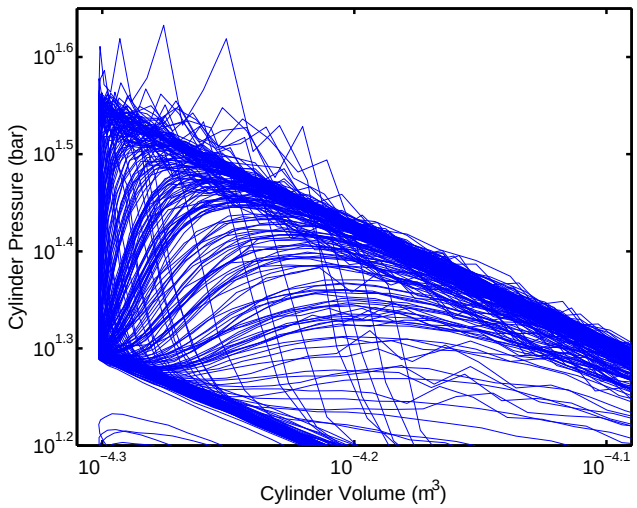

Figure 5.25: Logarithmic scale pressure vs. volume plot of cylinder 3 open-loop combustion data in pilot injection control data set

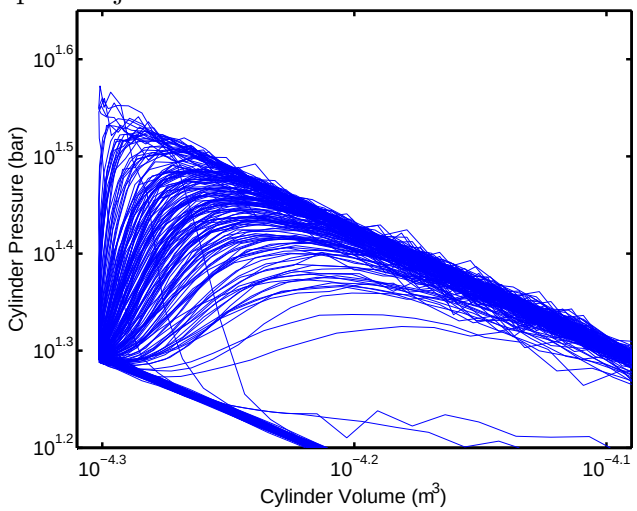

Figure 5.26: Logarithmic scale pressure vs. volume plot of cylinder 3 closed-loop combustion data in pilot injection control data set

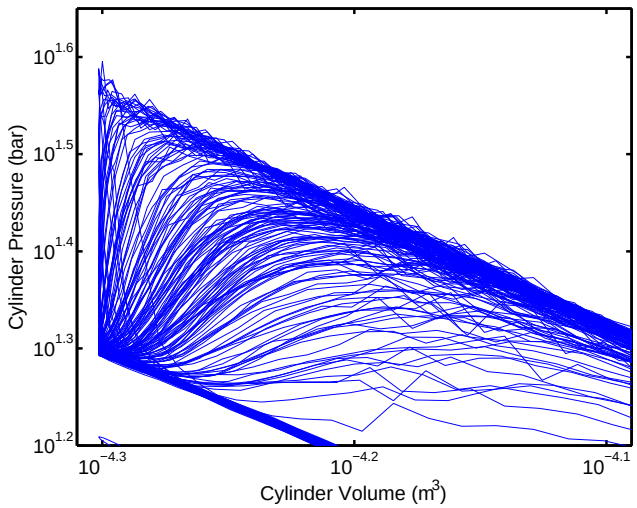

Figure 5.27: Logarithmic scale pressure vs. volume plot of cylinder 3 open-loop combustion data in fuel quantity control data set

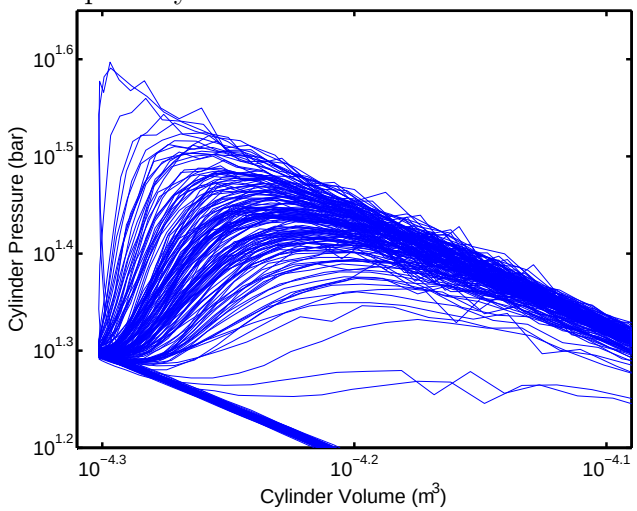

Figure 5.28: Logarithmic scale pressure vs. volume plot of cylinder 3 closed-loop combustion data in fuel quantity control data set

Table 5.4: Controller Comparison

Control Input	Exhaust Valve	Pilot Injection	Fuel Quantity
Mean θ_{50}, OL (CADaTDCc)	7.27	6.19	9.14
Mean θ_{50}, CL (CADaTDCc)	8.13	7.27	9.62
θ_{50} StdDev, OL	6.23	7.64	4.94
θ_{50} StdDev, CL	1.78	3.87	2.79
% Reduction in θ_{50} StdDev	***71.4***	***49.3***	***43.5***
Mean IMEP, OL (bar)	2.08	2.12	2.27
Mean IMEP, CL (bar)	2.19	2.24	2.32
IMEP CoV, OL (%)	13.1	14.9	9.96
IMEP CoV, CL (%)	4.23	6.46	5.80
% Reduction in IMEP CoV	***67.6***	***56.7***	***41.8***

Table 5.5: Implementation and Control Challenges for the Three Actuation Technologies Studied

Input	Ease of Implementing	Control Challenge	Ease of Control	Effectiveness at Reducing Cyclic Variations
Exhaust valve closing	Difficult	Geometric input non-linearity	Easy	High
Pilot injection timing	Easy	Non-obvious input non-linearity	Moderate	Moderately High
Fuel injection quantity	Easy	Non-minimum phase input, Linked to work	Difficult	Moderate

timing are more likely to be successful at reducing cycle variations than controllers that alter the main fuel injection quantity. There are two reasons that explain why the fuel quantity control scheme is difficult to achieve. First, the link between fuel quantity and work output makes it difficult to control combustion timing by changing fuel quantity while maintaining a constant work output. However, as the data in Table 5.4 demonstrate, small adjustments in fuel injection quantity can actually reduce the cyclic variations in work output instead of increasing them. If the commanded adjustments in fuel quantity grow sufficiently large, those adjustments would induce oscillations in the work output and possibly lead to misfire. Second, the two different physical effects observed in the cylinder, charge cooling and energy release, result in a non-minimum phase input that is used to damp out disturbances. The non-minimum phase nature of the input means that the system model needs to accurately capture the two different effects together so that the overall effect of fuel quantity on combustion timing can be incorporated into a controller that adjusts all the inputs simultaneously.

The comparison also suggests that investment in developing production-oriented technologies that can control valve timing on a cycle-to-cycle and cylinder-to-cylinder basis would push HCCI engines closer to market. The ability to directly influence the sensible energy in the cylinder prior to combustion makes controlling combustion timing much easier than needing to rely the two different thermal effects, charge cooling and energy release, that result from changing fuel quantity to control combustion timing.

Chapter 6

Conclusions and Future Work

Grappling with climate change is one of the major concerns confronting humanity in the 21st Century, and bringing technologies to market that reduce the amount of greenhouse gasses emitted into the atmosphere will make significant strides toward mitigating the effects climate change has. In the automotive sector, HCCI engines present one technology that over the short and medium term promises to reduce the amount of energy and the associated greenhouse gas emissions required to transport people and goods from one location to another. However, controlling combustion timing in HCCI engines remains a major challenge to their widespread implementation.

This dissertation makes several advancements in controlling combustion timing in HCCI engines. First, using classical control techniques, it transforms combustion timing control into a root locus control design problem for each of three different actuation strategies: exhaust valve timing control, pilot injection timing control, and main fuel injection quantity control. The root locus representation of the system allows for a simple, visual comparison of the characteristics of each control problem. It proves especially helpful in comparing the zero locations for the pilot injection timing and main fuel injection quantity control strategies since the zero locations are the primary differences between those two strategies and state-space representations of dynamic systems often obscure zero locations of systems, making it difficult to compare the zero locations in one system to another.

Second, three controllers, each using a different actuator, independently improve

the oscillatory dynamics observed at certain HCCI operating conditions. Each of the three controllers is simple enough to be easily implemented on any embedded processor on a production vehicle.

Finally, the improvements achieved at the operating conditions with oscillatory dynamics can be obtained using a gasoline direct injection fuel system, which is currently in production. However, further improvements at those conditions would be possible if better production-oriented variable valve timing technology existed that allowed for cycle-to-cycle and independent cylinder-to-cylinder control of exhaust valve timing.

6.1 Summary of Work

Chapter 2 presents the Stanford multi-cylinder HCCI engine and describes its features in detail. It specifically focuses on the aspects of the engine's design that make it suitable for controlling recompression HCCI combustion on a cycle-to-cycle basis. The variable valve actuation system and direct fuel injection system together provide the capability of adjusting the inputs of exhaust valve timing, fuel injection timing, and fuel injection quantity for each cylinder individually, and they all are adjustable from one cycle to the next. Similarly, an in-cylinder pressure sensor and a wide-band exhaust oxygen sensor provide feedback about the combustion occurring in each cylinder to controllers that improve the engine's operating performance.

Chapter 3 covers the model first introduced by Ravi et al. [32], where an HCCI engine cycle is modeled as a discrete-time process. First, the chapter breaks an engine cycle down into eight distinct, physical steps, and then it presents the inputs, outputs, and states of that model.

Chapter 4 discusses the linearization of the model in Chapter 3, and it illustrates that the source of the oscillations, different quantities of heat transfer that occur based upon combustion timing, is represented in the linearized model as a negative real axis eigenvalue. A simple, proportional controller manipulates that eigenvalue by changing the exhaust valve closing timing on each engine cycle to improve combustion stability and reduce the oscillations observed in combustion timing and power output

on the experimental engine.

In Chapter 5, the control concepts used to improve combustion stability are extended to work with a pilot fuel injection timing input and a main fuel injection mass input. Again, when the model is linearized using each input, the oscillations at certain operating conditions are driven by a negative, real-axis eigenvalue. In the pilot injection timing input case, a lag controller moves that eigenvalue by manipulating the end-of-injection angle of the pilot injection.

The non-minimum phase nature of the relationship between the main fuel injection mass input and the combustion timing output presents challenges to using the fuel mass input for controlling combustion timing. One particularly challenging aspect of their relationship is modeling the changing amounts of charge cooling that occur when the injected fuel mass is varied on a cycle-to-cycle basis. By bounding the amount of charge cooling that occurs and examining two different systems on root loci, Chapter 5 shows that a single lag controller, which is robust to the different charge cooling assumptions, works to improve the dynamics on the experimental engine as well.

Finally, all three controllers are compared at the end of Chapter 5 to determine the effectiveness of each controller. The exhaust valve closing input and the pilot injection timing input each exhibit more promise for reducing cyclic variations in late-phasing HCCI than the main fuel injection mass controller exhibits.

6.2 Future Work

Several advances could make significant strides toward HCCI becoming a realizable technology in mass-produced automobiles. In particular, improving three different aspects of the model in this thesis would lead to better HCCI performance. First, extending the nonlinear model in Chapter 3 to include unburned fuel from one cycle to the next may lead to results that more closely mimic the behavior observed on the experimental engine. The thermal coupling that the model relies upon does predict oscillations, but it understates the extent to which cyclic variations occur from one cycle to the next. Adding a chemical link between cycles could improve the agreement

between the model and the experimental results.

Second, updating the heat transfer models in Chapter 3 would also potentially lead to better modeling results. The two-step combustion model, in which heat transfer occurs both during a polytropic process and an instantaneous combustion event, could be replaced with a single-step combustion model where the amount of heat transfer to the cylinder head and wall would be a linear function of combustion timing. Using this kind of model would both simplify the model, since combustion would be occurring through only one mechanism, and improve its transparency, since it would be easier to identify the amount of heat transfer occurring during combustion. Additionally, the heat transfer model during recompression could be converted from one which features a tuned heat transfer coefficient and first law balance to one featuring a polytropic process modeling the recompression event. This change would likely allow the model to more accurately represent changes in state temperature due to changes in valve timing, and it would make the model easier to fit to experimental data.

Third, further study of the charge cooling effect due to varying fuel mass on a cycle-by-cycle basis would improve the effectiveness of the fuel quantity input. While the control approach used in this thesis is robust to the uncertainty in the amount of charge cooling taking place in the cylinder, it is unclear that integrating either of the two fuel mass models into a multi-input, multi-output system and then deriving a more complex controller, such as a model predictive controller, would yield desirable results. One potential avenue for improving the fuel mass model would be to use an identified model, wherein the amount of charge cooling occurring at a particular engine operating condition could simply be obtained experimentally. That identified model could then validate and possibly aid in tuning a physical model of charge cooling due to fuel quantity changes.

Three other advances could extend the work presented in this thesis. One way to advance HCCI's capabilities would be to integrate both the pilot injection timing input and the main fuel injection mass input into the switching controller presented by Liao et al. [24] that captures dynamics at both nominal-phasing and late-phasing operating conditions. Such a controller would allow each cylinder to move between operating regimes, opening up more feasible operating points that could be very

beneficial in the case of transient engine maneuvers between steady-state speeds and loads.

Another way to advance HCCI toward production would be to integrate the different inputs with a controller capable of explicitly controlling combustion in each cylinder individually. Integrating the fuel mass input and the switching region controller into the multi-cylinder control approach pioneered by Erlien et al. [8] would create a controller capable of operating in different operating regions and explicitly handling cylinder-to-cylinder differences while reducing the requirements of a possible cam phasing system.

Finally, increasing the robustness of HCCI to environmental conditions would improve its viability as an on-road technology. Fuel quality and composition and ambient air temperature and relative humidity all have an influence on combustion timing. Studying the impacts each of these quantities has on combustion timing would improve HCCI's odds of being used in production. Additionally, all the experiments in this work have been conducted at an engine speed of 1800 RPM. The control model's design allows it to simulate tests at different engine speeds, so expanding the speed range in which these results are valid would extend the work in a meaningful way.

Bibliography

[1] J. Bengtsson, P. Strandh, R. Johansson, P. Tunestål, and B. Johansson. Closed-loop combustion control of homogeneous charge compression ignition (hcci) engine dynamics. *International Journal of Adaptive Control and Signal Processing*, 18(2):167–179, 2004. ISSN 1099-1115. doi: 10.1002/acs.788. URL `http://dx.doi.org/10.1002/acs.788`.

[2] Johan Bengtsson. *ClosedLoop Control of HCCI Engine Dynamics*. PhD thesis, Lund Institute of Technology, Lund, Sweden, Nov 2004.

[3] Patrick A. Caton, Aaron J. Simon, J. Christian Gerdes, and Christopher F. Edwards. Residual-effected homogeneous charge compression ignition at a low compression ratio using exhaust reinduction. *International Journal of Engine Research*, 4(3), 2003.

[4] Hsin-Pao Chen, Ting-Hao Cheng, Der-Min Tsay, and M. J. Yan. Design and verification of piston-train cam linkage mechanism. SAE International, 04 2007. doi: 10.4271/2007-01-0251. URL `http://dx.doi.org/10.4271/2007-01-0251`.

[5] Magnus Christensen, Anders Hultqvist, and Bengt Johansson. Demonstrating the multi fuel capability of a homogeneous charge compression ignition engine with variable compression ratio. Copyright 1999 Society of Automotive Engineers, Inc., 10 1999. doi: 10.4271/1999-01-3679. URL `http://dx.doi.org/10.4271/1999-01-3679`.

[6] Steven Chu. The science of photons to fuel. In *Proceedings of the American*

Institute of Physics, volume 1044, pages 266–282. American Institute of Physics, March 2008. doi: http://dx.doi.org/10.1063/1.2993725.

[7] Kathi Epping, Salvador Aceves, Richard Bechtold, and John Dec. The potential of HCCI combustion for high efficiency and low emissions. Number 2002-01-1923. SAE, 06 2002. doi: 10.4271/2002-01-1923. URL `http://dx.doi.org/10.4271/2002-01-1923`.

[8] Stephen M. Erlien, Adam F. Jungkunz, and J. Christian Gerdes. Multi-cylinder HCCI control with cam phaser variable valve actuation using model predictive cont. In *Proceedings of the 5th Annual ASME Dynamic Systems and Controls Division Conference*, 2012.

[9] Ahmad Ghazimirsaied, Mahdi Shahbakhti, and Charles Robert Koch. HCCI engine combustion phasing prediction using a symbolic-statistics approach. *Journal of Engineering for Gas Turbines and Power*, 132(8):082805, 2010. doi: 10.1115/1.4000297. URL `http://link.aip.org/link/?GTP/132/082805/1`.

[10] Göran Haraldsson, Per Tunestål, Bengt Johansson, and Jari Hyvönen. HCCI combustion phasing in a multi cylinder engine using variable compression ratio. SAE International, 10 2002. doi: 10.4271/2002-01-2858. URL `http://dx.doi.org/10.4271/2002-01-2858`.

[11] Göran Haraldsson, Per Tunestål, Bengt Johansson, and Jari Hyvönen. HCCI closed-loop combustion control using fast thermal management. Copyright 2004 SAE International, 03 2004. doi: 10.4271/2004-01-0943. URL `http://dx.doi.org/10.4271/2004-01-0943`.

[12] Erik Hellström and Anna Stefanopoulou. Modeling cyclic dispersion in autoignition combustion. In *IEEE Conference on Decision and Control and European Control Conference*. IEEE, December 2011.

[13] Jari Hyvönen, Göran Haraldsson, and Bengt Johansson. Operating conditions using spark assisted HCCI combustion during combustion mode transfer to si

in a multi-cylinder vcr-hcci engine. Number 2005-01-0109. SAE International, April 2005.

[14] Gordon Cheever Jr, Charles Sullivan, Karl Schten, Ash Punater, and Clinton Erickson. Design of an electric variable cam phaser controller. volume 5, pages 403–413. SAE International, 04 2012. doi: 10.4271/2012-01-0433. URL `http://dx.doi.org/10.4271/2012-01-0433`.

[15] Adam F. Jungkunz, Nikhil Ravi, Hsien-Hsin Liao, and J. Christian Gerdes. Combustion phasing variation reduction for late-phasing HCCI through cycle-to-cycle pilot injection timing control. In *Proceedings of the 4th Annual Dynamic Systems and Control Division Conference*. American Society of Mechanical Engineers, 2011.

[16] Adam F. Jungkunz, Stephen Erlien, and J. Christian Gerdes. Late phasing homogeneous charge compression ignition cycle-to-cycle combustion timing control with fuel quantity input. In *In Proceedings of the American Control Conference*, 2012.

[17] Jun-Mo Kang. Sensitivity analysis of auto-ignited combustion in HCCI engines. SAE International, 04 2010. doi: 10.4271/2010-01-0573. URL `http://dx.doi.org/10.4271/2010-01-0573`.

[18] Jun-Mo Kang and Maria Druzhinina. HCCI engine control strategy with external egr. In *American Control Conference (ACC), 2010*, pages 3783 –3790, June 30-July 2 2010.

[19] Jun-Mo Kang, C.F. Chang, J.S. Chen, and M.F. Chang. Concept and implementation of a robust HCCI engine controller. Number 2009-01-1131. Society of Automotive Engineers, 2009.

[20] Lucien Koopmans, Ove Backlund, and Ingemar Denbratt. Cycle-to-cycle variations: Their influence on cycle resolved gas temperature and unburned hydrocarbons from a camless gasoline compression ignition engine. In *SAE 2002 World Congress*, number 2002-01-0110. SAE International, March 2002.

[21] Anup M. Kulkarni, Gayatri H. Adi, and Gregory M. Shaver. Modeling cylinder-to-cylinder coupling in multi-cylinder HCCI engines incorporating reinduction. volume 2007, pages 1597–1604. ASME, 2007. doi: 10.1115/IMECE2007-42487. URL `http://link.aip.org/link/abstract/ASMECP/v2007/i43033/p1597/s1`.

[22] H. Liao, M.J. Roelle, Jyh-Shin Chen, Sungbae Park, and J.C. Gerdes. Implementation and analysis of a repetitive controller for an electro-hydraulic engine valve system. *IEEE Transactions on Control Systems Technology*, 19(5):1102 –1113, Sept. 2011. ISSN 1063-6536. doi: 10.1109/TCST.2010.2076387.

[23] Hsien-Hsin Liao. *Control and Robustness Analysis of Homogeneous Charge Compression Ignition Using Exhaust Recompression*. PhD thesis, Stanford University, 2011.

[24] Hsien-Hsin Liao, N. Ravi, A.F. Jungkunz, Jun-Mo Kang, and J.C. Gerdes. Representing recompression HCCI dynamics with a switching linear model. In *American Control Conference (ACC), 2010*, pages 3803 –3808, June 30 - July 2, 2010 2010.

[25] Joel Martinez-Frias, Salvador M. Aceves, Daniel Flowers, J. Ray Smith, and Robert Dibble. HCCI engine control by thermal management. Copyright 2000 Society of Automotive Engineers, Inc., 10 2000. doi: 10.4271/2000-01-2869. URL `http://dx.doi.org/10.4271/2000-01-2869`.

[26] Yanbin Mo. *HCCI Heat Release Rate and Combustion Efficiency: A Coupled KIVA Multi-Zone Modeling Study*. PhD thesis, University of Michigan, 2008.

[27] Paul M. Najt and David E. Foster. Compression-ignited homogeneous charge combustion. Number 830264. SAE, Feb 1983.

[28] JanOla Olsson, Per Tunestål, and Bengt Johansson. Closedloop control of an HCCI engine. Number 2001011031. Society of Automotive Engineers, SAE, 2001.

[29] Gerald M. Rassweiler and Lloyd Withrow. Motion pictures of engine flames correlated with pressure cards. Number 380139. SAE International, 1938. doi: 10.4271/380139. URL `http://dx.doi.org/10.4271/380139`.

[30] Nikhil Ravi. *Modeling and Control of Exhaust Recompression HCCI Using Variable Valve Acutation and Fuel Injection*. PhD thesis, Stanford University, 2010.

[31] Nikhil Ravi, Hsien-Hsin Liao, Adam F. Jungkunz, Chen-Fang Chang, Han Ho Song, and J. Christian Gerdes. Modeling and control of an exhaust recompression HCCI engine using split injection. *Journal of Dynamic Systems, Measurement, and Control*, 2010.

[32] Nikhil Ravi, Matthew J. Roelle, Hsien-Hsin Liao, Adam F. Jungkunz, Chen-Fang Chang, Sungbae Park, and J. Christian Gerdes. Model-based control of HCCI engines using exhaust recompression. *IEEE Trans. on Control Systems Technology*, 18:1289 – 1302, Nov 2010.

[33] Nikhil Ravi, Hsien-Hsin Liao, Adam F. Jungkunz, Chen-Fang Chang, Han Ho Song, and J. Christian Gerdes. Modeling and control of an exhaust recompression hcci engine using split injection. *Journal of Dynamic Systems, Measurement, and Control*, 134(1):011016, 2012. doi: 10.1115/1.4004787. URL `http://link.aip.org/link/?JDS/134/011016/1`.

[34] Matthew J. Roelle, Nikhil Ravi, Adam F. Jungkunz, and J. Christian Gerdes. A dynamic model of recompression hcci combustion including cylinder wall temperature. volume 2006, pages 415–424. ASME, 2006. doi: 10.1115/IMECE2006-15125. URL `http://link.aip.org/link/abstract/ASMECP/v2006/i47683/p415/s1`.

[35] M. Shahbakhti and C. R. Koch. Characterizing the cyclic variability of ignition timing in a homogeneous charge compression ignition engine fuelled with n-heptane/iso-octane blend fuels. *I. J. Engine Research*, 9(5):361–397, 2008.

[36] M. Shahbakhti and C. R. Koch. Physics based control oriented model for HCCI combustion timing. *J. Dynamic Systems, Measurement, and Control*, 132, 2010.

[37] G.M. Shaver, M. J. Roelle, and J.C. Gerdes. Modeling cycle-to-cycle dynamics and mode transition in HCCI engines with variable valve actuation. *Control Engineering Practice*, 14:213–222, 2005.

[38] H.-H. Song and C. F. Edwards. Optimization of recompression reaction for low-load operation of residual -effected HCCI. In *SAE World Proceedings 2008*, number 2008-01-0016, pages 79–97. SAE, SAE, 2008.

[39] Rudolf H. Stanglmaier and Charles E. Roberts. Homogeneous charge compression ignition (HCCI): Benefits, compromises, and future engine applications. Number 1999-01-3682. SAE, 10 1999. doi: 10.4271/1999-01-3682. URL `http://dx.doi.org/10.4271/1999-01-3682`.

[40] Richard Stone. *Introduction to Internal Combustion Engines*. SAE International, 1999.

[41] The World Bank. CO2 Emissions, 2011. URL `http://data.worldbank.org/indicator`.

[42] The World Bank. Energy use (kt oil equivalent), 2011. URL `http://data.worldbank.org/indicator`.

[43] The World Bank. Passenger cars, 2011. URL `http://data.worldbank.org/indicator`.

[44] R. H. Thring. Homogeneous charge compression ignition (HCCI) engines. Number 892068. Society of Automotive Engineers, 1989.

[45] U. S. Energy Information Administration, 2010.

[46] Robert M. Wagner, K. Dean Edwards, C. Stuart Daw, Johney B. Green Jr., and Bruce G. Bunting. On the nature of cyclic dispersion in spark assisted HCCI combustion. Number 2006-01-0418. SAE, 2006.

[47] Anders Widd, Kent Ekholm, Per Tunestål, and Rolf Johansson. Experiemental evaluation of predictive combustion phasing control in an HCCI engine using

fast thermal management and vva. In *Control Applications, (CCA), Intelligent Control, (ISIC), 2009 IEEE*, pages 334 –339. IEEE, 2009.

[48] Anders Widd, Hsien-Hsin Liao, J.Christian Gerdes, Per Tunestål, and Rolf Johansson. Control of exhaust recompression HCCI using hybrid model predictive control. In *American Control Conference (ACC), 2011*, pages 420 –425, June 29 - July 1 2011.

[49] Koudai Yoshizawa, Atsushi Teraji, Hiroshi Miyakubo, Koichi Yamaguchi, and Tomonori Urushihara. Study of high load operation limit expansion for gasoline compression ignition engines. *Journal of Engineering for Gas Turbines and Power*, 128(2):377–387, 2006. doi: 10.1115/1.1805548. URL `http://link.aip.org/link/?GTP/128/377/1`.

[50] Hanho Yun, Jun-Mo Kang, Man-Feng Chang, and Paul Najt. Improvement on cylinder-to-cylinder variation using a cylinder balancing control strategy in gasoline HCCI engines. SAE International, 04 2010. doi: 10.4271/2010-01-0848. URL `http://dx.doi.org/10.4271/2010-01-0848`.